UNIVERSITY OF OKLAHOMA

GRADUATE COLLEGE

PROCESS BASED MODELING OF SURFACE ENERGY FLUXES, EVAPOTRANSPIRATION, SOIL MOISTURE, AND SOIL TEMPERATURE IN THE US SOUTHERN PLAINS

A THESIS

SUBMITTED TO THE GRADUATE FACULTY

in partial fulfillment of the requirements for the

Degree of

MASTER OF SCIENCE IN GEOGRAPHY

By

JORGE ANDRES CELIS R.
Norman, Oklahoma
2019

PROCESS BASED MODELING OF SURFACE ENERGY FLUXES, EVAPOTRANSPIRATION, SOIL MOISTURE, AND SOIL TEMPERATURE IN THE US SOUTHERN PLAINS

A THESIS APPROVED FOR THE
DEPARTMENT OF GEOGRAPHY AND ENVIRONMENTAL SUSTAINABILITY

BY THE COMMITTEE CONSISTING OF

Dr. Hernan A. Moreno, Chair

Dr. Jason Vogel

Dr. Renee A. McPherson

Acknowledgements

This thesis has a special dedication to my parents for all their unconditional support and encouragement to pursue my personal and professional goals and Santi for being always a motivation for me to be a good example.

There is an important acknowledgement to the US Army Research, Development and Engineering Command Army Research Office (ARO) for the funding of this project (W911NF-18-1-0007). Moreover, a big thanks to my advisor Dr. Hernan A. Moreno, for all his support, teachings, corrections, advice, feedback, and ideas. The success of this project would not be possible without his support and important help. Furthermore, the suggestions and advice from the committee members (Dr. McPherson and Dr. Vogel) helped me to organize better and focus on this study. Besides, there was excellent support from the Department of Geography and Environmental Sustainability and Dr. Moreno's research group members like Tri that helped during this process. Finally, it is necessary to mention the writing feedback, comments, and help of my dearest Christy and many thanks to my friend and colleague Filo, for being always supportive and proper upkeep during the development of this study. Big thanks to all the other people that contributed to the success of this project with their support, feedback , and commentaries.

Table of Contents

List of Tables

List of Figures

List of Important Acronyms

- ECT: Eddy Covariance Tower.
- ET: Evapotranspiration
- G: Ground heat flux.
- H: Sensible heat flux.
- LE: Latent heat flux.
- NR: Netradiation.
- SCE: Shuffled Complex Evolution.
- SEB: Surface Energy Balance.
- SEF: Surface Energy fluxes.
- SSM: Surface soil moisture.
- RSM: Root zone soil moisture.
- SST: Surface soil temperature.
- RST: Root soil temperature.
- tRIBS: Triangulated Irregular Network TIN-based Real Time Integrated Basin Simulator

Abstract

This study aims to evaluate the capability and transferability of a physically-based hydrologic model to understand the trade-offs between precipitation, soil moisture and surface energy fluxes at sites with different vegetation types in the U.S. Southern Plains. One of the benefits of training a process-based model is the capacity to use it as a complement to standard weather stations for predicting energy fluxes, soil temperature and moisture estimations.

Modeling of the terrestrial surface soil moisture and temperature, and boundary layer energy fluxes is key for understanding the spatio-temporal variability of hydro-meteorological conditions that drive normal and extreme (i.e. floods and droughts) events. Soil moisture (SM), surface energy fluxes (SEF) and soil temperatures (ST) play an important role in the ground and near surface hydro-energetic dynamics, especially in water exchange processes such as the evapotranspiration (ET). ET is an important variable for understanding the energy, water and biogeochemical budgets.

This study uses the Triangulated Irregular Network TIN-based Real Time Integrated Basin Simulator (tRIBS), a continuous physically-based distributed hydrological model, to provide estimations of the surface energy balance (SEB) components in typical environments of the U.S. Southern Plains. Both calibration and validation of the model are performed using available Eddy Covariance Tower (ECT) observations distributed on crops and grasslands in Oklahoma. The model calibration is based on a hybrid strategy that uses a manual procedure followed by an optimization algorithm based on the Shuffled Complex Evolution (SCE) theory. All data used to parametrize the model is free-access.

Satellite data is needed to represent dynamic vegetation conditions of albedo, leaf area index, vegetation throughfall coefficient, stomatal resistance and vegetation fraction. Model calibration is conducted during one hydrologic year at two stations with differing vegetation cover. Model validation is conducted at the same ECTs during a different year than the calibration. Transferability of the model parameterization is tested at other ECT with similar vegetation conditions in the Southern Plains. The model calibration and validation results showed the strong capabilities of tRIBS to predict the energy fluxes (Nash>0.5) and the soil temperature profile (Nash>0.7). In addition, the model predicts the soil water content well, but snow occurrences affected the model's performance.

Furthermore, tRIBS captures the seasonal and diurnal cycles of the energy partitioning with the use of remotely-sensed dynamic vegetation from MODIS and standard weather observations. Vegetation changes play a crucial role in the simulations accuracy. The onset of vegetation greening impacts the contribution of the different components of ET with increased contribution of plant transpiration (T) over soil evaporation (E). Finally, the model has potential to be transferable and of use as a forecasting tool in similar environments in the Southern Plains without parameter calibration. However, the quality of the weather forcing and satellite data will influence the accuracy of the results.

1.Introduction and Goals

The surface energy fluxes that make up net radiation (NR; i.e. latent heat flux (LE), sensible heat flux (H), ground heat flux (G)) impact the baroclinic wave, which plays an important role in the atmospheric conversion, and in some weather anomalies such as drought and flood events (Castelli, Rodriguez-Iturbe & Entekhabi, 1996; Oglesby 1991; Kuo, Reed & Low-Nam, 1990). Vegetation type and condition influence the energy exchange rates between the atmospheric boundary layer and the Earth's surface (McPherson 2007; Taylor, Said, & Lebel,1998), and the changes in vegetation cover impact albedo (near-infrared and visible wavelengths), solar radiation and evapotranspiration (ET) (Freedman et al., 2001; Anthes, 1984).

Furthermore, changes in Surface Energy Budget (SEB) partitioning affect the soil water content and land surface temperature that are key in cloud formation and convective storm rainfall patterns (Souza et al.,2000; Huber,Mechem, & Brunsell 2014; Xiang, Vivoni, & Gochis, 2014; Brusnell et al., 2010). The SEB also plays an important role on the ground and near-surface hydro-energetic dynamics (Campbell & Norman, 1998). H and LE can severely impact the performance of optical, infrared and acoustic sensors used by the military. LE is linked to evapotranspiration a key component of the water balance equation and critical atmospheric demand for different sectors like energy, food and water supply (Palladinoa et. al, 2013). Differences between actual and potential ET at high spatial resolutions, are of interest to agriculture, water resources, and even national security, as an indicator of crop water deficits. ET and soil moisture (SM) affect the

operational mobility of military operations and detection of landmines and unexploded ordinance (Van Dam et al., 2005).

One of the contemporary techniques to estimate surface energy fluxes is the eddy covariance method (EC), proposed by Montgomery (1948), Swinbank (1951), and Obukhov(1951) from measurements of heat, mass and momentum. The theory under the EC method proposes that under conditions of horizontal homogeneity, the net transport between the surface and the atmosphere exists in one dimension. Due to this, the method can be applied to estimate the flux density between the turbulent fluctuations of the element of interest and the vertical wind (Aubinet, 2012). The new generation of atmospheric instruments like sonic anemometers and gas analyzers at the end of the 1990's increased the use of the EC method, especially by the ecological scientific community, who were looking forward to carbon dioxide and carbon exchange measurements (Aubinet, 2012), contributing to the installation of the first EC towers with the application of the new techniques (Aubinet, et al., 2000).

The efforts of global networks such as FLUXNET and AmeriFlux, have contributed to increase the number of EC systems installed during the last decades. Due to the different environmental conditions between ecosystems, the EC technique has been improved from its initial theoretical considerations to the current tower's design, which varies from grassland to complex forest ecosystems, where measuring the microclimate and exchanges above the canopy presents different sets of difficulties (Aubinet, 2012). The specialized instrumentation and method used by the towers allow them to provide micrometeorological, energy, net ecosystem exchange and many other variables at a temporal resolution of 30 minutes. The towers have a standard configuration composed

of 6 groups of elements --data acquisition main enclosure, sensors, hardware, power, optional components, and software-- that are constantly upgraded and can be seen in more technical detail on the web page (AMERIFLUX, 2018). Although differences in sensors can be found across different locations, many scientists have studied the implications of the instruments' accuracy in different terrains, climate conditions and also number of maintenances, especially in very remote areas (Goodrich, et al., 2016).

Despite the multiple benefits of knowing SEF, SM and ST, the cost and complexity of measuring them make the availability of this data limited for most places, inhibiting our understanding of several atmospheric, hydrologic, and ecological processes (Pielke, et al., 1998). For this reason, some alternative techniques have been used to estimate the SEB, many of them focusing on LE and thus ET. Statistical and empirical approaches based on remote sensing models to estimate ET (Waglea et al., 2017) are useful over large areas (Glenn et al.,2007). Other approaches involve complex models based on the SEB equation, but due to the complexity of its parameterizations, had not been widely assessed. Waglea et al. (2017) compared and assessed the performance of five widely used SEB models over a sorghum crop field at Chickasha, Oklahoma for two growing seasons (2012, 2013) using (1) The Surface Energy Balance Algorithm for Land (SEBAL), (2) Mapping ET with Internalized Calibration (METRIC), (3) Surface Energy Balance System (SEBS), (4) Simplified Surface Energy Balance Index (S-SEBI), and (5) operational Simplified Surface Energy Balance (SSEBop). The results showed the best performance for the S-SEBI with substantial ET underestimations under wet conditions for that study period. However, the most important finding was that all SEB models overestimated sensible, ground, and latent heat flux values during dry periods, reflecting

the necessity to incorporate variables such as soil moisture or vegetation cover and activity to better represent plant transpiration. The changes in land cover, vegetation type and canopy biomass influence the soil moisture and surface energy fluxes through their relation with precipitation interception and transpiration (Sanchez et al.,2015; Lingli et al., 2013). Various authors (Moreno et al., 2016; Olajuyigbe et al., 2012; Dore et al., 2010) have found that disturbances, such as forest thinning, significantly shift the net radiation, surface temperature, wind speed, soil evaporation and different hydrological components in the long term. On the other hand, seasonality of vegetation can shift the energy and water balance components. MendezBarroso et al. (2014) found that seasonality has important effects on the ET partitioning and discussed how dynamic elements like albedo, stomatal resistance, and Leaf Area Index (LAI) are important. However, vegetation parameters are often considered static, reducing the simulation's accuracy. Additionally, vegetation can be exposed to insect infestation, fertilizers, disease and other elements that affect the plant health and condition, producing disturbances. Maggard, et al. (2016) showed how fertilizers affect the LAI and stomatal resistance in pines that are an important species in southern US.

To date, there is not a model that operationally runs continuously (at hourly time steps) at the scale of a ECT footprint to compute the SEB components, soil moisture and soil temperature at the shallow and root-zone layers for scientific and stakeholder applications in the Southern Great Plains. The overall goal of the study is to evaluate the capability of the tRIBS model to reproduce those variables and to test the model parameter transferability to standard weather stations (e.g. Oklahoma Mesonet) extending its usability through real-time modeling and providing new information on SEB at

standard weather stations. Furthermore, hydrology modeling often has disregarded or simplified vegetation to a static component, prescribing characteristics based on topography or climate (Kim & Eltahir, 2004; Dietrich & Perron, 2006), and the inclusion of the dynamics in vegetation cover and the phenology changes improve the long-term annual simulations (Ivanov, Bras, Vivoni, 2008; Donohue, Roderick, McVicar, 2010).

The Triangulated Irregular Network (TIN)-based Real Time Integrated Basin Simulator (tRIBS) was run over different locations in Oklahoma to fulfill the objectives of this study. tRIBS is a continuous, physically-based, distributed hydrological model (Garrote & Bras 1995; Ivanov, et al. 2004; Moreno, Vivoni, & Gochis, 2012), that uses spatially distributed atmospheric, land cover, soil and topographic parameters for each voronoi element (polygon) to reproduce the energy and water distribution within a basin. tRIBS' TIN geometry accurately represents the terrain variability, vegetation and soil distribution (Ivanov, et al. 2004 a b; Vivoni et al. 2005; Moreno, et al. 2016). This model has been successfully used to track the response of the energy and meteorological forcing across different environments (Mahmood and Vivoni, 2008; Mendez-Barroso et al., 2014; Rinehart et al., 2008; Vivoni et al., 2010). Furthermore, the model considers dynamic vegetation changes in a computationally efficient format, allowing tRIBS to improve the simulations accuracy and performance.

The general goal of this study is to assess the tRIBS model's ability to estimate surface energy fluxes, shallow and root-zone soil moisture, and surface and root layer temperatures at four eddy covariance towers of the U.S. Southern Plains and determine the mechanisms that control their event and seasonal scale shifts and model parameter transferability. The specific objectives to accomplish the general goal are to 1) Conduct

the tRIBS model parameter, initial and boundary conditions calibration according to the physical characteristics and location of each calibration ECT, using a combined manual/automated routine. 2) Perform tRIBS model validation at the calibration ECT for years different than the calibration period. 3) Analyze the impacts of precipitation, soil moisture and surface temperature on the SEB partitioning and STP in the calibration/validation ECT. 4) Assess the tRIBS model performance in different ECT of Oklahoma aiming to evaluate parameter transferability and potential use of the model to provide real-time estimations of SEB, and soil conditions over Oklahoma's Mesonet locations.

2. Study Area, Data & Methods

2.1. Study Area

The study is focused on four ECTs in the state of Oklahoma (see Figure 1). The state has multiple climate divisions (Panhandle, North Central, Northeast, West Central, Central, East Central, Southwest, South Central, Southeast), the location and characteristics of the climate regions provide a diverse sample of the Southern Great Plains (SGP) climate conditions. Oklahoma is characterized by a cool-mild average annual temperature of 15.3 °C and the precipitation in the state can range between 500mm/y to 1397 mm/y. The southeast climate zone is the warmest and receives most of the state's precipitation (Oklahoma Climatological Survey, 2004).

The Oklahoma department of agriculture, food, and forestry indicates that the state has twelve ecoregions. In fact, Oklahoma has more than 492 vegetative species (Oklahoma Department of Wildlife Conservation, 2017), but the highest recurrences are found in 85 species at the tree, shrub and herbaceous stratums. Cross timbers, Central Mixed Grass, High Plains Shortgrass, and Osage Tallgrass are the most common grasslands types, covering over a third of the state area (Oklahoma Department of Wildlife Conservation , 2017). Row crops and oak forest are almost half of the state area, which is why a better understanding of the SEB, SM and ST over crops and grasses land-cover is very beneficial. The rest of Oklahoma is covered by species that made up less than 10.000 ha each (Oklahoma Department of Wildlife Conservation , 2017).

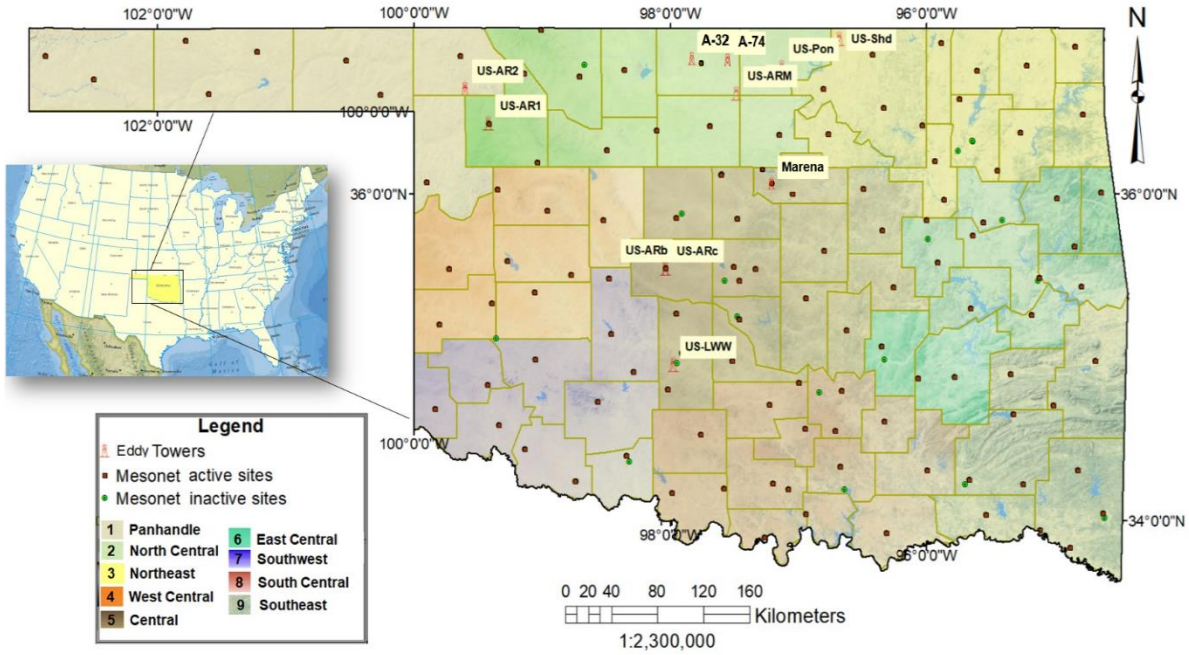

Figure 1. Spatial distribution of ECT and Oklahoma Mesonet stations on an Oklahoma climate region background map. Towers used in the study US-Arm, Marena, US-A32 and US-A74 at north central Oklahoma.

The ECTs shown in Figure 1, excluding Marena, are under the management of the AmeriFlux network, which provides quality-controlled and free of charge data of the main variables required to study water and energy flux dynamics. Additionally, the Mesonet stations are strategically distributed over the state, providing potential for testing the results of this study at multiple locations. The calibration and validation procedures were performed over the US-ARm, a location characterized by mixed crops, and the Marena site, also known as MOISST (Marena Oklahoma In-Situ Testbed) experiment, that has a rangeland/pasture land-cover. The transferability of the model in crops is tested over the US-A74 Milo field station, and the grasslands at the US-A32 ARm hay pasture site.

The ECTs utilized in this study are exposed to different surrounding vegetation, and management (grazing/fire/thinning) in the case of Marena. Table 1 briefly illustrates some aspects of relevance of the sites selected for this study.

Table 1. Micro-meteorological sites selected for model calibration, validation and transferability runs along with their vegetation and relevance to this project.

ID	Lat	Lon	Utility	Vegetation	Relevance
US-ARm	36.60N	97.48W	Cal/Val	Crop Field(winter wheat, soy, corn, alfalfa)	Provides more than 200 variables and it's the reference tower for the Atmospheric Radiation Measurement (ARM) quality data program. This tower is going to be used as a calibration point for the model.
Marena (MOISST)	36.04 N	97.21W	Cal/Val	Rangeland with grazed cattle pasture	The site has 4 in-situ testbed for soil moisture and soil temperature, and the MARE Mesonet station. The testbeds have Stevens Water Hydra Probe, Delta-T Theta Probe, EC-TM Probe and 5 other sensors that obtain

ID	Lat	Lon	Utility	Vegetation	Relevance
					measurements between the 2.5 to the 100cm.
US-A32	36.81N	97.81W	Parameter Transferability	Grasslands	The site is located at E32 ARM Southern Great Plains (SGP) extended facility.
US-74	36.80N	97.54W	Parameter Transferability	Croplands	The ARM SGP milo filed has a humid subtropical with no dry season and hot summer.

The US-ARm measuring tower is located over a silty clay loam soil, a cropland land-use and its soil depth is 0.25 m (Wang et al., 2012). The area is a mixed crop field (winter wheat, corn, soy, alfalfa; see Figure 2a). The site has 8 years of continuous measurements available on the AmeriFlux and FLUXNET networks. In addition, the experiment site has 3 additional ECTs under the ARm network management with data available up to the present, having sonic anemometer systems located at 4 m, 25 m and 60 m height. The Marena site is managed by Oklahoma State University (OSU) and includes the "MARE" Mesonet station, that is quality-assured 5 minutes' data (McPherson et. al, 2007). The land cover type is a grazed cattle pasture/rangeland pasture and the soil type is sandy clay loam/loam (see Figure 2b). In addition, sections of the field are burned for salt cedar control every three years. The site was proposed as an in-situ testbed for calibration and validation of the soil moisture obtained by new satellite products like NASA-SMAP. The US-ARm site, however experienced numerous gaps in the time series of SM, so this variable was not used for the calibration or validation in the study. On the other hand, the sensors deployed at the Marena site have Stevens water hydra probes, delta-t probes and some other soil moisture sensors at 2.5, 5, 10, 20, 50 and 100cm depth that were built in calibration equations that proven to be reliable in previous experiment sites (Cosh et al., 2005), allowing us to validate the model's ability to estimate

real time soil moisture and soil temperature at the surface and root zone layers. The information used in this study was from the MOISST experiment site A, and the soil moisture data obtained from the Stevens Hydra probes; more information about the experiment site, the in-situ techniques, and the instruments technical details can be found at the Soil Moisture Active Passive In Situ Sensor Testbed experiment plan at the USDA web site. For the ECTs US-ARm, Marena, US-A32 and US-74, I calculated the eddy flux footprint, in order to delimit the extension of the model domain for the terrain, soil and vegetation parameters and model output integration comparison (see Figures 3, 4 and 5). The computation of the flux footprint used was the Kljun model.

Kljun et al. (2015) has presented a model grounded on trajectory and based on the Langrarian model for various turbulence stratifications with backward paths, but less restricted than other models (i.e. Sogachev & Lloyd, 2004; Kormann and Meixner, 2001) improving its applicability. Kljun's model requires a two dimensional parameterization for Flux Footprint Prediction (FFP) and considers the roughness of the terrain, making it the most adequate to use in this study. Relevant information about the different fetch models and timeline up to the model we chose is presented in the appendix table A.

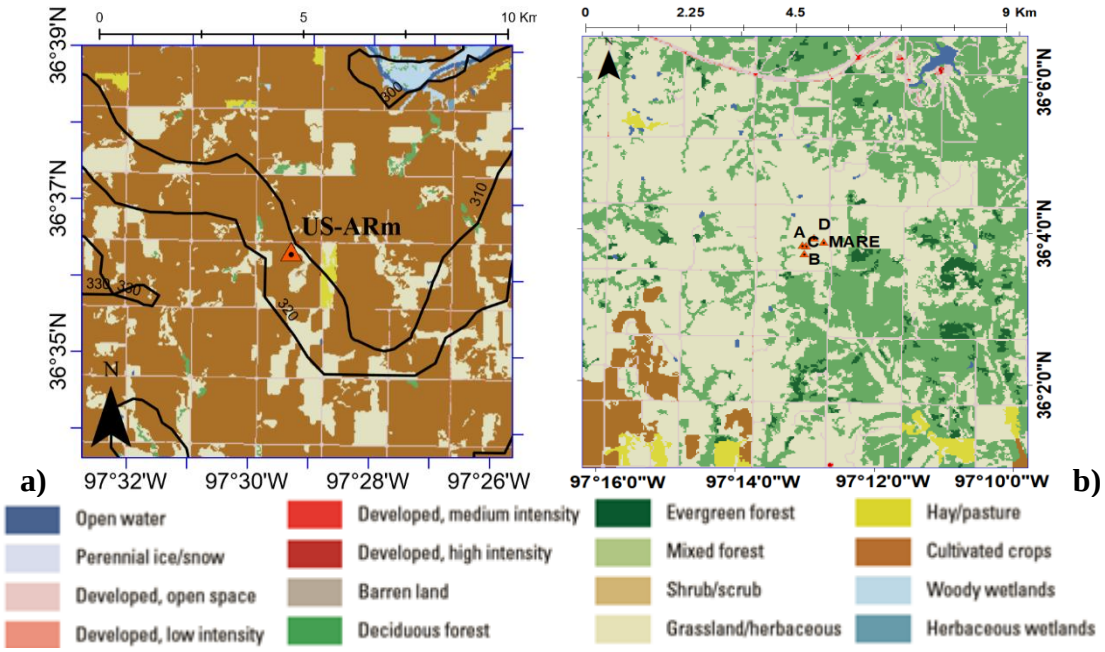

Figure 2. Land cover maps for (a) US-Arm (b) Marena, study sites.

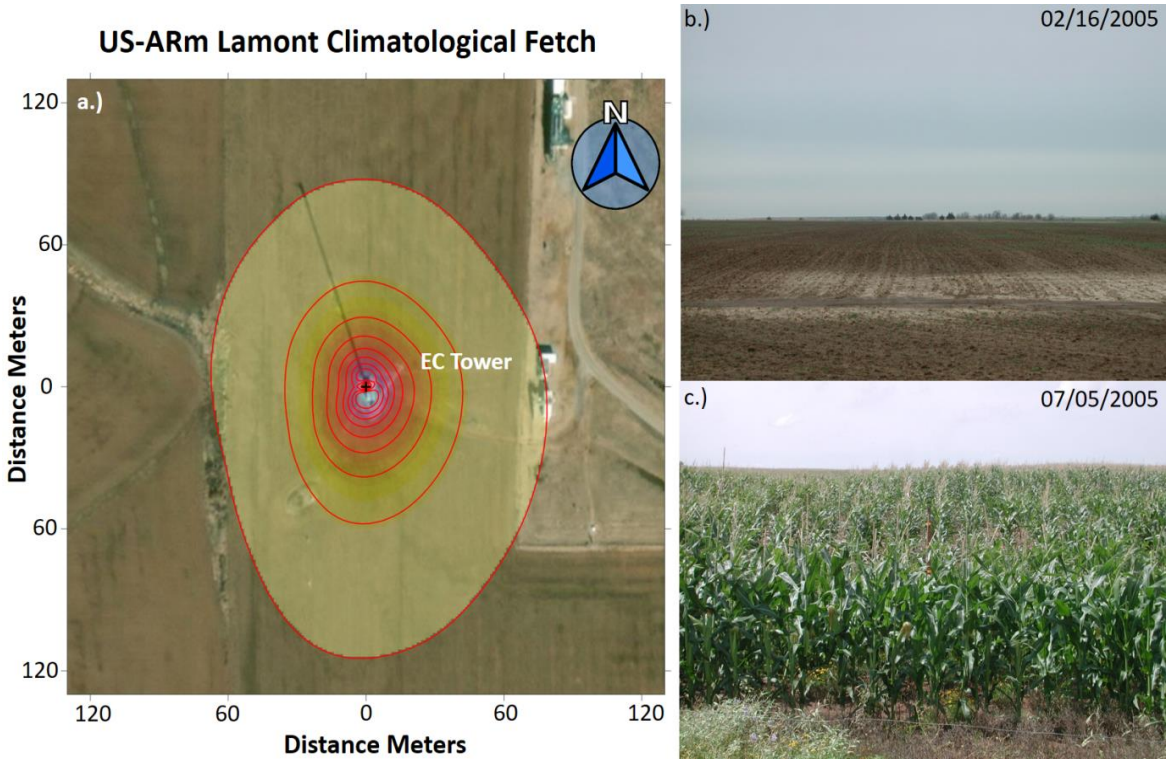

Figure 3. US-ARm site flux footprint 01/2004 to 01/2006 based on *Kljun et al. (2015)* (a). Phenocam images from winter and summer seasons are displayed in b) and c) respectively. Each of the FFP contour

lines represent 10% of contribution, being the last one the 10% remaining to complete 100% of the fetch area.

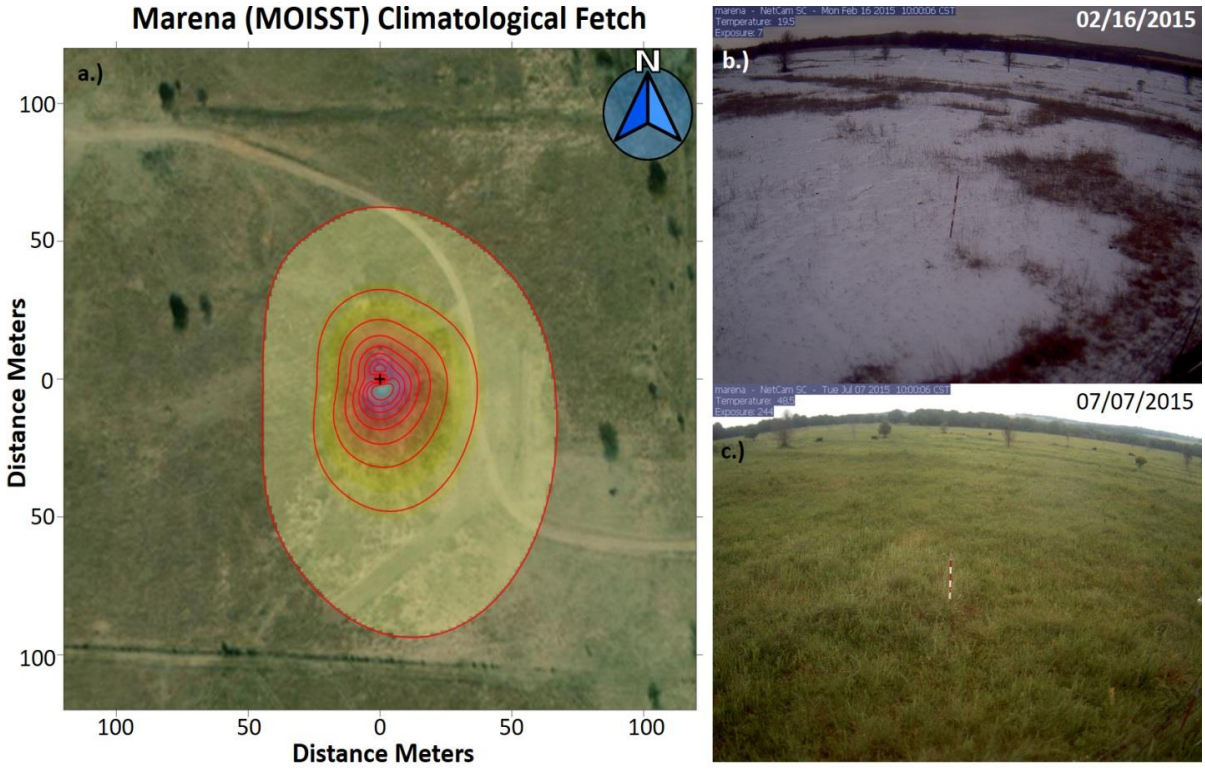

Figure 4. Marena (MOISST) site flux footprint 02/2015 to 07/2015 based on *Kljun et al. (2015)* (a). Phenocam images from winter and summer seasons are displayed in (b) and (c) respectively. Each of the FFP contour lines represent 10% of contribution, being the last one the 10% remaining to complete 100% of the fetch area.

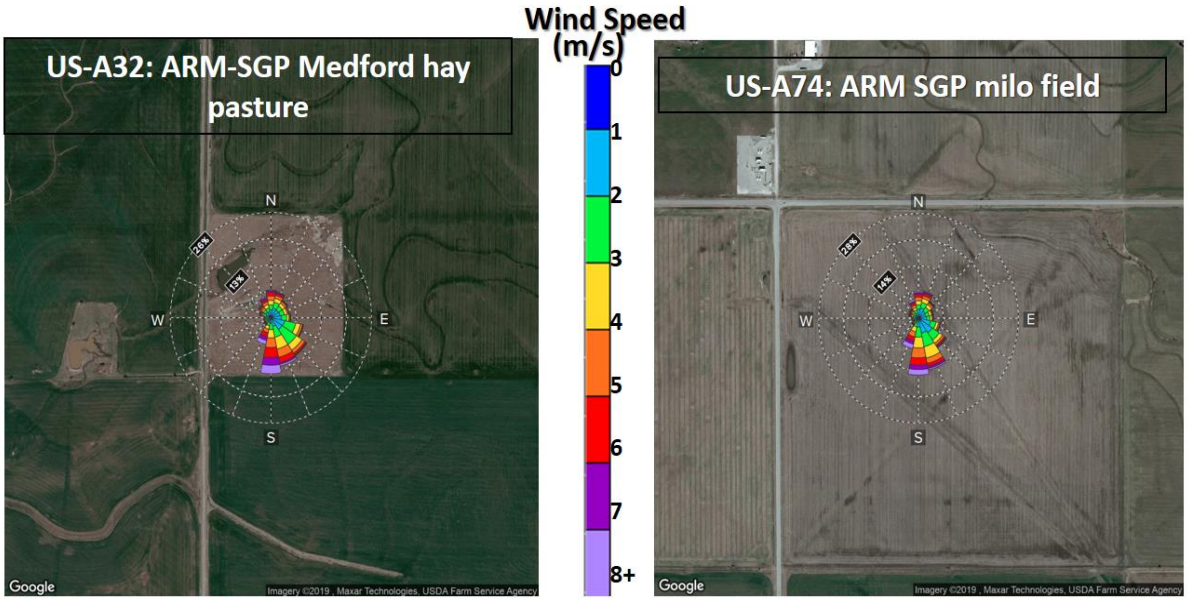

Figure 5. Annual mean wind rose for US-A32 and US-A74 respectively. Estimated by Ameriflux using 16 cardinal wind directions. (Ameriflux, 2018)

2.2. Data

2.2.1. Weather forcing, energy flux, soil moisture and temperature data

The data used in this study are measured at each ECT at 30-minute resolution. The weather forcing data that are used as input to the tRIBS model for the simulations are: incoming shortwave radiation (IS), air temperature (T), vapor pressure (VP), wind speed (WS), atmospheric pressure (Pa) and precipitation (P). Additionally, the data that are used as standard for calibration and validation are LE, H, G, NR, surface soil moisture (SSM), root-zone soil moisture (RSM), surface soil temperature (SST) and root-zone soil temperature (RST). These variables are measured directly by the ECTs and it is widely accepted to direct measure the surface energy fluxes components using the EC systems (Paw et al., 2000). FLUXNET and AmeriFlux both have special guidelines and controls for every tower's team to ensure the data quality. In the case of AmeriFlux, the network uses a mobile eddy covariance tower across their sites to validate the other towers'

measurements (AMERIFLUX, 2018). The instrumentation is standard and most of the towers currently use GA_OP-LI-COR LI-7500 to measure LE, SA-Gill Windmaster Pro for H, ground heat plates for G, RAD-Net radiometer for NR, and RAD-SW Pyranometer Class2 for the incoming short wave radiation. The specific details about instruments type and height for each of the ECT in the network can be found on their web page (www.ameriflux.lbl.gov/wp-content/).

In addition, within this Oklahoma study area 75% of the towers are part of the ARM Climate Research Facility that possesses around 7000 research data fields and is well known for producing data of *"known and reasonable quality"* for use by researchers on climate (Peppler et al., 2016). The goal of the ARM data quality program is to assess the quality of all the measured variables, and according to the data quality assessment history, the early programmatic efforts were focused on the first field site "*Southern Great Plains (SGP)"* that resulted in special benefit for our research because of the inclusion of one of our study sites. Also, in many cases both AmeriFlux and FLUXNET provide gap filled values using credible statistical techniques. For the case of Marena, OSU and the U.S. Department of Agriculture provide maintenance and manage the data derived in conjunction with the MOISST experiment.

2.2.2. Terrain and vegetation information

The Table 2 illustrates the different remote sensing products utilized for the hydrologic model simulations in relation to the terrain and dynamic vegetation parameters.

Table 2. Remote sensing data used to capture terrain and vegetation variability in the tRIBS simulations.

Parameter	Source	Product	Spatial Resolution	Temporal Resolution	Data set Download Period
Land cover	USGS	NLCD	30m	N.A.	2011 Map
Digital Elevation	USGS	SRTM	30 & 90m	N.A.	-
Leaf Area Index (LAI)	MODIS	MCD15A3H	500m	4 Days	2002-2012
Photosynthetically Active Radiation (FPAR)	MODIS	MCD15A3H	500m	4 Days	2002-2012
Albedo	MODIS	MCD43A	500m	Daily	2002-2012
NDVI	MODIS	MOD13Q1	250m	16 Days	2002-2012
Red & NIR Bands	MODIS	MCD43A4	500m	Daily	2002-2012

2.3. Tools and Methods

2.3.1. tRIBS Model

tRIBS is a physically-based distributed hydrological model developed at the Ralph M. Parsons Laboratory, Massachusetts Institute of Technology. It uses spatially distributed atmospheric, land cover, soil and topographic parameters for each voronoi cell to reproduce the energy, and water distribution within the basin. A Triangular Irregular Network (TIN) represents accurately the terrain variability, vegetation and soil distribution (Vivoni et al., 2004; Ivanov et al., 2004; & Moreno et al. 2016).

This study used tRIBS model simulations to evaluate the response of the energy and water budgets to meteorological forcing and vegetation transitions as successfully has been done across different environments (Vivoni et al. 2010; Mendez-Barroso et al. 2014; & Moreno et al. 2016)**.** Furthermore, we chose tRIBS over other similar models such as the mesoscale Weather Research and Forecasting model (WFR) on its extension

WRF-Hydro (Xiang et al., 2017; Gochis et al., 2014; Yucel et al., 2015; Senatore et al., 2015) based on tRIBS high spatial resolution, computational efficiency and computational architecture, that produces important savings on computational demands, using a domain adjustment to better fit the terrain. WRF-Hydro estimates as tRIBS several atmospheric and hydrological variables, but requires an extensive parametrization. For example, the estimation of surface energy exchange processes and inclusion of dynamic vegetation parameters (LAI and vegetation fraction), requires an additional multiparametrization of the land surface model Noah-MP (Niu et al., 2011) embedded within WRF-Hydro (Xiang et al., 2017), becoming more complex and less efficient.

In addition, the spatially-distributed physical descriptors of terrain, soil and vegetation can be input in tRIBS unprecedented, hyper-resolution differently from most GCM or CONUS models. Finally, tRIBS includes state of the art process-based conceptualizations of all processes linking energy and water fluxes at the scale of the voronoi element that can be a limitation in other models, becoming an appropriate tool to acquire the main goal of this study (Ivanov et al. 2004a, b).

The functionality of all the tRIBS modules of relevance for this research are not going to be explained in detail. However, Penman-Monteith energy and mass transfer techniques are used to estimate potential and actual evaporation, which are used to estimate evaporation from wet canopy, plant transpiration, and bare soil evaporation (Pan and Mahrt, 1987; Wigmostoa et. al, 1994). Table 3 provides a gist of the main model physics used to estimate the output variables of interest. For more detailed information

about the model components, physics, and structure the please refer to the user manual (http://vivoni.asu.edu/tribs/userManual.html).

Table 3. tRIBS module functionality and methods of relevance for this study.

Variable	Author	Method
Latent heat flux	(Penman 1948);(Monteith 1965)	Combines energy and mass transfer techniques for the estimation $$\lambda E = \frac{\Delta(Rn - G) + \gamma \frac{\rho m\, \lambda v\, \rho qa}{\gamma a}}{\Delta + \gamma(1 + \frac{\gamma a}{\gamma s})}$$
Sensible heat flux	(Rogers and Yau 1989);(Shuttleworth 1992)	Use an aerodynamic resistance approach to compute from air temperature and the surface temperature gradient $$H = \frac{\rho m\, Cp}{\gamma a}(Ts - Ta)$$
Ground Heat Flux	Lin (1980); Hu &Islam(1995)	Use the Force-restore method based in surface and deep soil temperatures $$G = \frac{1}{2}\, Csd1(\xi \frac{ds}{dt} + \omega(Ts - Td))$$
Soil heat capacity(Cs)	(Campbell and Norman 1998)	Based on equation 3 is estimated by: $$\rho sCs = \phi m \rho mCm + \theta \rho wCw + \phi 0 \rho 0C0$$
Thermal conductivity (Ks)	(DeVries1968)	It is a weight summation of the conductivities of the constituents $$Ks = \frac{\phi w * \varepsilon w * kw + \phi g * \varepsilon g * Kg + \phi m * \varepsilon m * km}{\phi w * \varepsilon w + \phi g * \epsilon g + \phi m * \varepsilon m}$$
Soil Temperature Profile	(Wang &Brass1999)	Relates Soil surface temperature and ground heat flux, is based on dimensional diffusion equation(Ivanov, Bras et al. 2008). $$G(t) = \sqrt{\frac{Ks * Cs}{\pi}} \int \frac{dTg(s)}{\sqrt{t - s}}$$
Soil water content	Green & Ampt (1911); Ivanov (2002)	The standard Green-Ampt model follows from assuming that for the moisture front infiltrating into a semi-infinite, homogeneous soil at uniform initial volumetric water (O, = const) content. qn= $-Ks\frac{\mathrm{hf-h0-Nf}}{Nf}$

2.3.2. Modeling Inputs

The model inputs can be summarized into terrain, atmospheric forcing, soil and vegetation parameters. Topographic data is required to retrieve the Triangular Irregular Network that the model uses to run. A 10 m resolution Digital Elevation Model (DEM) was used from the National Elevation Dataset to derive the model TINs at each simulation

site. Atmospheric model forcing variables such as, precipitation (P), atmospheric pressure, air temperature, wind speed, relative humidity and incoming short wave radiation were obtained from the ECTs' measurements at 30 min resolution. The flux footprint of each eddy covariance towers (Figures 3 and 4) was used to determine the average extent of the dynamic input files.

The land surface characteristics used to parametrize the hydrological processes related to the soil are presented in Table 4. The values come from local databases such as the Oklahoma Geological Survey, but for locations with not enough information available, well constrained soil values were obtained through the use of pedotransfer functions, helping us to represent more precisely the physics of the study site.

Further, the land cover or land use parameters are obtained from field measurements information and different biophysical relations at each EC site. The parameters shown in Table 5 are related to the interception and evaporation processes of the vegetative cover. Some of these parameters underlined in Table 5 were estimated and inputted into the model dynamically using remote sensing data. The dynamic vegetation parameters utilized to characterize the vegetation conditions were estimated using the Moderate Resolution Imaging Spectroradiometer (MODIS) sensor data (Xiang et. al, 2017; Mendez-Barrozo et. al, 2014; Mascaro & Vivoni, 2012). The Albedo (Al) was derived from the bi-hemispherical reflectance(BRDF) (white sky albedo) on the visible bands (Zhou et al. 2003; Lucht et al. 2000) from the version 6 of the MCD43A3 MODIS BRDF daily product.

Vegetation fraction (Vf) was estimated using the Normalized Vegetation Index (NDVI) (Pettorelli, 2005). The NDVI was calculated at a daily time scale from the

MCD43A4 MODIS 500m surface reflectance product. The other dynamic parameters described in Table 6, such as canopy field capacity (S), free throughfall coefficient (p), and optical transmission coefficient (Kt) were estimated based on the 500m MCD15A3H leaf area index (LAI) 4-day composite product. The light extinction coefficient (k) used in the Lambert equation to estimate K_t at the ARm site was 0.62± 0.17 (croplands) and 0.5 ± 0.15 (grasslands) for the Marena site (Zhang et al., 2014). Stomatal resistance (Rs) that is based in LAI and the photosynthetically active radiation (PAR) was estimated in an hourly scale to reproduce the diurnal changes of vegetation. The LAI cloud-free MODIS composites were linearly interpolated to daily and then to hourly values to include smaller changes in vegetation. Then, because PAR is driven by the incoming short wave radiation (IS) that is measured every 30 minutes, it allowed us to average PAR estimations into hourly values and compute stomatal resistance at 1-hour time scale to reproduce the diurnal cycles. In Table 5, the vegetation parameters that are dynamically changing in the model are then p, S, Al, Kt, LAI, Rs and Vf. The others are static vegetation parameters and are calibrated using an automated algorithm (see section 2.3.3). The set of process-based equations used to link MODIS remote sensing data with the vegetation parameters (shown in Table 5) are presented on Table 6. For additional details of this approach, see MendezBarroso et al. (2014).

Table 4. tRIBS soil parameters

P	Description	Units
Ks	Saturated Hydraulic Conductivity	[mm/hr]
θ_s	Soil Moisture at Saturation	[]
θ_r	Residual Soil Moisture	[]
m	Pore distribution index	[]

P	Description	Units
ψ_B	Air Entry Bubbling Pressure	[mm] (negative)
f	Decay parameter	[mm^{-1}]
As	Saturated Anisotropy Ratio	[]
Au	Unsaturated Anisotropy Ratio	[]
n	Porosity	[]
ks	Volumetric Heat Conductivity	[J/msK]
Cs	Soil Heat Capacity	[J/m^3K]

Table 5. tRIBS vegetation static and dynamic (underlined) parameters.

Parameter	Description	Time Scale	Units
P	Free Throughfall Coefficient - Rutter	4-day	[]
S	Canopy Field Capacity - Rutter	4-day	[mm]
K	Drainage Coefficient - Rutter	Static	[mm/hr]
b_2	Drainage Exponential Parameter - Rutter	Static	[mm^{-1}]
Al	Land-Use Albedo	1-day	[]
H	Vegetation height	Static	[m]
Kt	Optical Transmission Coefficient	4-day	[]
R_s	Canopy-average Stomatal Resistance	1-hour	[s/m]
Vf	Vegetation Fraction	1-day	[]
LAI	Canopy Leaf Area Index	4-day	[]
θ^*_s	Stress threshold for Soil Evaporation	Static	[]
θ_s	Stress threshold for Plant Transpiration	Static	[]

Table 6. Physics-based equations used to link remote sensing data with tRIBS vegetation parameters

Parameter	Equation	Remarks
Maximum Canopy Storage(S)	$S = 0.5 * LAI$	Controls rainfall interception as a function of LAI (Pitman 1989)
Free Throughfall Coefficient(p)	$p = e^{-1.5*LAI}$	Fraction of rainfall not captured by plants. (Pitman 1989)
Optical Transmission Coefficient (Kt)	$p = e^{-k*LAI}$	Based on Beer-Lambert law, in which k is the light extinction coefficient. The k value was determined from Zhang, et al.(2014)

Parameter	Equation	Remarks
Minimum stomatal resistance(rs)	$rs = \frac{\left[\frac{Q_{50} + Q}{g_{max} * Q}\right]}{LAI}$	Based on the energy-limited relation by Schulze et al. (1995).
Vegetation Fraction	$Vf = \left[\frac{NDVI - NDVI_{min}}{NDVI_{max} - NDVI_{min}}\right]^2$	Based on (Carson and Ripley 1997). Vegetation fraction carries out transpiration in the model (MendezBarroso et al. 2014).

2.3.3. Model Calibration

Model calibration was conducted for the soil and static vegetation parameters described in section 2.3.2 since another set of vegetation parameters were inferred from the remotely-sensed information that fed the equations presented in Table 6. A One-At-a Time (OAT) sensitivity analysis was initially used to determine the most important parameters for each simulation condition (Moreno, Vivoni, & Gochis, 2016); after this, the Shuffled Complex Evolution (SCE) algorithm was applied as an optimization method to achieve automatic calibration (Duan et al. 1993). The comparisons of observed and simulated values of soil moisture and temperature, and energy balance components were based on the Mean Absolute Error (MAE), Correlation Coefficient (CC), bias, and Nash-Sutcliffe model efficiency coefficient (NS). The SCE determined the best set of parameters after an approximately of 15,000 iterations of the model. The objective function was calculated based on the statistical assessment of each of the runs performed by the SCE, comparing the RN, LE, H, G, and soil moisture and soil temperature at the

root zone and shallow layers' estimations with simultaneous observations at each of the two ECTs.

The sites selected for tRIBS model calibration were the US-ARm and the Marena.

The US-Arm site was chosen based on the data quality and continuity, being the site with the longer and most complete time series over Oklahoma available in Ameriflux. The Marena site was selected because of the high availability of soil moisture sensors for being a testbed site for satellite validation. However, the site has several gaps in the weather forcing variables, representing a continuity issue for the model parametrization that can be fixed using Mesonet data. Furthermore, the US-ARm site serves for the validation stage 3 of some of the MODIS products and Marena is used to validate SMAP. The input data time scale for both sites was standardized into hourly averages or sums (in the case of P) and the model outputs were continuous and at a 1-hour temporal resolution.

The calibration for the US-ARm site was for a hydrologic year from 05/09/2004/06:00 to 06/29/2005/22:00; the 200 hours previous the calibration period starting in 04/30/2004/23:00 represent the model spin-up period. The total calibration period had 10,000 hours. The time period was selected based on the low amount of gaps and that among the available data (2002-2012), this time frame did not show precipitation anomaly compared with the other years. The calibrated output variables were LE (actual ET), H, G, NR and ST.

The Marena (MOISST) site was calibrated from 12/09/2013/07:00 to 09/10/2014/11:00 with the first 200 hours starting in 12/12/2013/00:00 representing the model spin-up period and the total calibration period having 7,300 hours. The selected time interval was based on the quantity and quality of available data, being this period

the second one with less data gaps; the period with less gaps was used for the validation. The atmospheric forcing data were obtained from the Oklahoma Mesonet site at Marena. The calibrated output variables were LE, H, G, NR and ST and SM at the surface and the root-zones. Since the model simulations were conducted at the footprint scale, the soil parameters were constant over the time to avoid an over-parametrization (Ivanov et. al, 2008.; Ivanov, 2002). The set of soil parameters and the ranges used during the calibration were found in similar studies (Ivanov et. al, 2008; Xiang et. al, 2014; Ivanov, et al. 2004; MendezBarroso, et al. 2014), and through the use of soil pedo-transfer functions based on bulk density, and particle fractions proposed in Campbell & Norman (1998) and Rawls et. al (1982). The vegetation parameters for the calibration at each site were obtained following the information described in section 2.3.2.

2.3.4. Model Validation

A model validation was performed at each of the calibration sites for a different time period than the one used in the calibration. During the validation process, the atmospheric and dynamic vegetation parameters (that depend upon site and remote sensing data) are the only elements to be changed. Normally, the atmospheric forcing can be found from a standard meteorological station and the satellite data are globally available. The US-ARm site was validated for a total of 8,780 hours for the period 07/01/2008/0:00 to 07/01/2009/20:00. This time period was selected for the low number of gaps in the observation dataset from Fluxnet. The output variables were the same as

the corresponding to the calibration process. The Marena site was validated for a 10,000 hours' timestamp period between 11/09/2015/07:00 to 29/12/2016/23:00, time frame with the more complete dataset. The atmospheric forcing data were obtained from the Oklahoma Mesonet site at Marena (Mare). The validation metrics to assess the model performance were the CC, RMSE, bias, and NS.

2.3.5. Best Subsets Analysis and Contribution of Dynamic Vegetation

This section aims to evaluate the contribution of the model forcing, soil moisture, soil temperature, and vegetation parameters in the estimation of the SEB components, helping us to analyze the impacts of precipitation, soil moisture, vegetation activity and surface temperature on the SEB partitioning at each of the test environments. The analysis was based on a variance contribution quantification conducted for variable arrays containing some of the SEB components and other independent variables such meteorological (P, IS, RH, WS), soil moisture and temperature (SSM and RSM), and the vegetation activity changes represented in the dynamic parameters (Al, Vf, Sr, Kt) described in section 2.3.2.

The best subset method includes all measured predictors into multiple linear combinations to find a subset that explains the highest percent of the variance in the predictands. Best subsets (Heinze et al.2018; Olejnik et al. 2010) is a technique that relies on exhaustive searches for the best groups of the variables using an efficient branch-and-bound algorithm. The procedure fits 2^P (i.e. 16) models, where P=4 is the number of

predictors in the dataset and might vary between different studies. The Akaike information criterion (AIC; Akaike, 1973) and the coefficient of determination (R^2) facilitated model selection by providing an estimator of the relative quality of statistical models for a given set of data.

Finally, in order to characterize the influence of dynamic vegetation in the SEB were run simulations with non-changing vegetation for each of the sites. The tRIBS parameter sets obtained in the calibration at the US-ARm and Marena were used to run a scenario of static vegetation (with average annual parameter values) and compared with the results obtained by using dynamic vegetation parameters for each site. Further, ET partitioning results were compared for both cases illustrating how these changes affect the proportion of contribution to ET from E and T.

2.3.6. Model Transferability

The final stage of this research focused on assessing the tRIBS model performance in sites where no calibration had been conducted. tRIBS was tested at two additional ECTs of the U.S. Southern Plains, with the goal of evaluating parameter transferability and potential use of the model to provide real-time estimations of SEF, soil moisture and soil temperature over similar environments including the area covered by the Mesonet network. The model transferability assessment thus depends on the set of meteorological forcing and dynamic vegetation parameters at each location, using the set of soil parameters and static conditions of vegetation obtained during the calibration at the initial ECTs. Thus, calibration or re-calibration is not performed or considered at this stage.

The transferability test over crops evaluated the model at the US-A74 ECT, also known as the ARm Milo field. The transferability test of Marena was performed at the US-A32 tower, known as the ARm hay pasture site. The results from this section provided an initial assessment of the model's capacity for operating as a complementary tool for soil moisture, soil temperature, ET and SEF estimations at standard weather stations that measure the forcing data needed to parametrize the model. The time period for the transferability test was determined based on the data availability and continuity. The transferability test was conducted at US-A32 and US-A74 between 01/2016 and 06/2017. The same assessment metrics that compare simulations and observations, namely CC, bias, RMSE and NS were used to evaluate tRIBS model performance during this stage.

3. Results

3.1 Calibration Results

3.1.1 US-ARm

Figure 6 illustrates time series of the atmospheric forcing variables for the calibration period (i.e. Jul 2004 to Jul 2005) at US-ARm. These time series illustrate the clear seasonal variability of incoming short wave radiation and temperature while precipitation, relative humidity and wind speed seemed less influenced by seasonality. Furthermore, similarities are observed between relative humidity and wind speed that appear to be related to the diurnal cycle. The highest rates of incoming energy occur during the summer months of June and July and the lowest values during the winter period, as dictated by both solar declination and seasonal cloud cover. Furthermore,

during this period precipitation has its highest values in July and August 2004. Figure 7 illustrates the seven dynamic vegetation parameters also used during the tRIBS model calibration at US-ARm. Evidently, the onset of vegetation greening in early Spring significantly affects the representation of the vegetation parameters in the model. For example, vegetation fraction (Vf) increases from 0.0 to 0.2 in March 2005 and then rises to 0.6 during May 2005, resulting in a positive gradient growth that has peaks during the summer months. Vf shows a strong seasonal behavior, where the Fall season is characterized by a strong negative slope and followed by a Winter season of low vegetation activity. The abrupt decline of Vf can be related to the end of the harvest season and the peaks in the summer time to the maximum biomass productivity period. Furthermore, albedo (Al) and Leaf Area Index (LAI) have a similar behavior particularly during Winter and Spring. LAI and Vf do not show a similar seasonal pattern since vegetation cover and activity might not necessarily be entirely linked. Finally, as interception throughfall coefficient (p), optical transmission coefficient (Kt), and stomatal resistance (Rs) are inversely-related to LAI, they display a strong seasonal correlation with this variable with higher values during the Winter and lower during the Summer season.

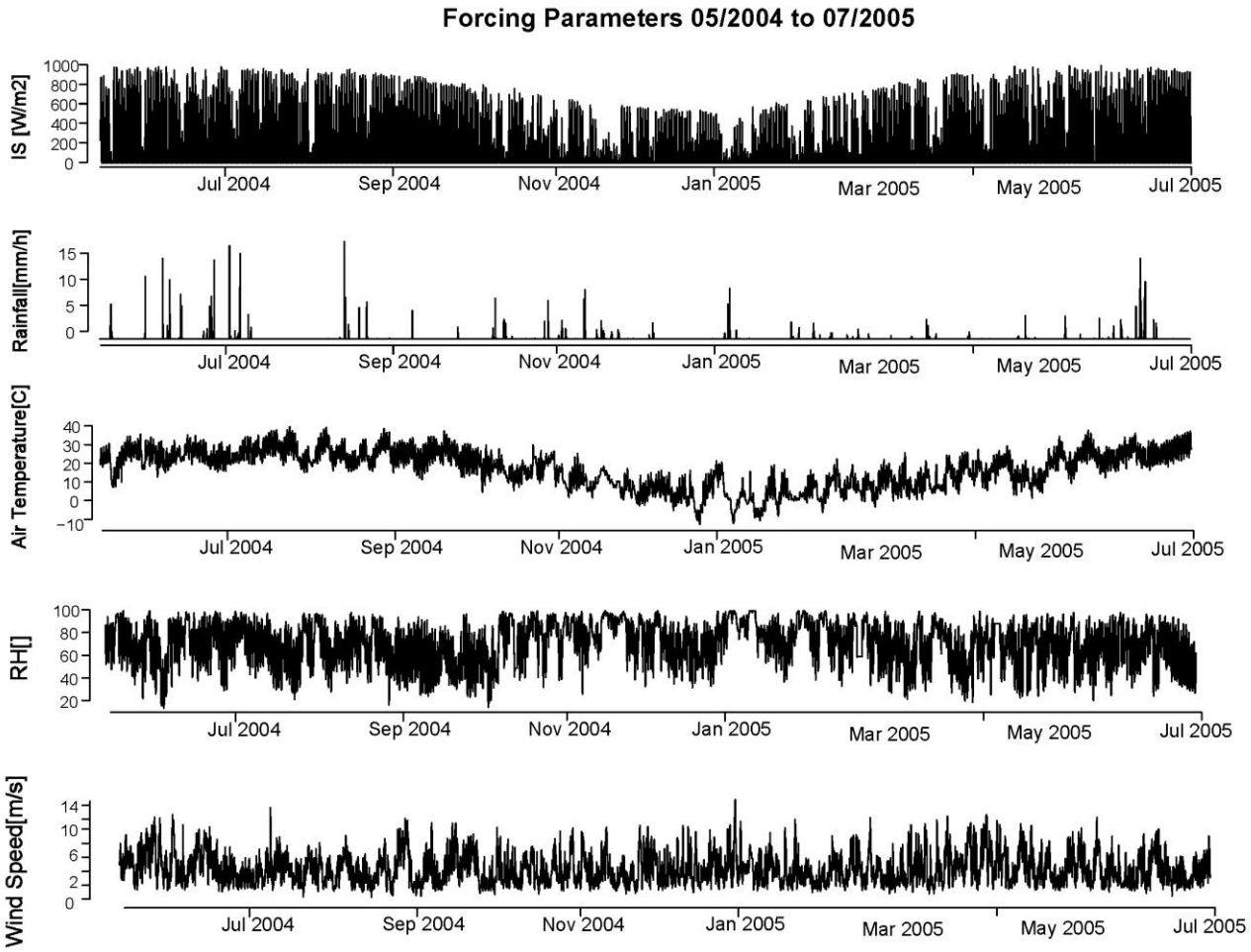

Figure 6. ARm observed atmospheric forcing for model calibration. From the top down the time series correspond to incoming solar radiation (IS, W/m^2), precipitation (P, mm/h), air temperature (T, °C), relative humidity (RH, %) and wind speed (WS, m/s).

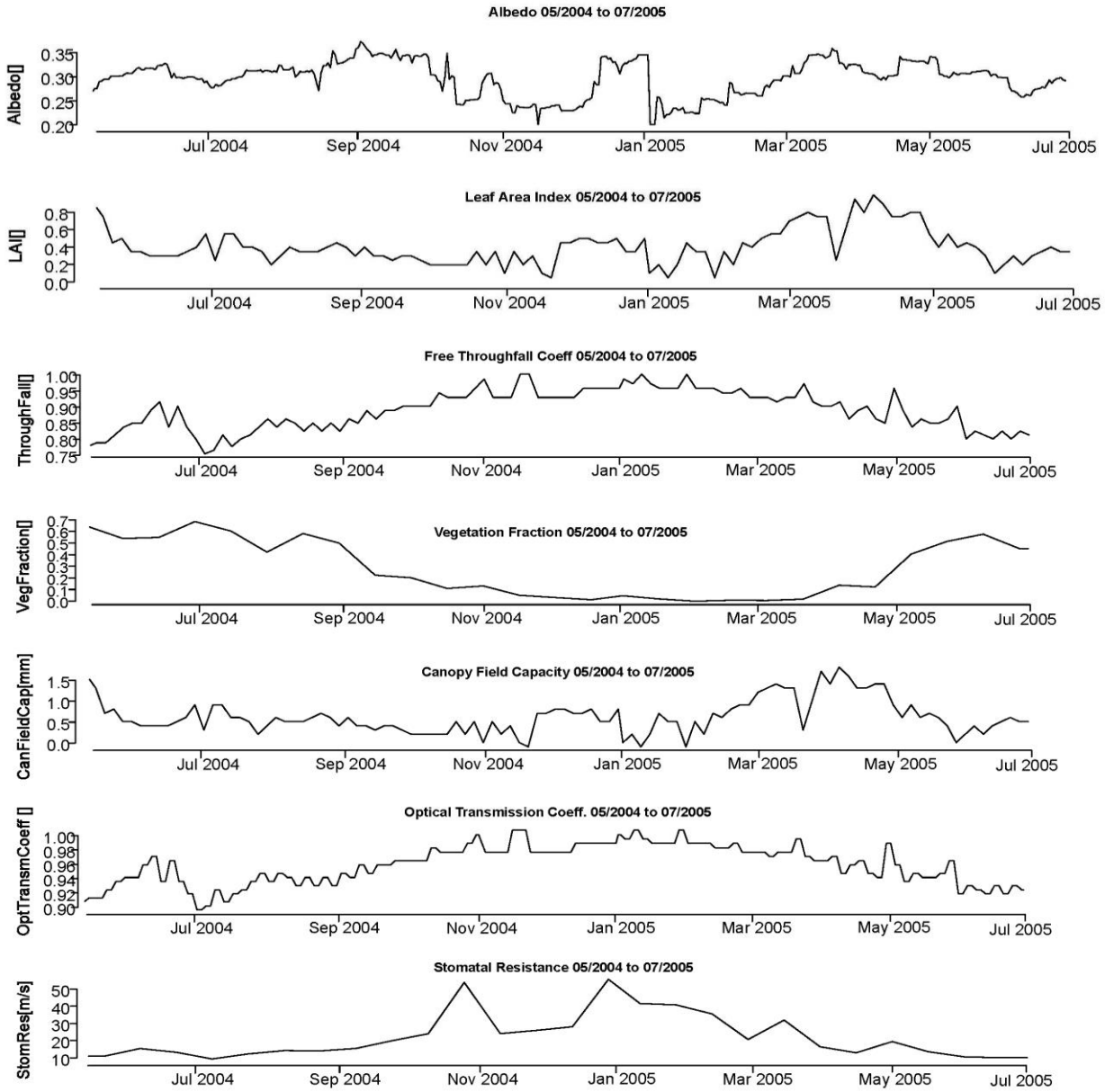

Figure 7. Remotely-sensed derived vegetation parameters for tRIBS model calibration at US-Arm. From the top down, the time series correspond to the albedo (Al), Leaf Area Index (LAI), throughfall coefficient (s), vegetation fraction (Vf), canopy field capacity (p), optical transmission coefficient (Kt) and plant stomatal resistance (Rs)

The OAT results for US-ARm are shown in the Appendix A. Pore-size distribution index (m), soil heat capacity (Cs) and saturated hydraulic conductivity (Ks) are the parameters that mostly influence the simulations. Some studies have lighted the importance of these parameters in the infiltration and water exchange processes (S. Assouline, 2006; Alvenäs, et. al 1997). For the automated calibration, 10,000 iterations led to high CC between simulated and observed values with asymptotic increases of only $1\text{-}E^{-6}$ % to $1\text{-}E^{-7}$%. The use of the correlation coefficient helped to normalize the assessment of the six simulation variables, constraining the simulation results to the objective function established on the SCE. Table 7 shows the final calibrated parameters using the SCE at US-Arm.

Table 7. tRIBS soil and static vegetation (underlined) parameter calibration results at US-ARm. The initial ground water table is also shown. The soil type at US-Arm is silty clay loam.

Parameter	**Optimal value**	**Units**
$\mathbf{K_s}$	21.84	[mm/hr]
$\boldsymbol{\theta_s}$	0.552	[]
$\boldsymbol{\theta_r}$	0.017	[]
m	0.57	[]
$\boldsymbol{\Psi_b}$	-0.373	[mm] (negative)
f	5.00E-07	[mm^{-1}]
As	1.109	[]
Au	1.109	[]
n	0.431	[]
Ks	0.989	[J/msK]
$\mathbf{C_s}$	1061340	[J/m^3K]
$\underline{\mathbf{K}}$	0.2911	[mm/hr]
$\underline{\mathbf{B_2}}$	3.209	[mm^{-1}]
$\underline{\mathbf{H}}$	0.2953	[m]
$\underline{\theta^*_s}$	0.55	[]
$\underline{\theta_s}$	0.1792	[]
Water Table	19460	[mm]

tRIBS model calibration results are presented below using density scatter plots (Figure 8), time series of hourly values during the entire simulation period (Figure 9) and an example summer month comparison (Figure 10) between simulated and observed values. Additionally, simulation statistics describing each calibrated output variable are shown on Table 8.

The density scatterplots in Figure 8 show NS values all above 0.5, except for G, which suggest a model with sufficient quality for the majority of simulated variables. Criss & Winston, 2008 suggests that a NS value of 1 indicates a perfect agreement between the model and the observation to a value of minus infinity, but negative values do not necessary indicates that the model's performance is extremely poor. For G, due errors in the model scheme to parameterize the heat transfer to the soil and perhaps observation uncertainties derived from heat flux plate calibration and technology could explain the lower than 0.5 NS. However, NS>0 still represents that the model outputs are better estimators than the historic mean. For the case of LE, despite both CC (>0.75) and NS (>0.5) are satisfactory, the model shows the best accuracy for the low to mid LE values (<100 W/m^2) but slightly biased for high values (>350 W/m^2) where the model tends to overestimate. Analogously, soil surface temperature illustrates that, despite the general simulation skill of the model, low and high values have the largest biases above and below the observed values.

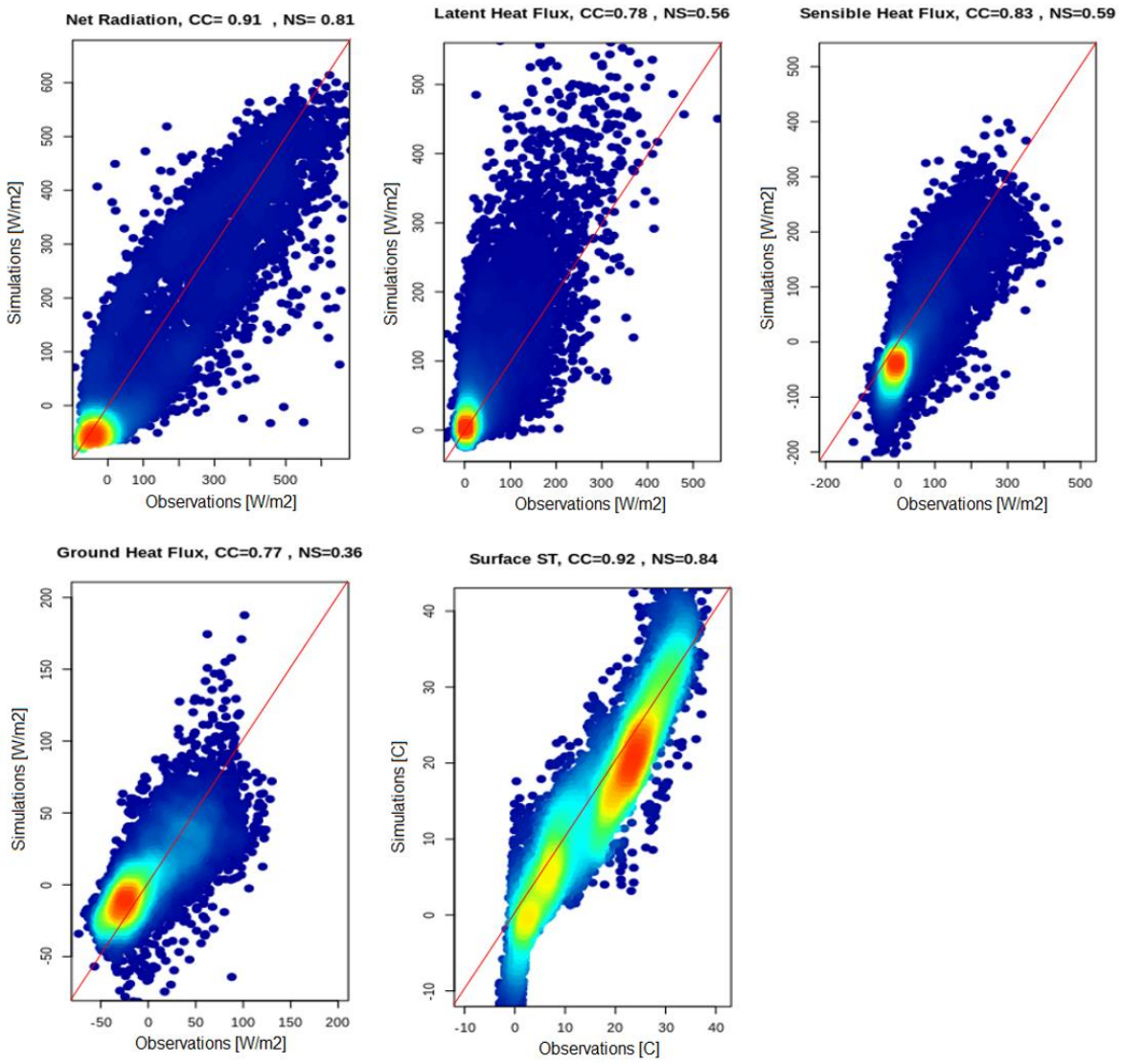

Figure 8. Density scatterplots of the calibration results at US-ARm. In all panels the x-axis represents the observed and the y-axis the simulated values.

Table 8. US-ARm calibration metrics for each of the output variables respect to observed values. Net radiation (NR, W/m^2), latent heat flux (LE, W/m^2), sensible heat flux (H, W/m^2), ground heat flux (G, W/m^2), and soil surface temperature (SST, °C).

Variable→	**NR(W/m^2)**	**LE(W/m^2)**	**H(W/m^2)**	**G(W/m^2)**	**SST(C)**
CC	0.91	0.78	0.83	0.77	0.92
BIAS	0.24	-0.36	-8.99	-8.76	0.08
RMSE	77.55	66.64	60.54	22.13	4.57
NS	0.81	0.56	0.59	0.36	0.84

The simulation results of the calibration process displayed on Figure 9 illustrate that the model shows ability to represent the temporal responses and general range variability and seasonality of all calibrated variables as visually the simulations (red) and observations (black) lines exhibit a tied behavior, which is supported with statics displayed on table 8.

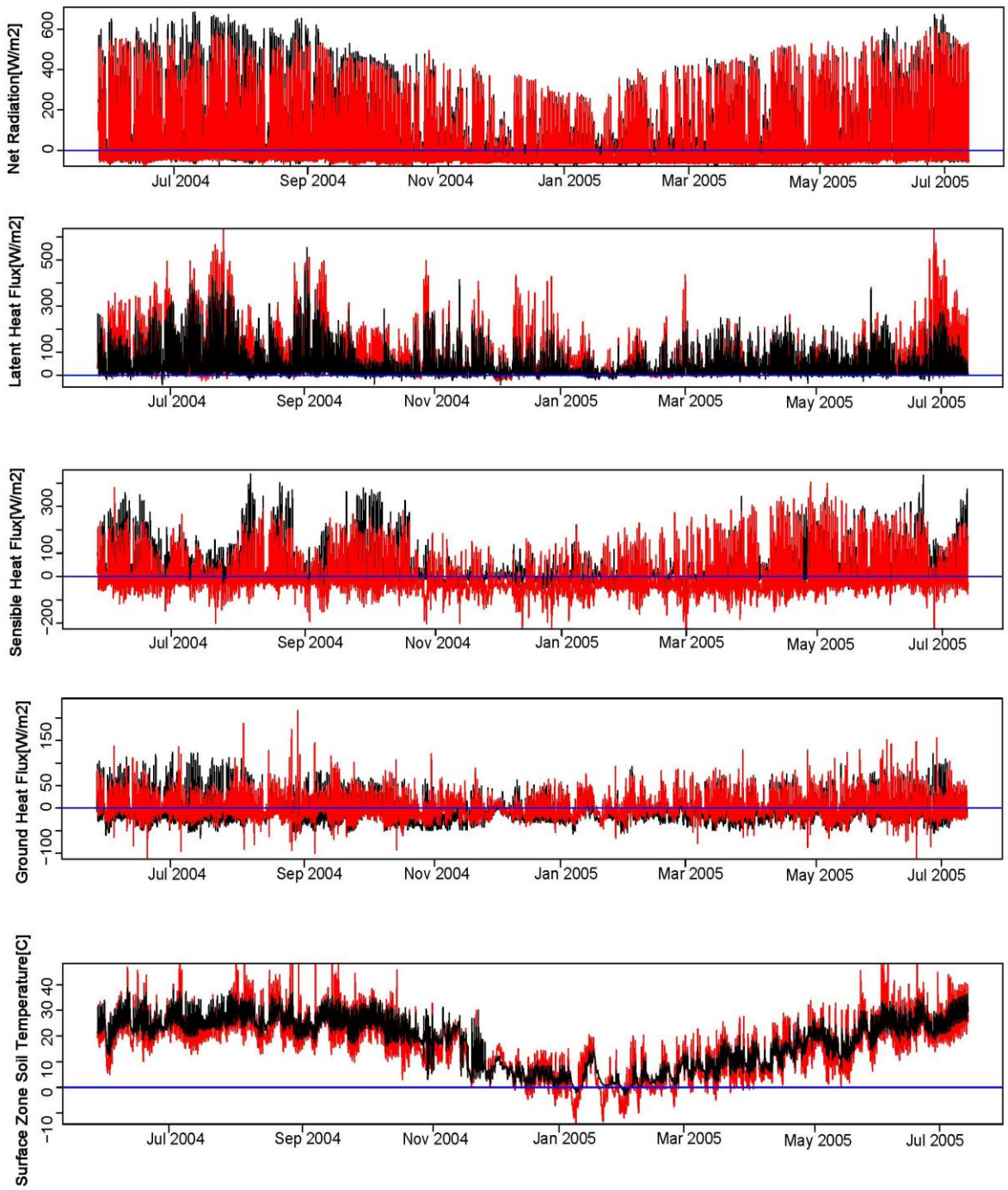

Figure 9. US-ARm calibration time series results. Red and black lines represent simulated and observed values respectively. From top down the variables are net radiation (NR, W/m^2), latent heat flux (LE, W/m^2), sensible heat flux (H, W/m^2), ground heat flux (G, W/m^2), and soil surface temperature (SST, °C).

To gather a detailed view of the model value at simulating the diurnal cycles of the variables of interest, Figure 10 illustrates these values during the month of June of 2004. From Figure 10 it can observed that the model physics captures the diurnal cycle of the radiative forcing and the responses to the precipitation inputs. The results showed that even soil moisture model's predictions follow the general trend of the existent observations during this month. The netradiation is well represented by the model that is capturing the high values (>400 W/m^2) and the low values. LE is well simulated CC (0.86) and NS (0.70), but during the moments of the day with higher latent heat flux the model has a small systematic overestimation. Finally, G displays the higher limitation for the model that is generally underestimating it.

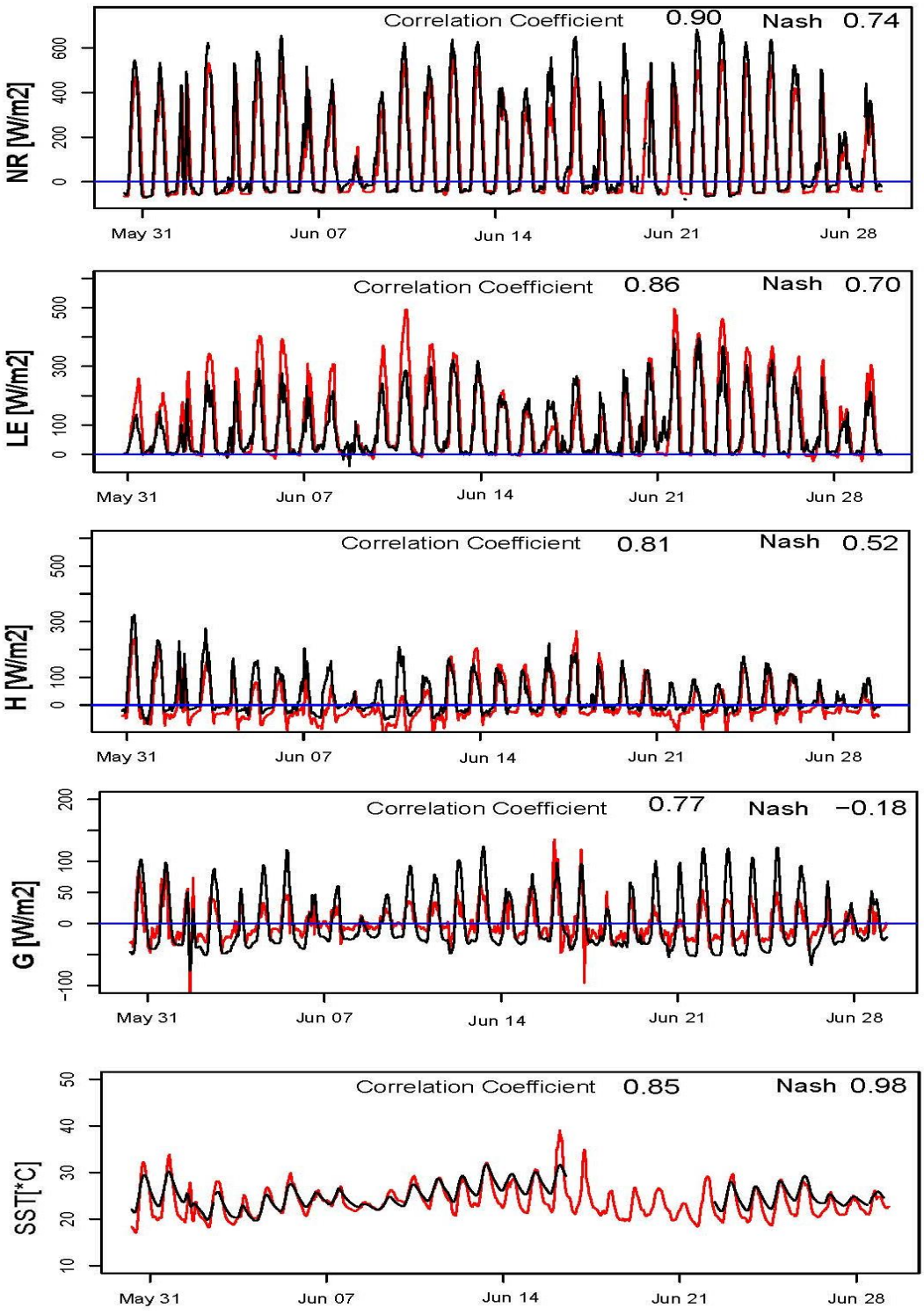

Figure 10. US-ARm calibration results during the month of June, 2004. Red and black lines represent simulated and observed values. From the top down, the output variables are: net radiation (NR), latent heat flux (LE), sensible heat flux (H), ground heat flux (G), and soil surface temperature (SST).

Despite surface soil moisture was not directly calibrated because there were many gaps and inconsistencies with the data series, the Figure 11 presents results for this variable against the observed data. The soil moisture was excluded from the calibration, due a lack of quality of observations. However, the good performance of the model at simulating SEB components could support the use of tRIBS for filling the gaps in observations of this variable. Figure 11 shows the precipitation on top, driving the soil moisture responses of the model (red line). However, besides the evident amount of gaps in the observations (black line) the precipitation events are not well captured by the sensor.

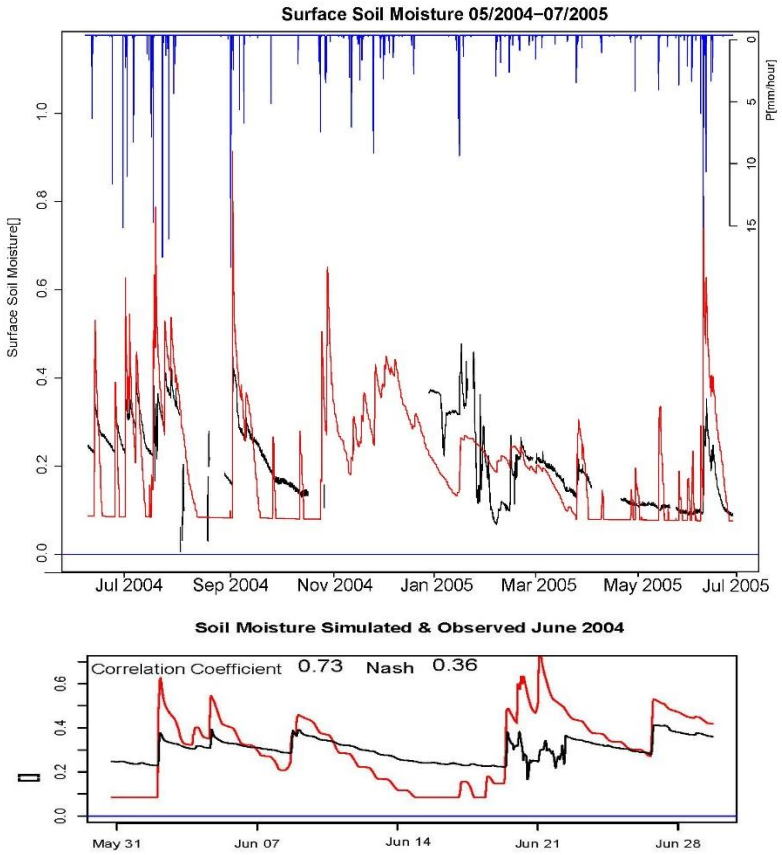

Figure 11. US-ARm results for the surface soil moisture simulations (SSM) during the calibration period in the figure at top. The blue lines on the top represent precipitation values. Red and black lines represent simulated and observed values, respectively. Results during the month of June, 2004 are shown at the bottom.

3.1.2 Marena (MOISST)

Figure 12 illustrates the times series of the atmospheric forcing variables for the calibration period (i.e. December 2013 to October 2014) at Marena. Analogously to US-ARm, these time series help us to visualize the seasonal variability of incoming short wave radiation and temperature while precipitation, relative humidity, and wind speed seemed less influenced by seasonality. Then again, the relative humidity and wind speed exhibit variability control from the diurnal scale. Furthermore, incoming shortwave radiation had the highest values between late Spring and early Summer seasons, and then

its range of values has less variability. Relative humidity and air temperature show high variability during the first part of the year, and during the second half of the year, there were narrower ranges but persistent high values. Wind speed presents high variability during the first part of the year, but lower, less variable values occur during the second half. Finally, the highest peaks in precipitation occur during the summer period. The onset of vegetation greening in April starts driving some changes in the dynamic vegetation parameters and, consequently, in the model variable representations. Vf and LAI have a similar behavior to air temperature with lowest values between January and April. On the other hand, the free throughfall coefficient and stomatal resistance behavior is inversely-related to the vegetation fraction. It is essential to highlight that during the active precipitation window in June 2014, the albedo value had an evident decrease that can be explained by the influence of the soil water content and the reflectance of ponded areas, affecting the albedo value directly and decreasing it from 0.30 to 0.24. Finally, optical transmission coefficient (Kt) and stomatal resistance (Rs) are inversely-related to Vf, they display a strong seasonal correlation with this variable with higher values between January and April.

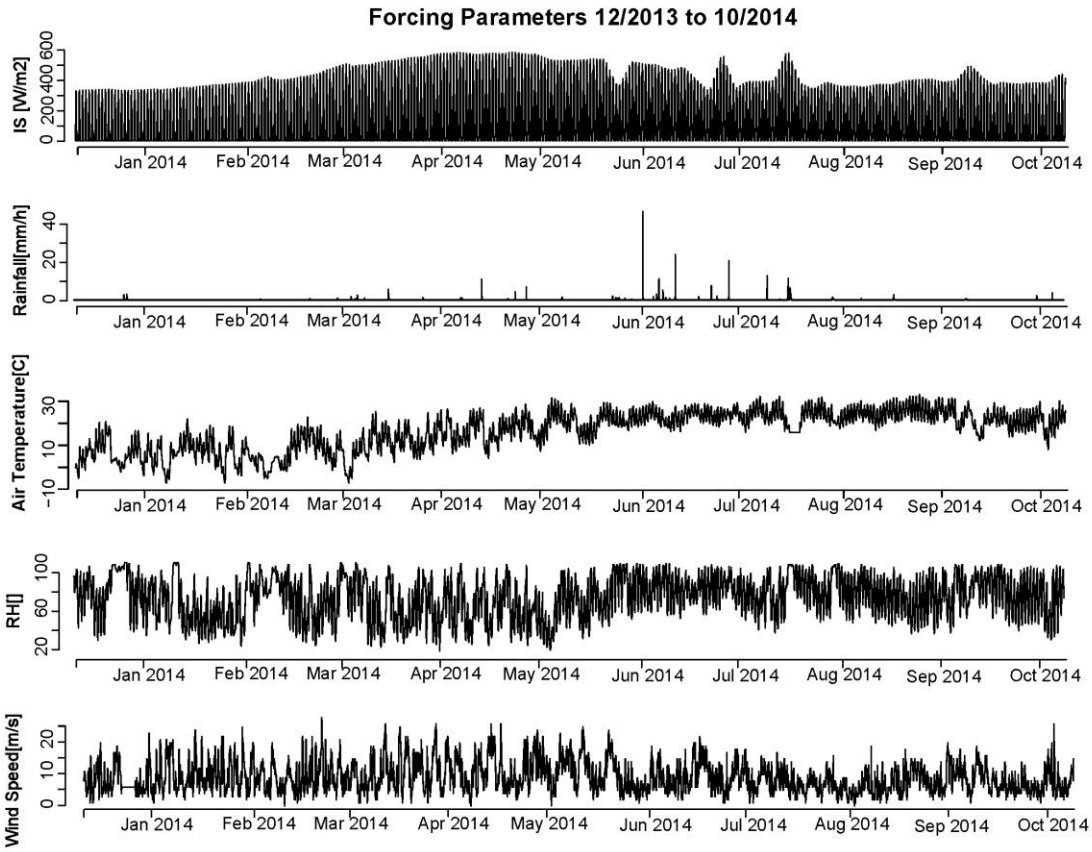

Figure 12. Marena observed atmospheric forcing for model calibration. From the top down the time series correspond to incoming solar radiation (IS, W/m^2), precipitation (P, mm/h), air temperature (T, °C), relative humidity (RH, %) and wind speed (WS, m/s).

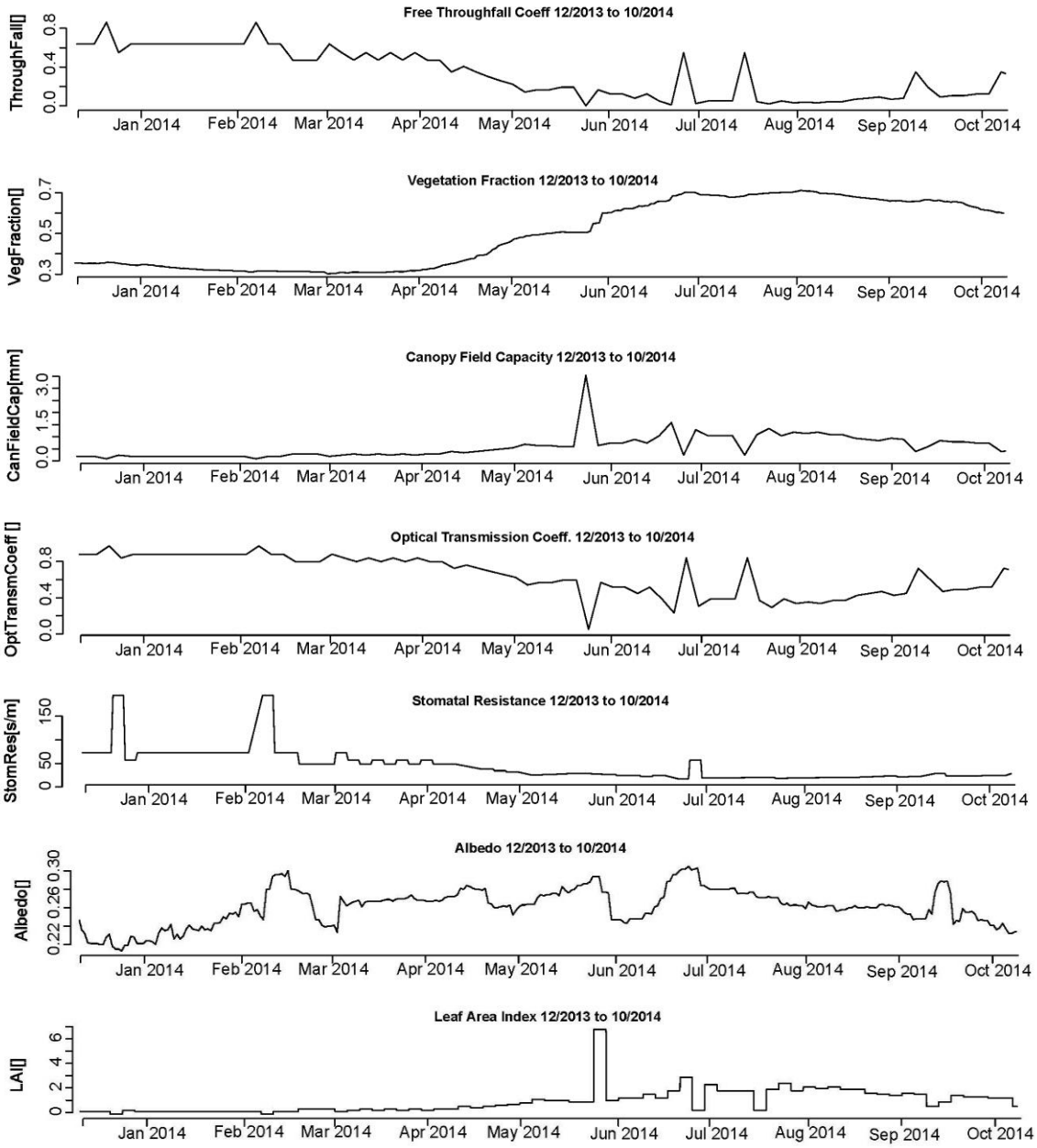

Figure 13. Remotely-sensed derived vegetation parameters for tRIBS model calibration at Marena. From the top down, the time series correspond to the albedo (Al), Leaf Area Index (LAI), throughfall coefficient (s), vegetation fraction (Vf), canopy field capacity (p), optical transmission coefficient (Kt) and plant stomatal resistance (Rs)

The OAT results of Marena's calibration are displayed in Appendix B. The air bubbling pressure (Ψ_b), decay parameter (f), pore-size distribution index (m), soil heat

capacity (Cs), and saturated hydraulic conductivity (Ks) are the parameters that mostly influenced the simulations. Further, after 12,000 iterations of the SCE, there were no improvements in the simulation results. Table 9 presents the best set of soil parameters obtained after model calibration at this location. Also, it is necessary to highlight that during the automated calibration procedure, the residual soil water content, pore distribution index, and depth to water table were found to be the parameters that most significantly impact the soil moisture variable. The parameter values in Table 9 are similar to the ones proposed by literature but these ones, because they were obtained through dynamic vegetation simulations, have an added value for this region of the Southern Plains.

Table 9. tRIBS soil and static vegetation (underlined) parameter calibration results at Marena. The initial ground water table is also shown. The soil type at Marena is loam clay.

Parameter	**Optimal value**	**Units**
$\mathbf{K_s}$	4.85	[mm/hr]
$\boldsymbol{\theta}_s$	0.61	[]
$\boldsymbol{\theta_r}$	0.11	[]
m	0.52	[]
$\boldsymbol{\Psi_b}$	-99.2	[mm] (negative)
f	0.07	[mm^{-1}]
As	388	[]
Au	388	[]
n	0.51	[]
Ks	1.6	[J/msK]
$\mathbf{C_s}$	1383	[J/m^3K]
$\underline{\mathbf{K}}$	0.2911	[mm/hr]
$\underline{\mathbf{B_2}}$	3.5272	[mm^{-1}]
$\underline{\mathbf{H}}$	0.4476	[m]
$\underline{\theta^*_s}$	0.1577	[]
$\underline{\theta_s}$	0.4939	[]
Water Table	7847	[mm]

tRIBS model calibration results are presented below using density scatter plots (Figure 14), time series of hourly values during the entire simulation period (Figure 15) and an example summer month comparison (Figure 16) between simulated and observed values. Additionally, simulation statistics describing each calibrated output variable are shown in Table 10.

The density scatterplots in Figure 14 show NS values all above 0.5, except by surface soil moisture, indicating a model with satisfactory quality. There was presence of snow during few winter days at the site. For SSM, errors associated with the snow module in the model scheme that was inactive to parameterize and calibrate the site could explain the lower than 0.5 NS. However, NS>0 still represents that the model outputs are better estimators than the historical mean, and the model still scoring an adequate NS=0.20. Soil temperature is better represented at the root zone layer than at the surface layer. Nonetheless, observing the density scatter plots and time series, it is easy to identify that despite the gains in simulation skill, tRIBS is underestimating the SST during low temperature days. This again is related to the failure to account for snow processes during the winter season. On the other hand, the best estimations of soil moisture occur at the root zone level. Table 10 presents the statistic assessment of the simulations, where the latent heat flux is the energy component with the smaller RMSE. Such results allow us to identify the strengths of the model representing the variables, but also recognize some of its limitations in the accuracy at simulating the targeted variables.

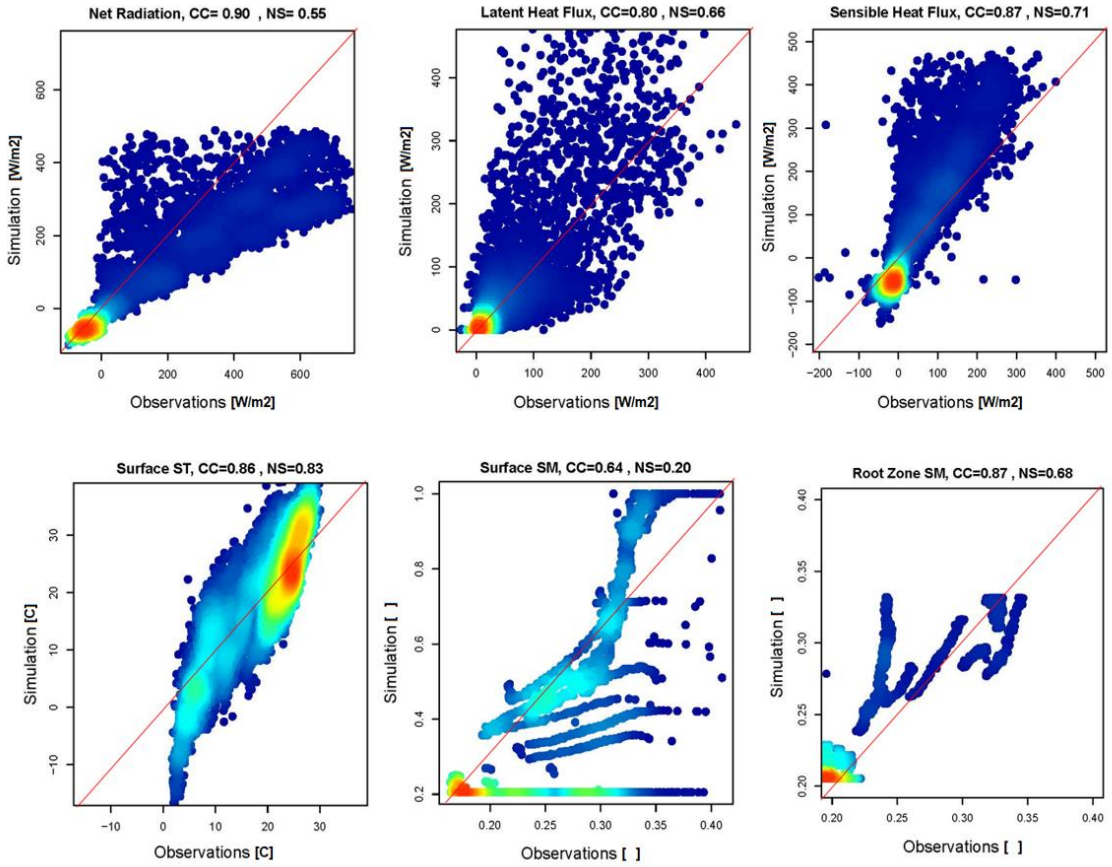

Figure 14. Density scatterplots of the calibration results at Marena. In all panels the x-axis represents the observed and the y-axis the simulated values.

Table 10. Marena calibration result's statistics. Net radiation (NR), latent heat flux (LE), sensible heat flux (H), soil surface temperature (SST), shallow soil surface soil moisture (SSM), and soil root zone soil moisture (RSM).

Variable→	**NR(W/m^2)**	**LE(W/m^2)**	**H(W/m^2)**	**SST**	**SSM**	**RSM**
CC	0.9	0.81	0.87	0.86	0.64	0.87
BIAS	0.68	1.54	-0.35	-0.02	-0.26	-0.05
RMSE	126.20	63.77	85.43	5.79	0.193	0.0229
NS	0.55	0.66	0.71	0.83	0.20	0.68

The simulation results displayed in figures 15 and 16 indicate that the model is capturing the surface energy partitioning, soil temperature, and soil moisture seasonal responses well as it is supported visually and with the statistical results of table10, where all the variables have correlation coefficients over 0.80 and NS results higher than 0.55 with the exception of surface soil moisture.

For the case of the surface soil moisture (variables with the lowest skill scores) the discrepancies between the model and observations are the highest. The soil moisture time series expresses more sensitivity to precipitation events, but changes seem more abrupt that the small progressive changes of the observations.

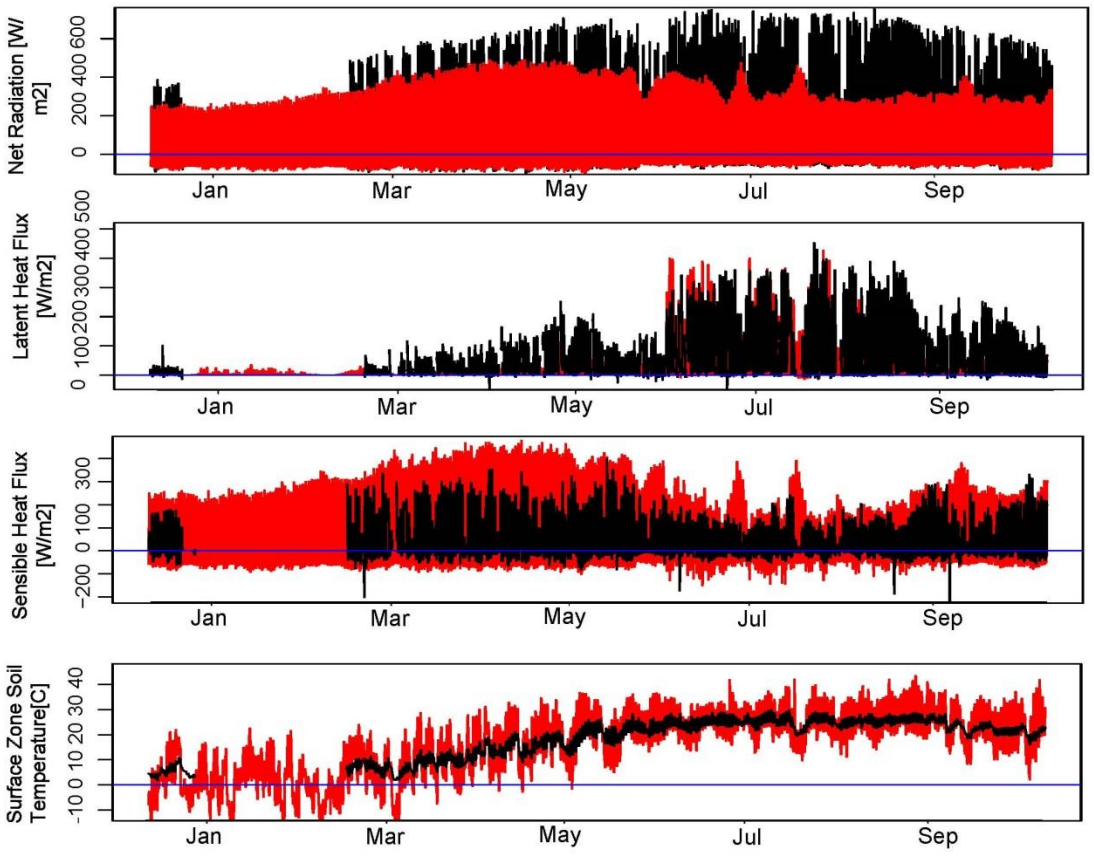

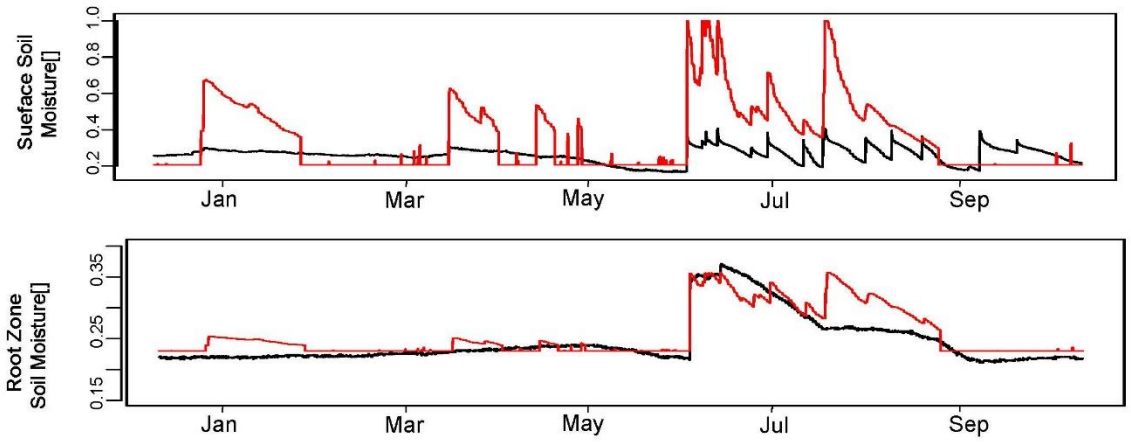

Figure 15. Marena calibration time series results. Red and black lines represent simulated and observed values respectively. From top down the variables are net radiation (NR), latent heat flux (LE), sensible heat flux (H), soil surface temperature (SST), shallow soil surface soil moisture (SSM), and soil root zone soil moisture (RSM).

The performance of tRIBS representing the diurnal cycle for the different variables is presented in Figure 16. Despite underestimations of NR, the model simulates well the root zone soil moisture during August (CC=0.94 NASH = 0.39) as n indication of the skill at capturing the precipitation pulses. The monthly time series displayed in figure 16 show the capability of tRIBS to represent the transient responses and to capture the diurnal cycle. The sensible heat flux is the best represented, followed by latent heat flux. However, soil surface temperature observations do not reflect the expected variability of the diurnal cycle, instead it shows a stronger sensibility and higher variability. Finally, the soil moisture observations at the root zone exhibit minimum variation, while the root zone and shallow soil moisture simulations keep a similar behavior between them.

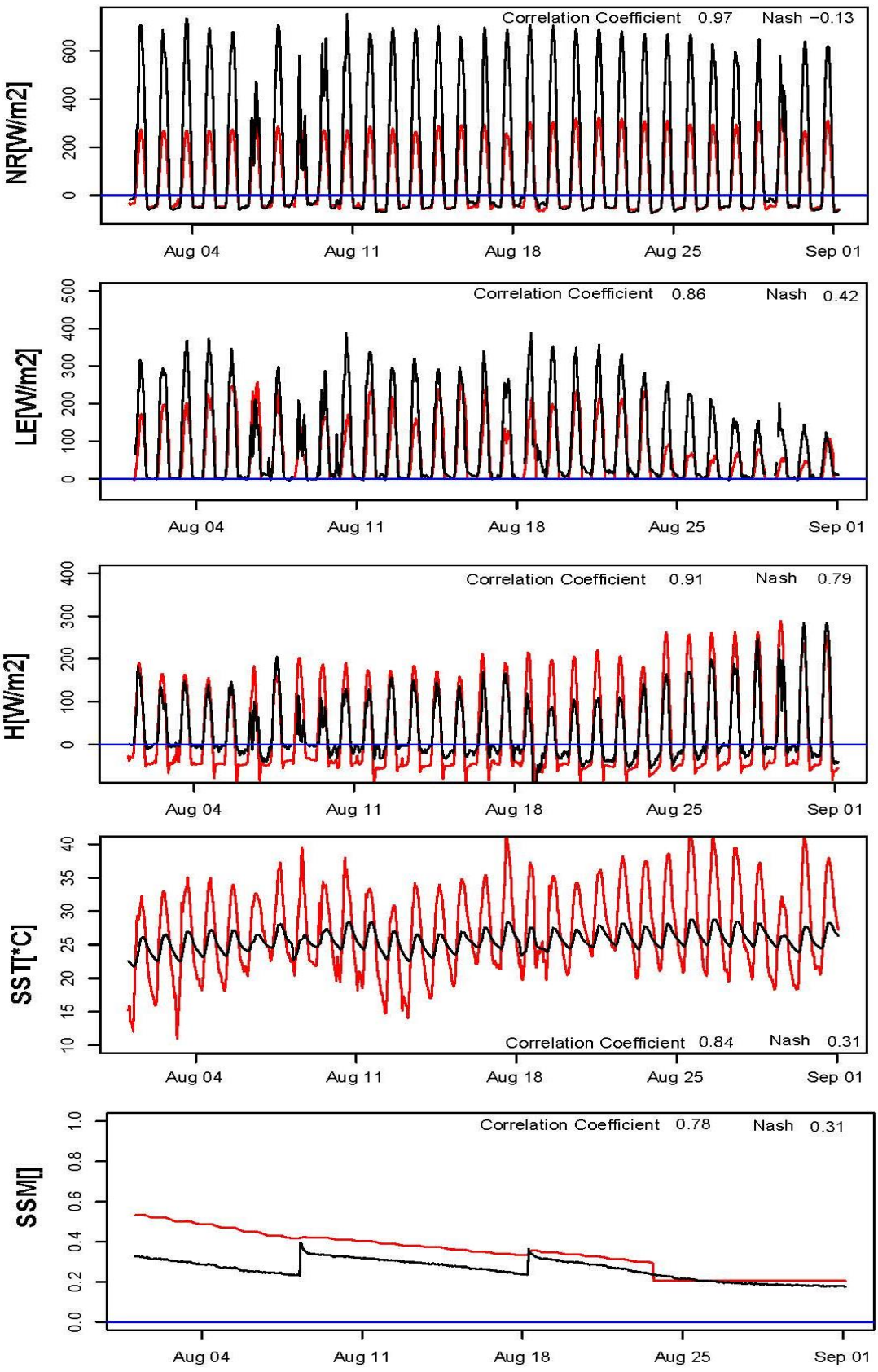
Correlation Coefficient 0.97 Nash −0.13
NR[W/m2]
0
200
400
600
Aug 04
Aug 11
Aug 18
Aug 25
Sep 01
Correlation Coefficient 0.86 Nash 0.42
LE[W/m2]
0
100
200
300
400
500
Aug 04
Aug 11
Aug 18
Aug 25
Sep 01
Correlation Coefficient 0.91 Nash 0.79
H[W/m2]
0
100
200
300
400
Aug 04
Aug 11
Aug 18
Aug 25
Sep 01
Correlation Coefficient 0.84 Nash 0.31
SST[*C]
10
15
20
25
30
35
40
Aug 04
Aug 11
Aug 18
Aug 25
Sep 01
Correlation Coefficient 0.78 Nash 0.31
SSM[]
0.0
0.2
0.4
0.6
0.8
1.0
Aug 04
Aug 11
Aug 18
Aug 25
Sep 01

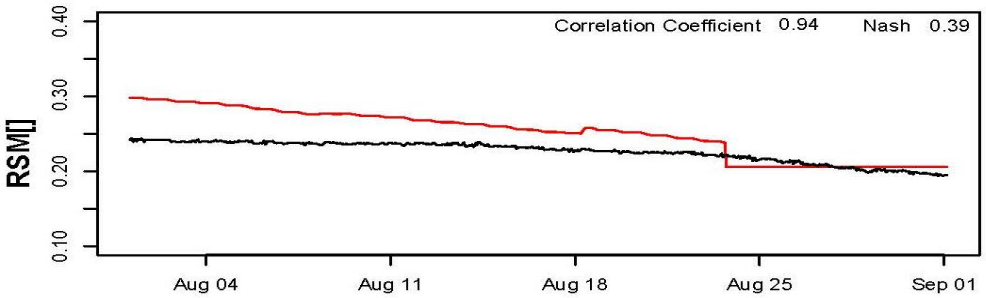

Figure 16. Marena calibration results during the month of August, 2014. Red and black lines represent simulated and observed values. From the top down, the output variables are: net radiation (NR), latent heat flux (LE), sensible heat flux (H), soil surface temperature (SST), surface soil moisture (SSM), and root soil moisture (RSM).

3.2 Validation Results

3.2.1 US-ARm

The time series of atmospheric forcing and vegetation parameters of the model for the validation period (July 2008 to July 2009) at the US-ARm site are displayed in Figures 17 and 18. These time series help us to visualize the seasonal variability of the model inputs. Similar to the calibration period, IS has a typical seasonal behavior, with the peak values in July and lowest in December. Air temperatures are maximum during the summer and minimum during the wintertime. In contrast, wind speed and relative humidity do not seem to have consistent seasonal patterns and exhibit sturdier diurnal patterns. Vegetation fraction (Vf) reflects the effect of the greening onset since late April. For example, the vegetation fraction (Vf) increases from 0 to 0.15 in March 2008 and then rises to 0.4 during April, resulting in a high positive growth gradient that peaks during the summer months.

Vf is based on the maximum and minimum NDVI values, and LAI's algorithm uses red and NIR bands that as it happens with the NDVI. This relation explains some of

the similarities with the Vf and LAI patterns. The stomatal resistance, optical transmission coefficient, and throughfall coefficients are inversely-related to canopy field capacity and LAI. This is the reason why Rs, Kt, and s are maximum during the Winter. Also, it is important to remark the influence of precipitation on the vegetation green-up, where a significant precipitation event in late April is evident responsible of the abrupt increase of vegetation fraction at the beginning of May.

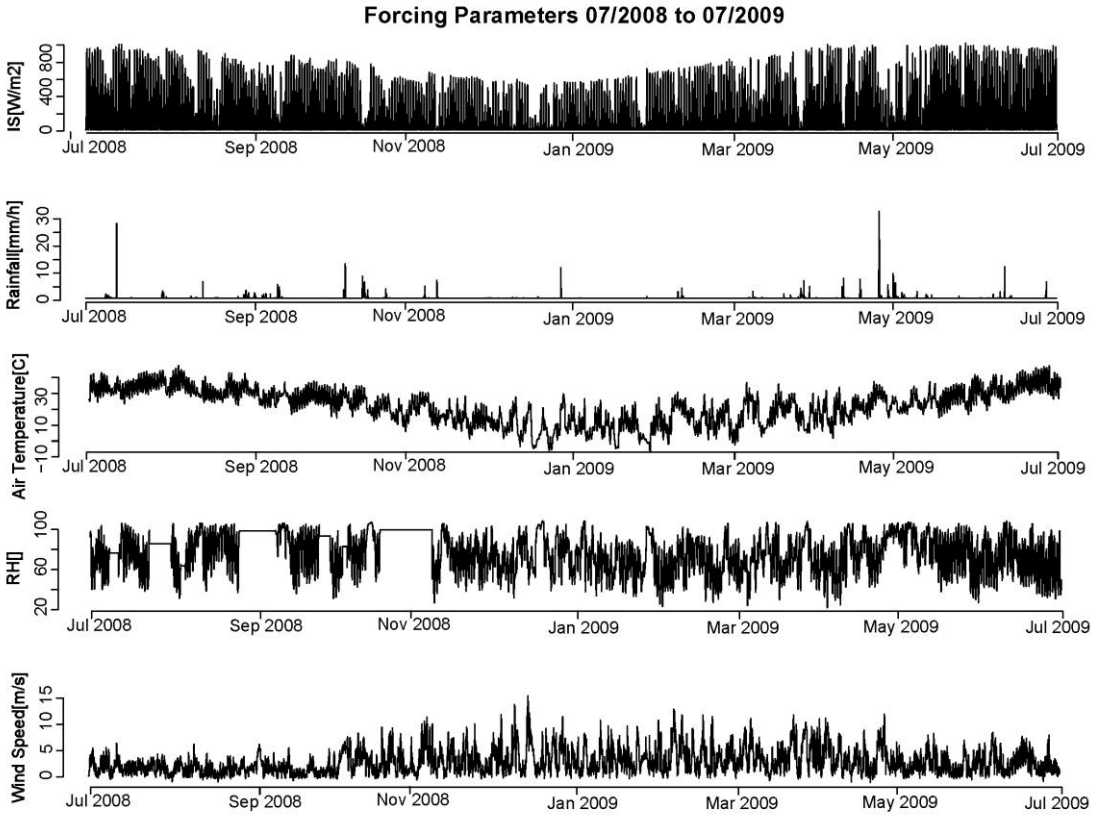

Figure 17. US-ARm Validation atmospheric forcing for model calibration. From the top down the time series correspond to incoming solar radiation (IS, W/m2), precipitation (P, mm/h), air temperature (T, °C), relative humidity (RH, %) and wind speed (WS, m/s).

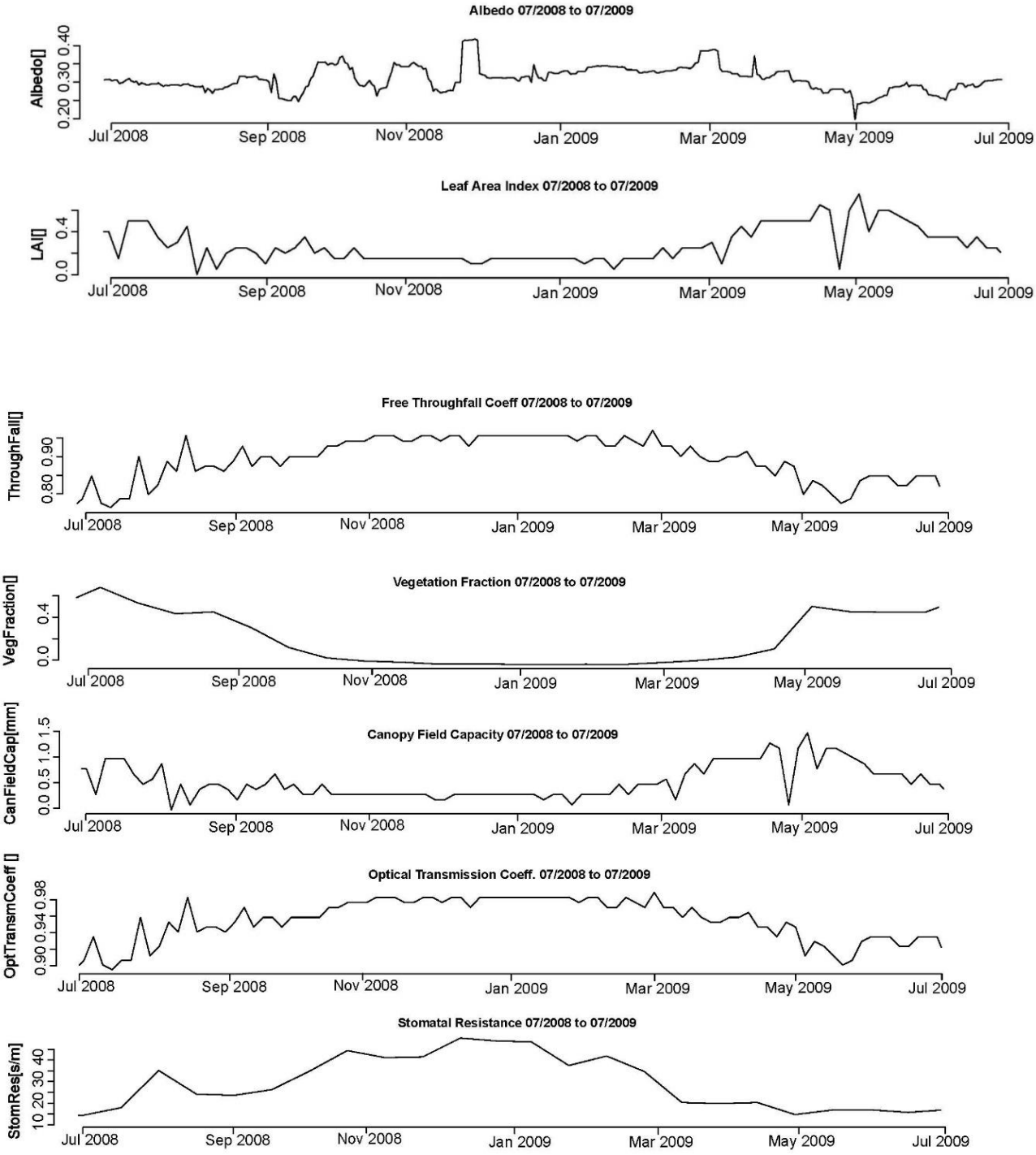

Figure 18. Remotely-sensed derived vegetation parameters for tRIBS model validation at US-Arm. From the top down, the time series correspond to the albedo (Al), Leaf Area Index (LAI), throughfall coefficient (s), vegetation fraction (Vf), canopy field capacity (p), optical transmission coefficient (Kt) and plant stomatal resistance (Rs).

As mentioned before, for the ARm site, the shallow soil moisture and root zone soil moisture were not included in the calibration stage. However, aiming to enhance the model assessment, the scarce soil moisture data available was used to conduct some comparisons with the simulated time series (see Figures 19, 20 and 21). Results in Figures 19, 20 and 21 and Table 11 show that the model maintain its simulation skill during the validation period with NS>0.5 in all cases. It also represents well the soil moisture data with NS=0.42. The validation results state that the model can be used as a predictive tool since the predictability assessment ended up in NS > 0.50 proving its parameter stability and extended usability across years, at the same eddy station.

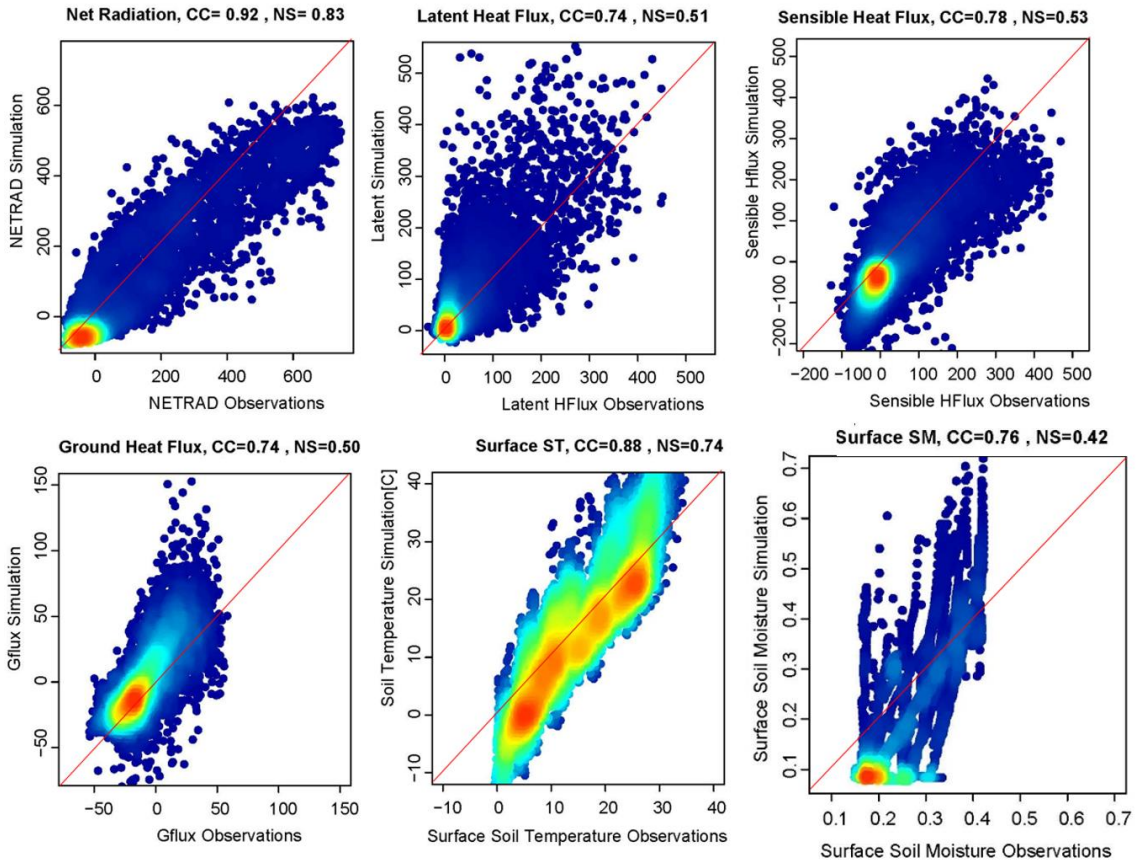

Figure 19. Density scatterplots of the validation results at US-ARm. In all panels the x-axis represents the observed and the y-axis the simulated values.

Table 11. US-Arm validation result statistics.

Variable→	**NR(W/m^2)**	**LE(W/m^2)**	**H(W/m^2)**	**G(W/m^2)**	**SST(C)**
CC	0.92	0.74	0.78	0.74	0.88
BIAS	0.13	-0.32	-16.55	-26.45	0
RMSE	78.47	63.39	71.97	20.86	6.30
NS	0.83	0.51	0.53	0.5	0.74

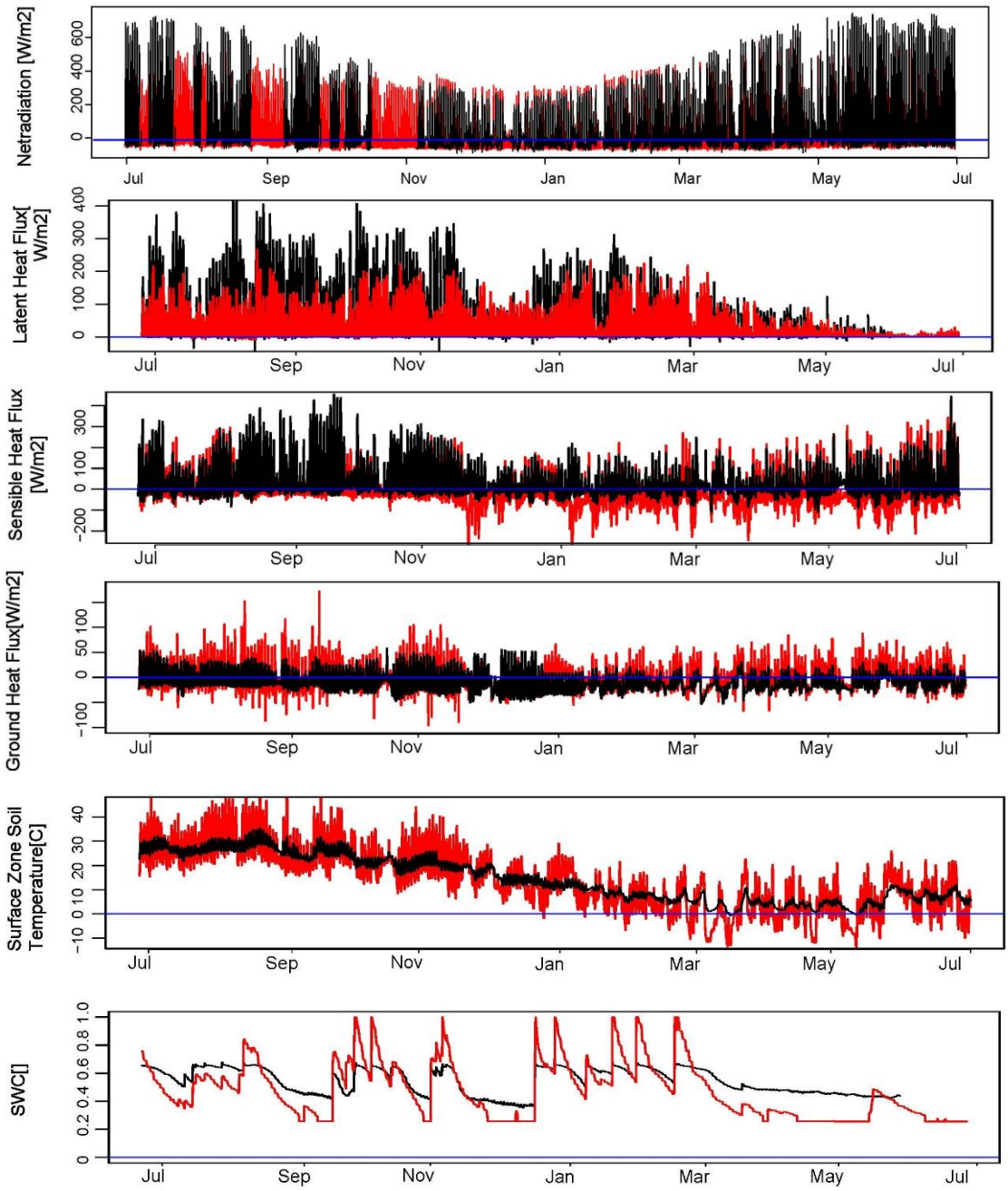

Figure 20. US-ARm Validation time series results. Red and black lines represent simulated and observed values respectively. From top down the variables are net radiation (NR) latent heat flux (LE),sensible heat flux (H), soil surface temperature (SST), and soil surface soil moisture (SSM).

Figure 21 illustrates the model's ability to simulate the surface energy fluxes, keeping positive NS values from 0.33 to 0.85. The model performance during the selected

month validates the positive results obtained during the entire validation period and allows observing the seasonal and diurnal responses of the different variables.

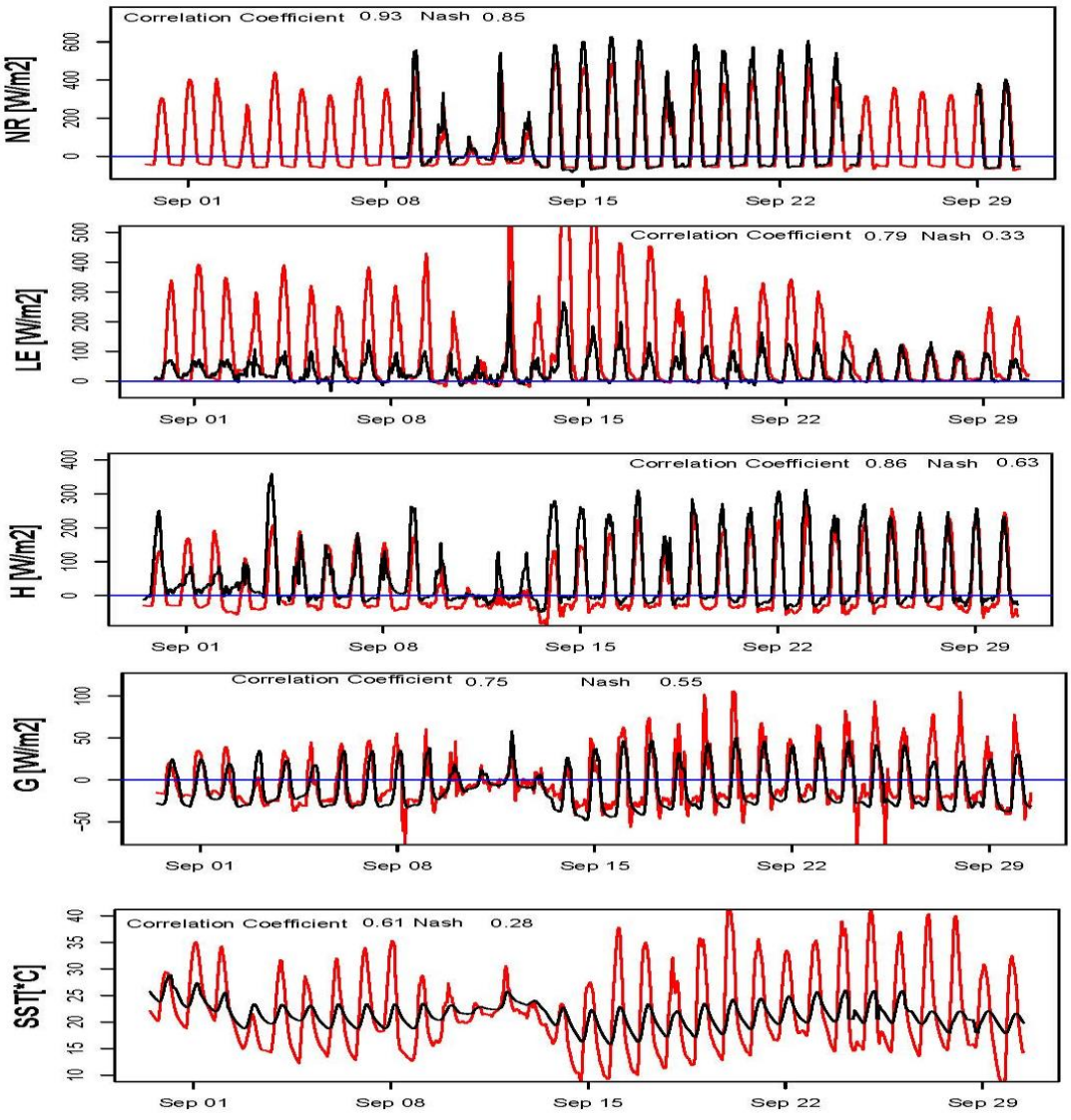

Figure 21. US-ARm validation results during the month of June, 2004. Red and black lines represent simulated and observed values. From the top down, the output variables are: net radiation (NR), latent heat flux (LE), sensible heat flux (H), ground heat flux (G), and soil surface temperature (SST).

3.2.2 Marena (MOISST)

Figure 22 illustrates the model forcing time series. During this period, there are more precipitation events than during the calibration year. Incoming shortwave radiation presents a seasonal pattern, and relative humidity does not appear to follow a seasonal pattern. Vegetation-wise, LAI shows minimum values during the Winter until late April when values appear to be more proportional to Vf. Stomatal resistant is generally under 100 s/m, but during early October it has a peak value of almost 150 s/m. All parameters derived from LAI share the Rs peak, which overlaps with an abrupt decrease of LAI when the values were as low as in the winter season. LAI, Vf, p, and Al keep a proportional behavior. Meanwhile, free throughfall coefficient (s), optical transmission coefficient (Kt), and stomatal resistance (Rs) have comparative behavior that is inverse to vegetation fraction.

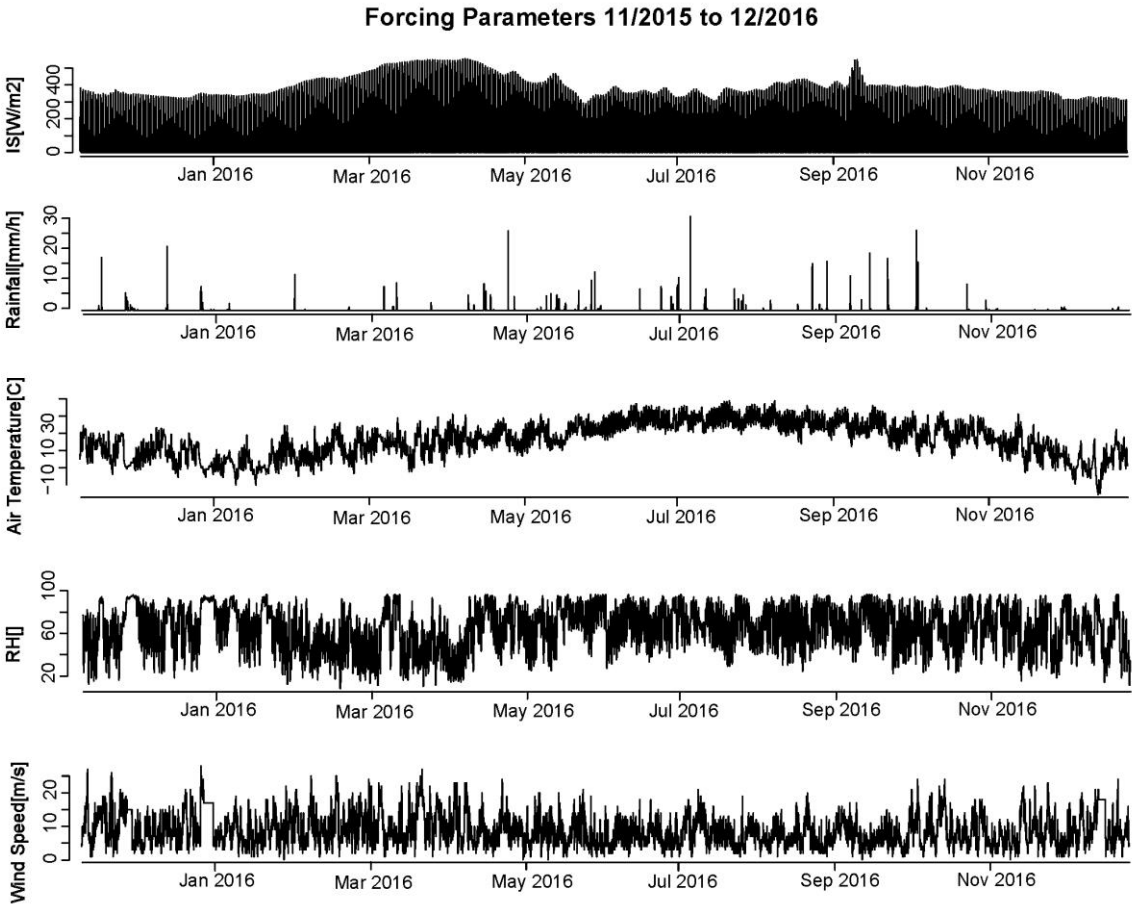

Figure 22. Marena observed atmospheric forcing for model validation. From the top down the time series correspond to incoming solar radiation (IS, W/m2), precipitation (P, mm/h), air temperature (T, °C), relative humidity (RH, %) and wind speed (WS, m/s).

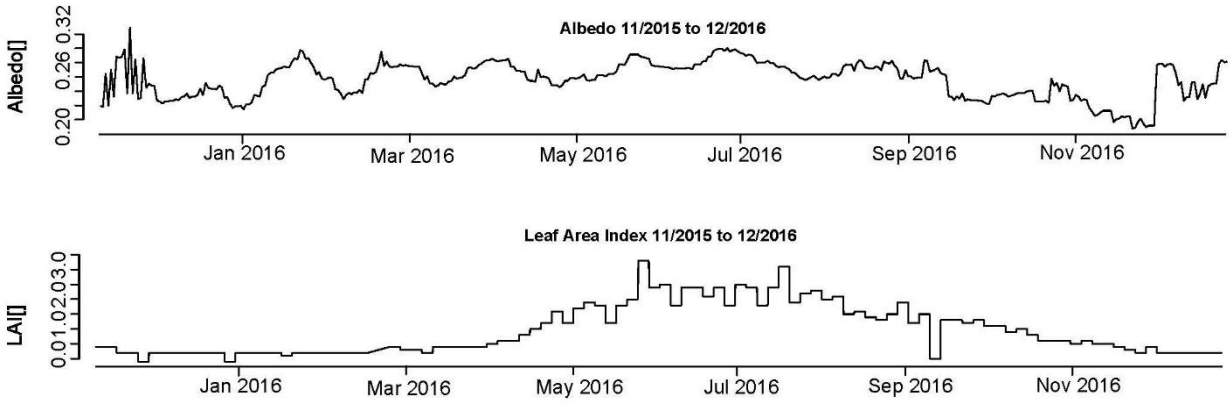

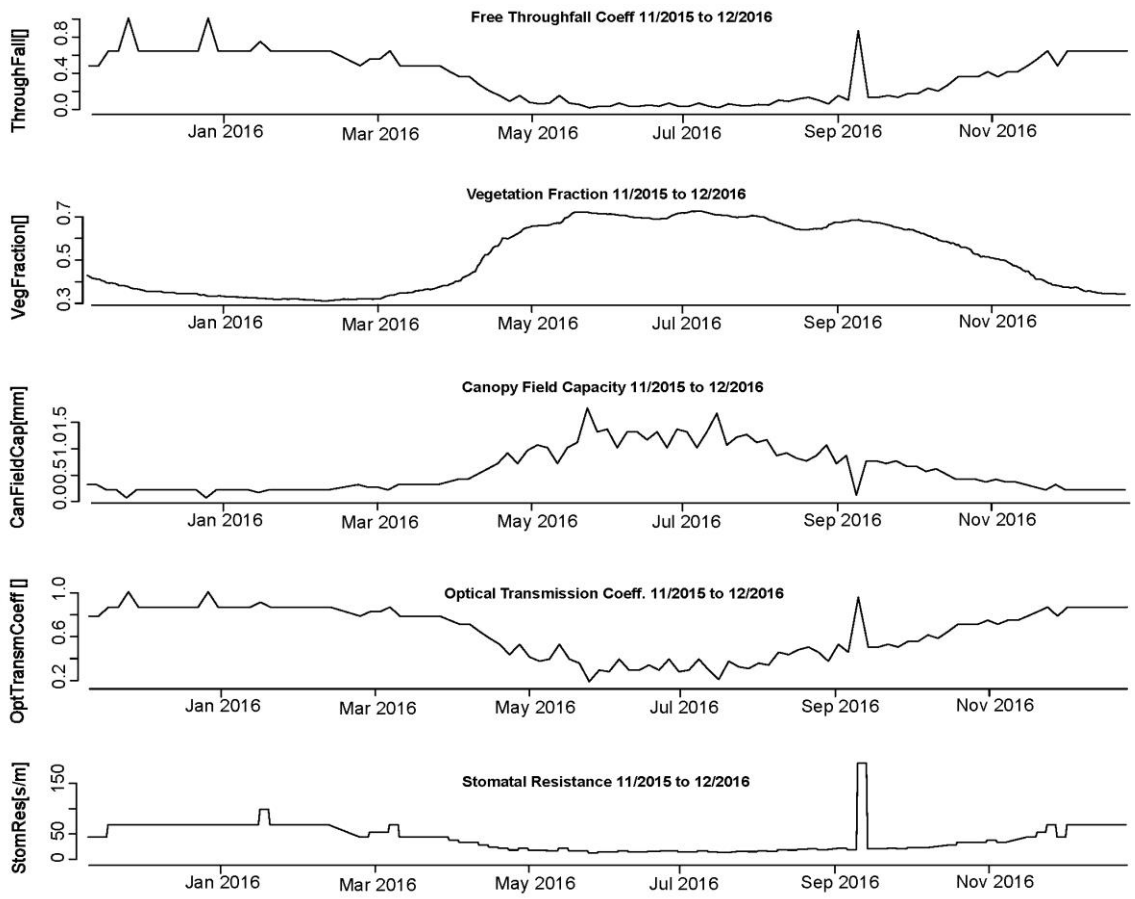

Figure 23. Remotely-sensed derived vegetation parameters for tRIBS model validation at Marena. From the top down, the time series correspond to the albedo (Al), Leaf Area Index (LAI), throughfall coefficient (s), vegetation fraction (Vf), canopy field capacity (p), optical transmission coefficient (Kt) and plant stomatal resistance (Rs)

Figures 24, 25 and 26 and Table 12 illustrate the utility of the tRIBS model to perform SEF and ST and SM simulations at this station as all NS values area above 0.5.

Although, the model seems to be systematically under and overestimating SST, this could be further corrected when snow and cold processes are included into tRIBS. Finally, the model keeps representing well the surface soil moisture with a correlation coefficient of 0.73 and a NS value of 0.55. The root zone predictions of the model have a strong correlation coefficient, capturing the general seasonal and diurnal behaviors

The time series presented in Figures 24 through 26 verify the models capacity to be used as a virtual tool for predictions of the SEB at stations where previous parameter calibration is conducted.

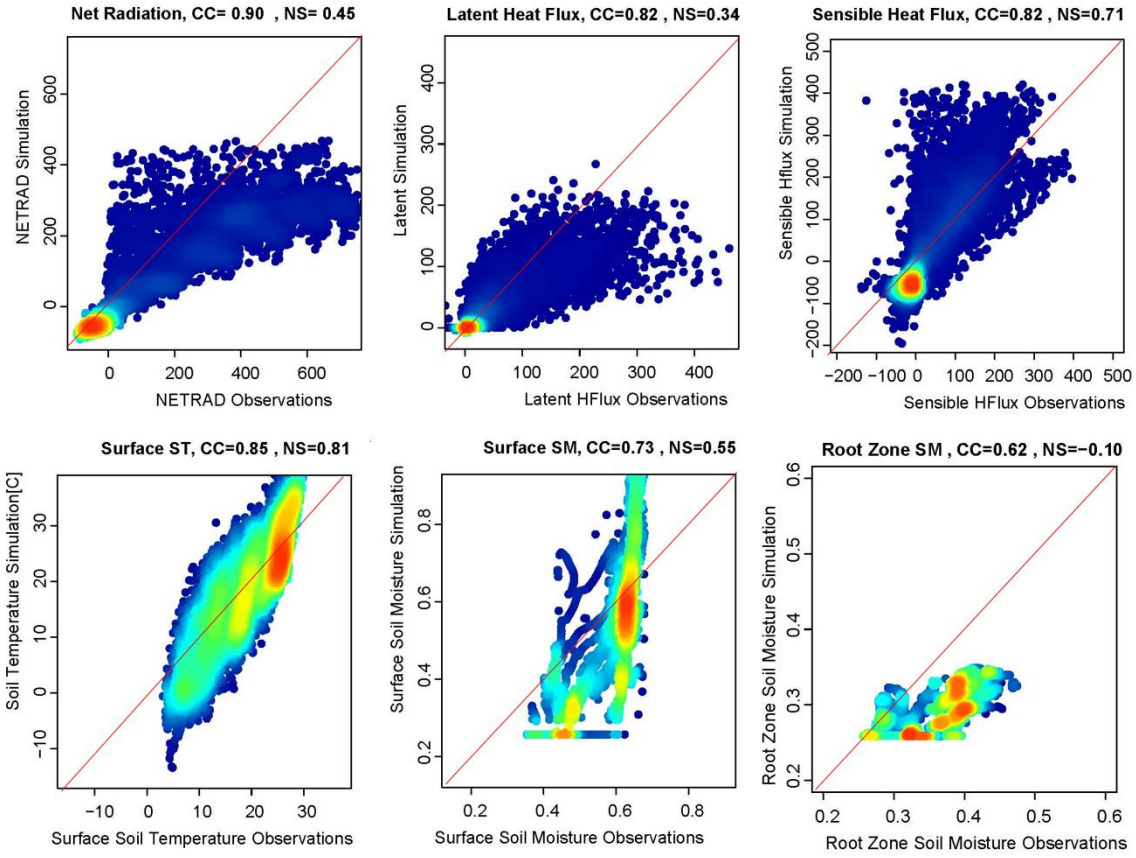

Figure 24. Density scatterplots of the Validation results at Marena. In all panels the x-axis represents the observed and the y-axis the simulated values.

Table 12. Marena validation result statistics. Net radiation (NR), latent heat flux (LE), sensible heat flux (H), soil surface temperature (SST), shallow soil surface soil moisture (SSM), and soil root zone soil moisture (RSM).

Variable→	**NR(W/m^2)**	**LE(W/m^2)**	**H(W/m^2)**	**SST(C)**	**SSM()**	**RSM()**
CC	0.9	0.82	0.82	0.85	0.73	0.62
BIAS	1	0.41	0.17	-0.06	-0.15	-0.17
RMSE	130.5	46.25	69.45	5.45	0.16	0.093

NS	0.45	0.34	0.71	0.81	0.55	-0.10

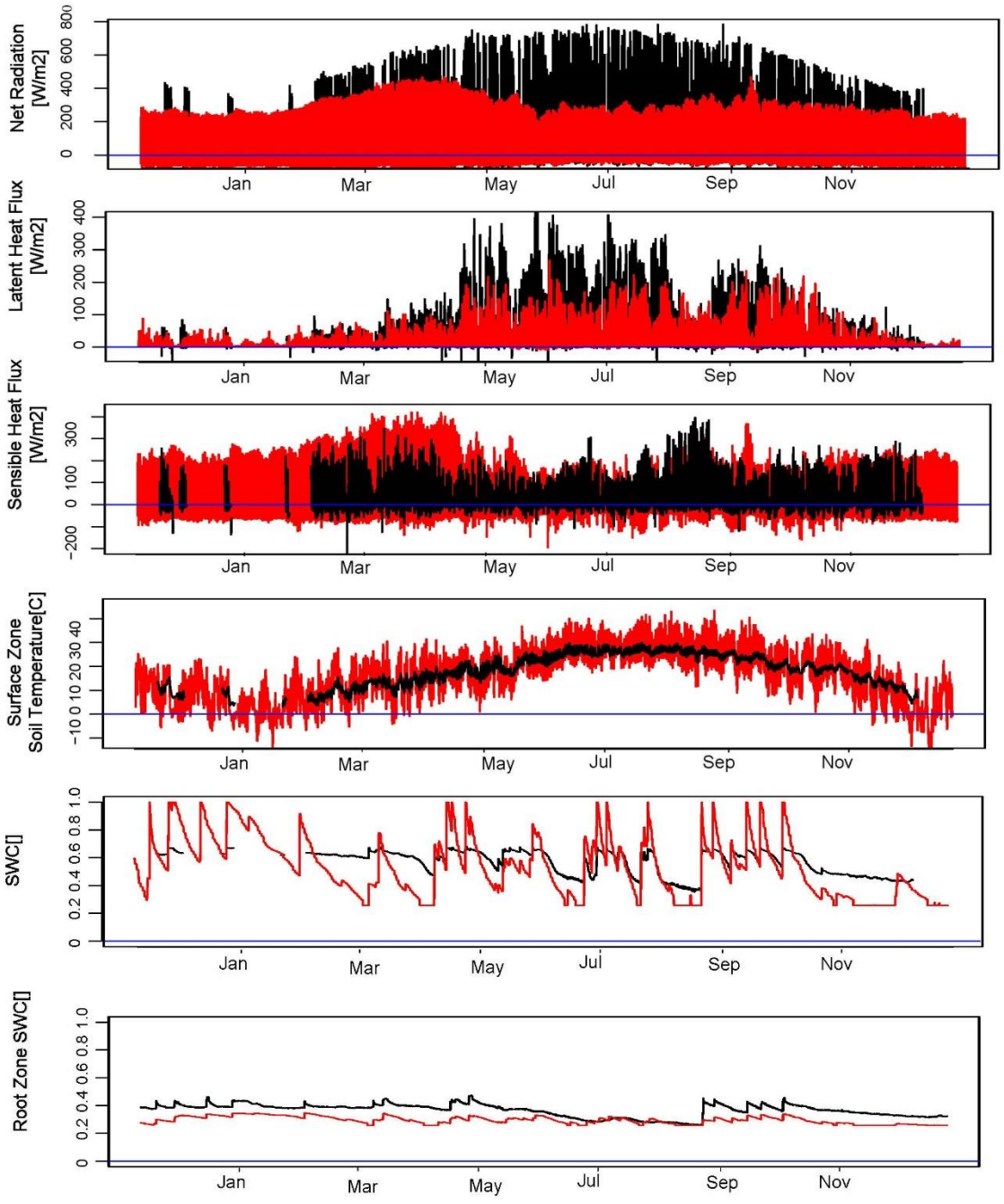

Figure 25. Marena validation time series results. Red and black lines represent simulated and observed values respectively. From top down the variables are net radiation (NR), latent heat flux (LE), sensible heat flux (H), soil surface temperature (SST), shallow soil surface soil moisture (SSM), and soil root zone soil moisture (RSM).

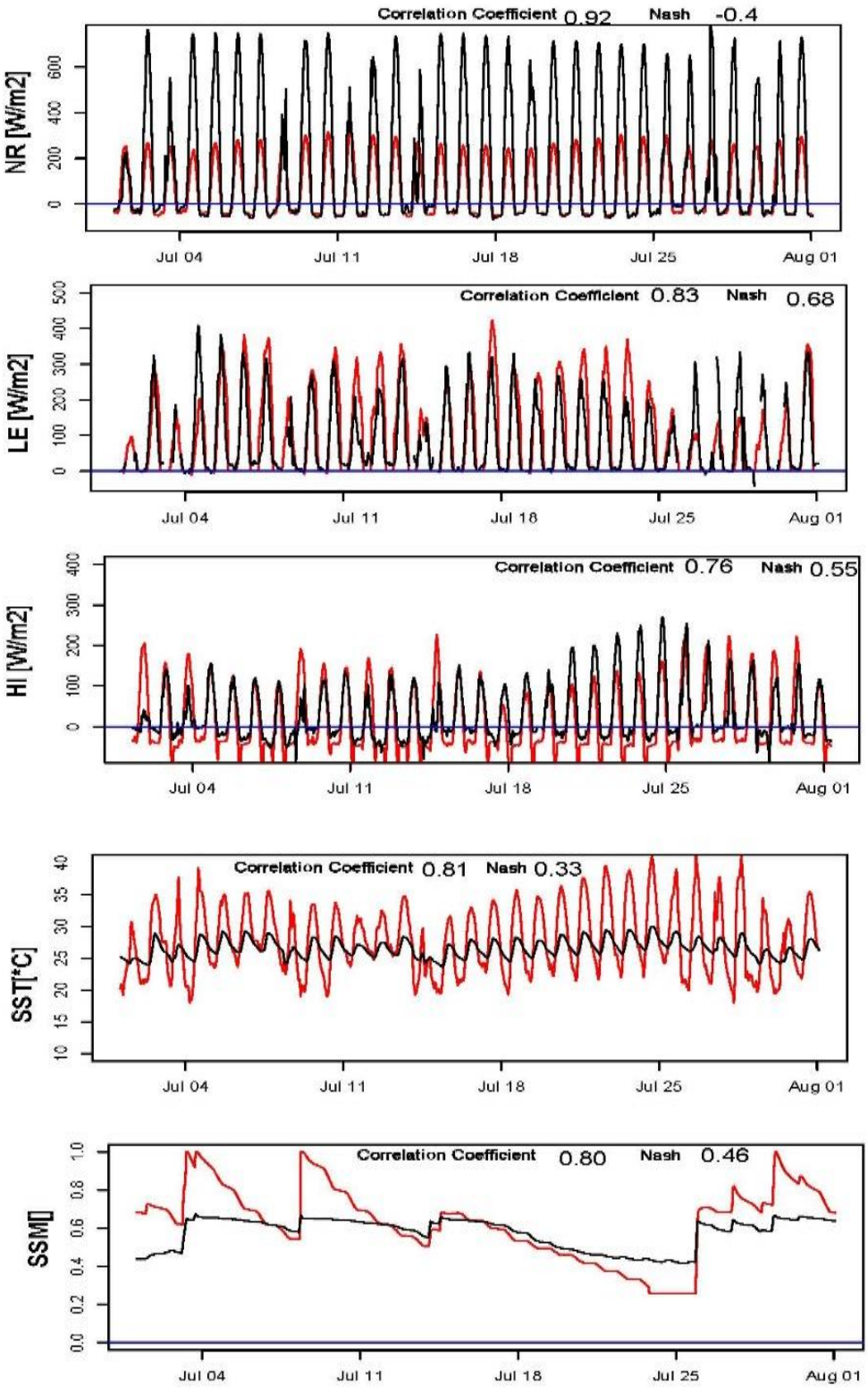
Correlation Coefficient 0.92 Nash -0.4
NR [W/m2]
0
200
400
600
Jul 04
Jul 11
Jul 18
Jul 25
Aug 01
Correlation Coefficient 0.83 Nash 0.68
LE [W/m2]
0
100
200
300
400
500
Jul 04
Jul 11
Jul 18
Jul 25
Aug 01
Correlation Coefficient 0.76 Nash 0.55
HI [W/m2]
0
100
200
300
400
Jul 04
Jul 11
Jul 18
Jul 25
Aug 01
Correlation Coefficient 0.81 Nash 0.33
SST[°C]
10
15
20
25
30
35
40
Jul 04
Jul 11
Jul 18
Jul 25
Aug 01
Correlation Coefficient 0.80 Nash 0.46
SSM[]
0.0
0.2
0.4
0.6
0.8
1.0
Jul 04
Jul 11
Jul 18
Jul 25
Aug 01

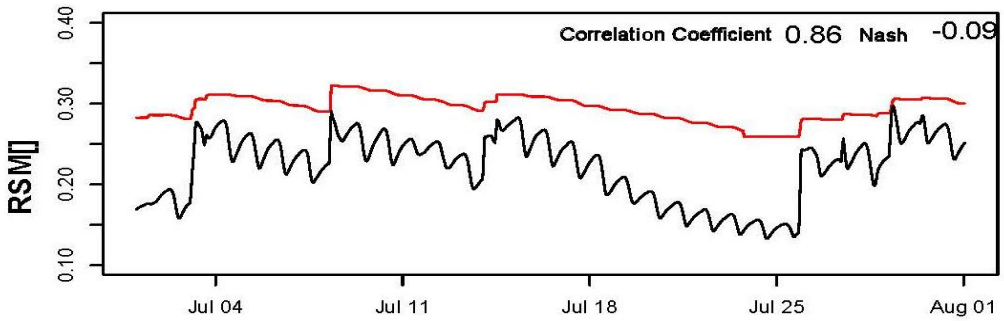

Figure 26. Marena validation results during the month of August, 2014. Red and black lines represent simulated and observed values. From the top down, the output variables are: net radiation (NR), latent heat flux (LE), sensible heat flux (H), soil surface temperature (SST), surface soil moisture (SSM), and root soil moisture (RSM).

3.3 Predictor Contribution Assessment and The Effect of Dynamic Vegetation

3.3.1 US-ARm

The best subsets analysis helps to identify the predictors that have the largest influence on the variability of a predictand. Seeking to better understand the influence of vegetation, precipitation, soil water content, soil temperature and other forcing variables on the surface energy partitioning, we used the best-subsets approach to identify the best predictors of NR, LE, H and G. Figures 27 and 28 indicate that incoming short wave radiation explains more than 80% of all the energy flux variables. Air and soil temperatures are necessary to predict the surface energy partitioning, especially the ground heat flux (G). Further, soil water content is also valuable in the prediction of the energy balance components with shallow and deep-soil water content having more influence in the values of latent heat flux (LE) than in the other components of the energy partitioning. Wilson et. al, 2002 found a strong influence on the surface energy fluxes

produce by the interannual differences in soil water content. Similarly, wind speed has also influence on LE and H.

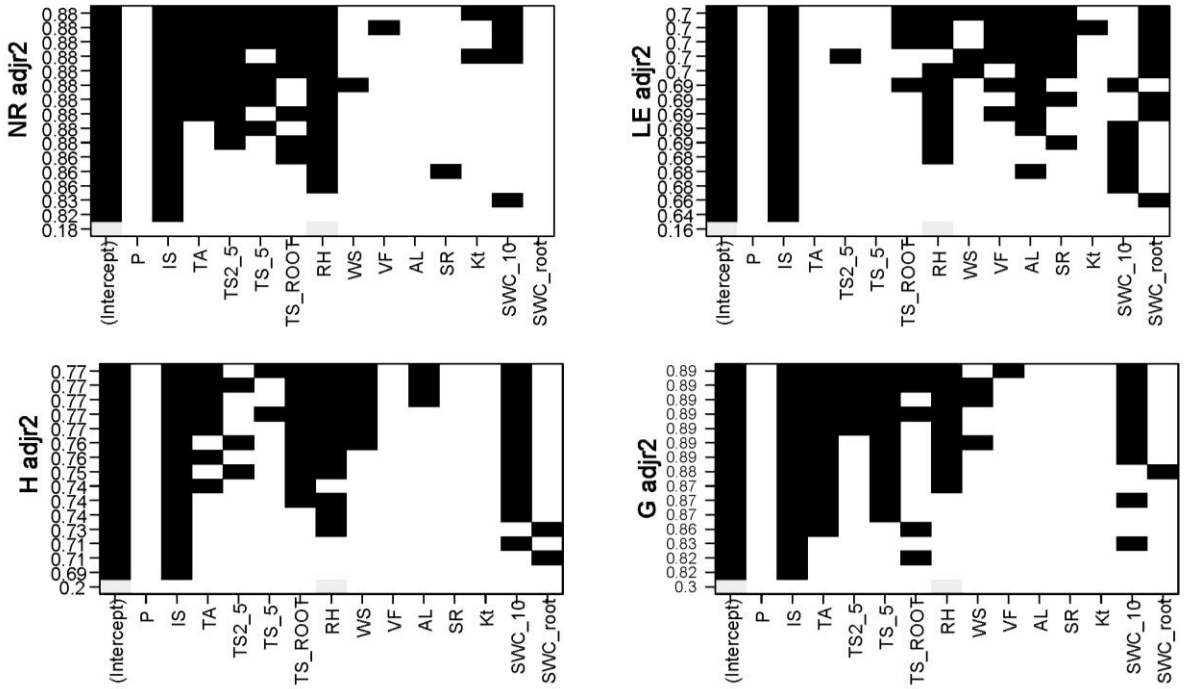

Figure 27. Results of the best subsets analysis to identify best predictors in the estimation of the energy fluxes at US-ARm. The predictands in the x axis are precipitation (P), incoming short wave radiation (IS), air temperature (TA), surface soil temperature at 2.5 cm depth (TS2_5), soil temperature at 5.0 cm depth (TS_5), root zone soil temperature at 100 cm depth (TS_Root), relative humidity (RH), wind speed (WS), vegetation fraction (Vf), albedo (AL), stomatal resistance (SR), optical transmission coefficient (Kt), surface soil water content (SWC_10), and root zone soil water content (SWC_Root).

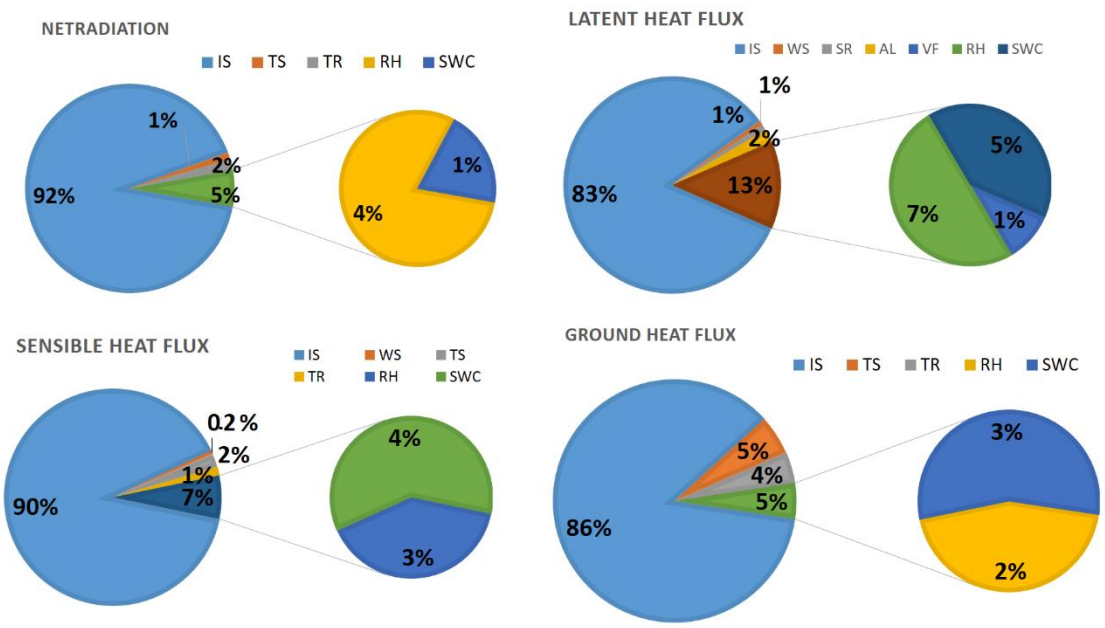

Figure 28. Summary results of the best-subsets analysis at US-ARm. Incoming solar radiation(IS.),wind speed(WS), relative humidity (RH), soil temperature (TS), root soil temperature (TR), vegetation fraction (Vf), albedo (AL), stomatal resistance (SR), and soil water content (SWC).

Finally, in order to assess the importance of dynamic Vs. static vegetation parameters, Figure 29 shows a comparison of the two simulation results, where one of them was made using dynamically-changing vegetation parameters (a) and the other one (b) keeping the vegetation parameters static (as traditional models do). The partitioning components of ET (E and T) are also shown in both plots. The assumption of constant vegetation, as shown Figure 29 (a) represents an underestimation of ET during the wintertime, having maximums values of 5 mm/day, which accounts to almost 30 mm/month less than in the dynamic scenario displayed at the bottom of the Figure 29 (b). In the static vegetation scenario, there is a constant overestimation of transpiration (T) and underestimation of evaporation across the months.

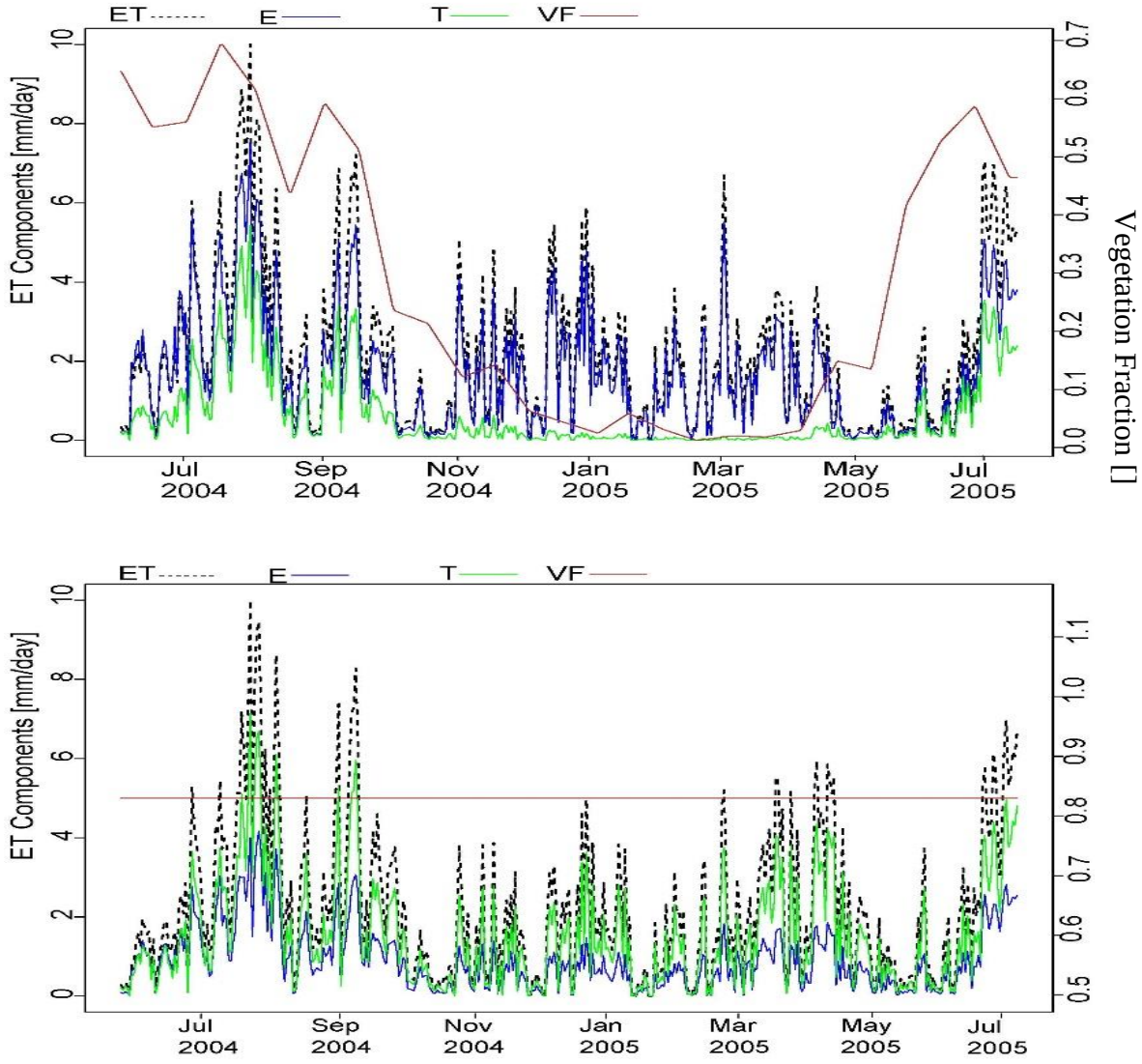

Figure 29. US-ARm vegetation dynamic (a) and static (b) scenarios. In both panels Total ET (dashed lines) is partitioned on Evaporation from soil and intercepted water (E) and plant transpiration (T) and the values are presented on the left- Y axis. Vegetation. Vegetation fraction (Vf) values are on the right Y-axis of the figure.

3.3.2 Marena (MOISST)

Figures 30 and 31 indicate that IS has less influence at Marena than it had at the US-ARm site. IS controls more than 80% of NR and H, but only 51% of LE. Air and soil

temperatures are important variables to predict the energy fluxes. Relative humidity (RH) and vegetation fraction (Vf) are also important variables to describe these fluxes, but Vf has a higher predicting power on H. The soil surface temperatures (SST) explain up to 34% of LE, gaining more control with the vegetation fraction in contrast with the ARm site.

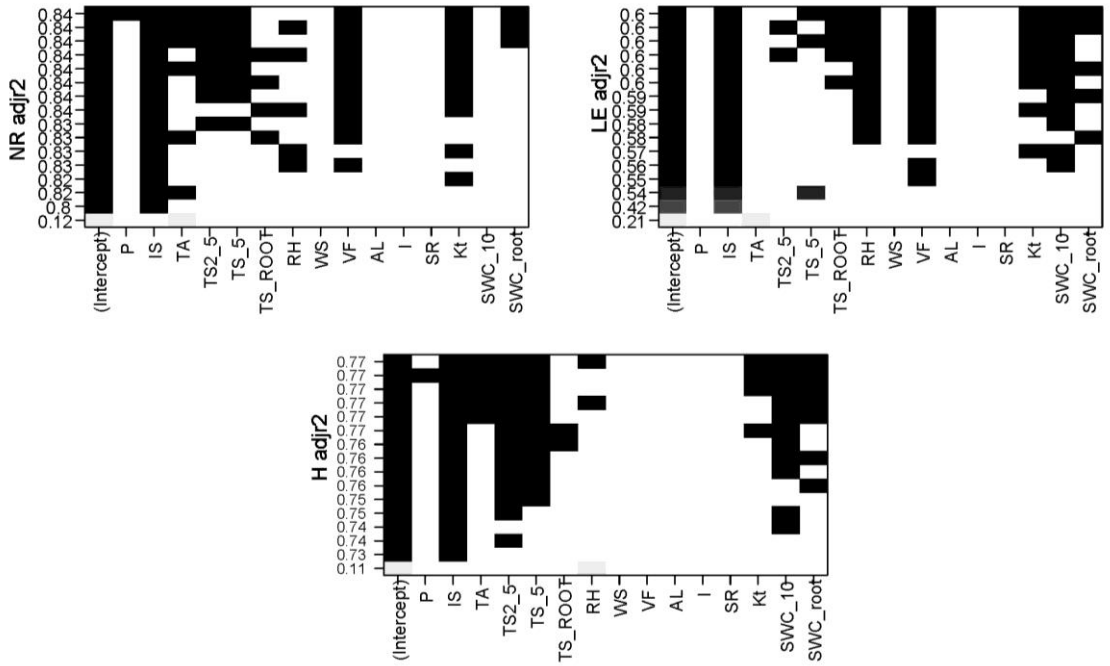

Figure 30. Results of the best subsets analysis to identify best predictors in the estimation of the energy fluxes at Marena. The predictands in the x axis are precipitation (P), incoming short wave radiation (IS), air temperature (TA), surface soil temperature at 2.5 cm depth (TS2_5), soil temperature at 5.0 cm depth (TS_5), root zone soil temperature at 100 cm depth (TS_Root), relative humidity (RH), wind speed (WS), vegetation fraction (Vf), albedo (AL), stomatal resistance (SR), optical transmission coefficient (Kt), surface soil water content (SWC_10), and root zone soil water content (SWC_Root).

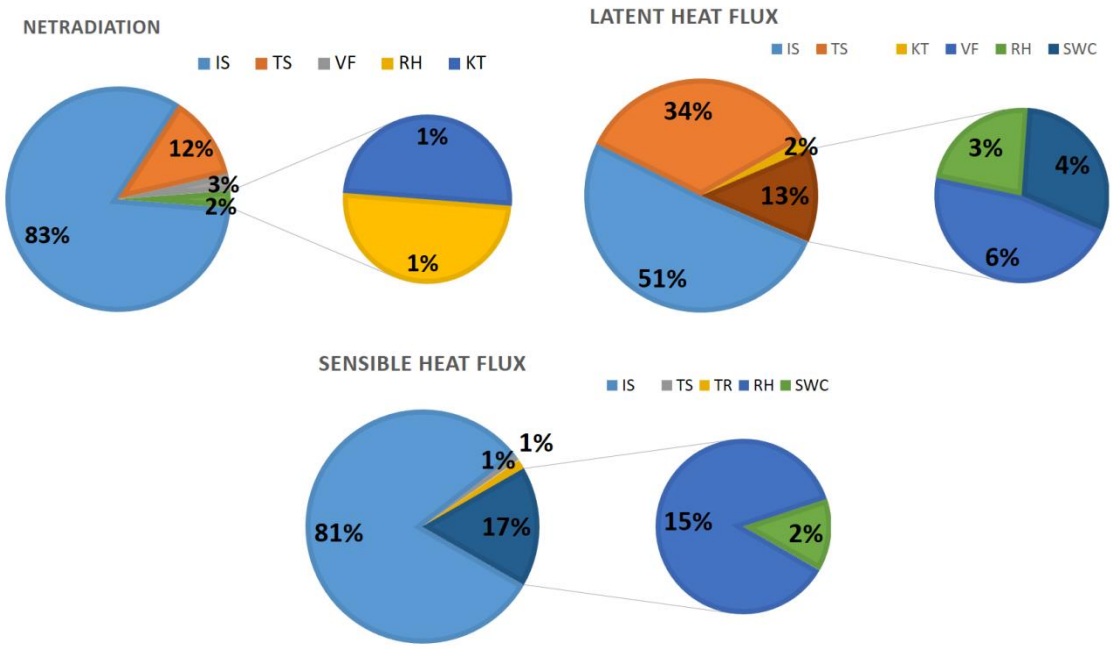

Figure 31. Summary results of the best-subsets analysis at Marena. Incoming solar radiation(IS.),wind speed(WS), relative humidity (RH), soil temperature (TS), root soil temperature (TR), vegetation fraction (Vf), albedo (AL), optical transmission coefficient (Kt), stomatal resistance (SR), and soil water content (SWC).

Figure 32 states the influence of vegetation on the ET partitioning at Marena. When vegetation is constant (Figure 32 a), there is an underestimation of ET and overestimation of transpiration (T) values. Both E and T result similar when the vegetation fraction varies as it occurs in nature. For example, transpiration during the summer was, on average, 4mm/day with a dynamic land cover, meanwhile with the static was 6mm/day. The dynamic biophysical parameters mentioned in Table 5 are tied to NDVI and LAI and this conditions the seasonal effects on vegetation. Across both sites, the consideration of dynamic vegetation implies lower transpiration but higher evaporation values as a result of the fluctuations in vegetation activity and cover.

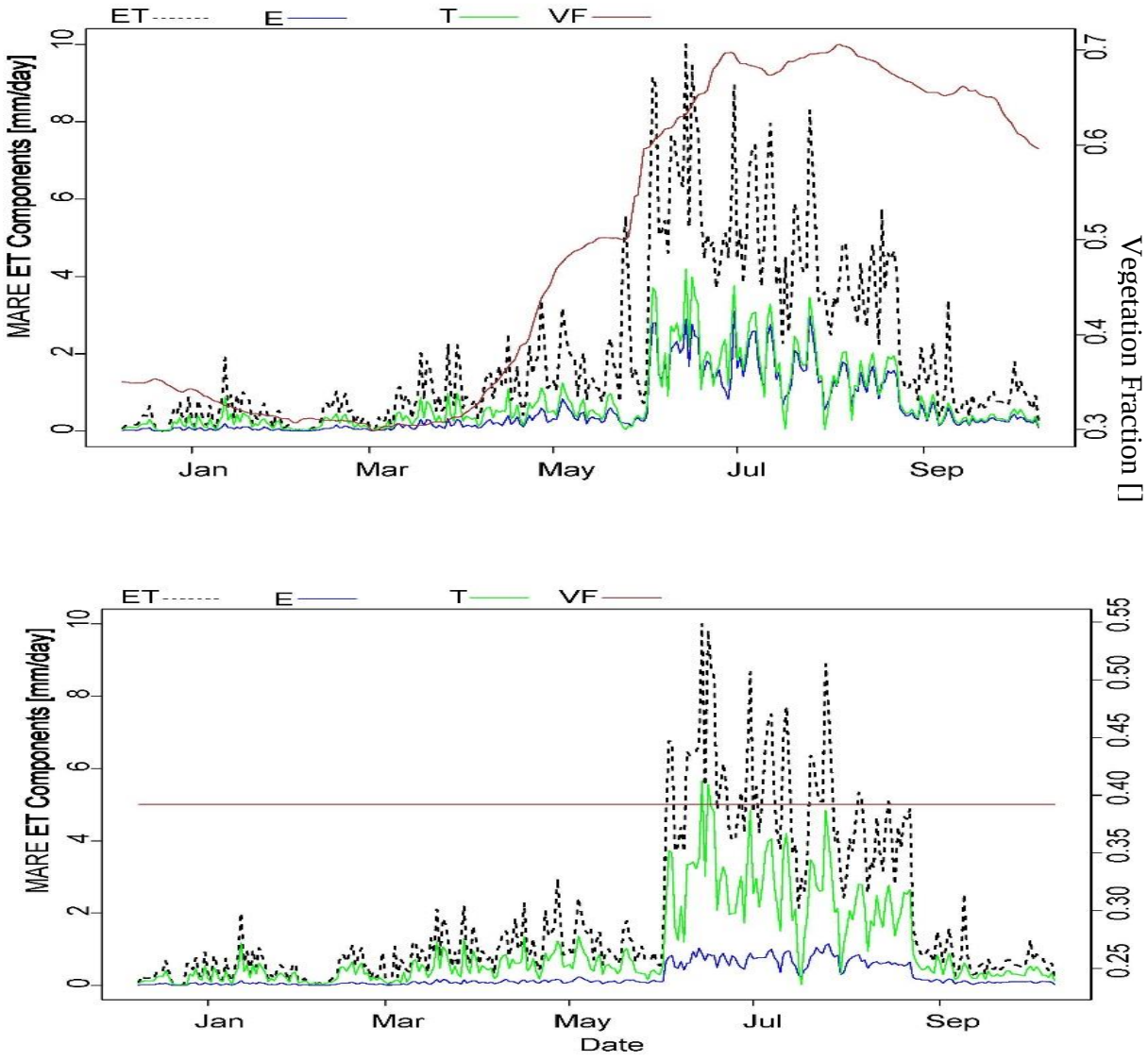

Figure 32. Marena vegetation dynamic (a) and static (b) scenarios. In both panels Total ET (dashed lines) is partitioned on Evaporation from soil and intercepted water (E) and plant transpiration (T) and the values are presented on the left- Y axis. Vegetation fraction (Vf) values are on the right Y-axis of the figure.

3.4. Model Parameter Transferability

3.4.1 US-A74

The transferability of the model parameters was tested using the ARm calibration results at the A74 site. As shown by Figures 33 and 34, both weather forcing and vegetation parameters hold similitude with US-ARm, where the stronger precipitation events are happened during July-August and vegetation fraction reaches highest values in July. The maximum incoming short wave values were found between late April to July, and minimum were found in November. Summer was characterized by high temperatures, high relative humidity, low wind speed and most of the larger precipitation events of the year.

The albedo had a similar behavior with leaf area index, but more variable than LAI. Between the months of July and September both Al and LAI have their peaks. On the other hand, Vf does not show a strong seasonality effect, although its highest values are found during July and August and the minimum during the winter season. The optical transmission coefficient (kt) shows a stronger seasonal influence that is disrupted by two events in July and August, dates where the LAI registered subnormal values for the season.

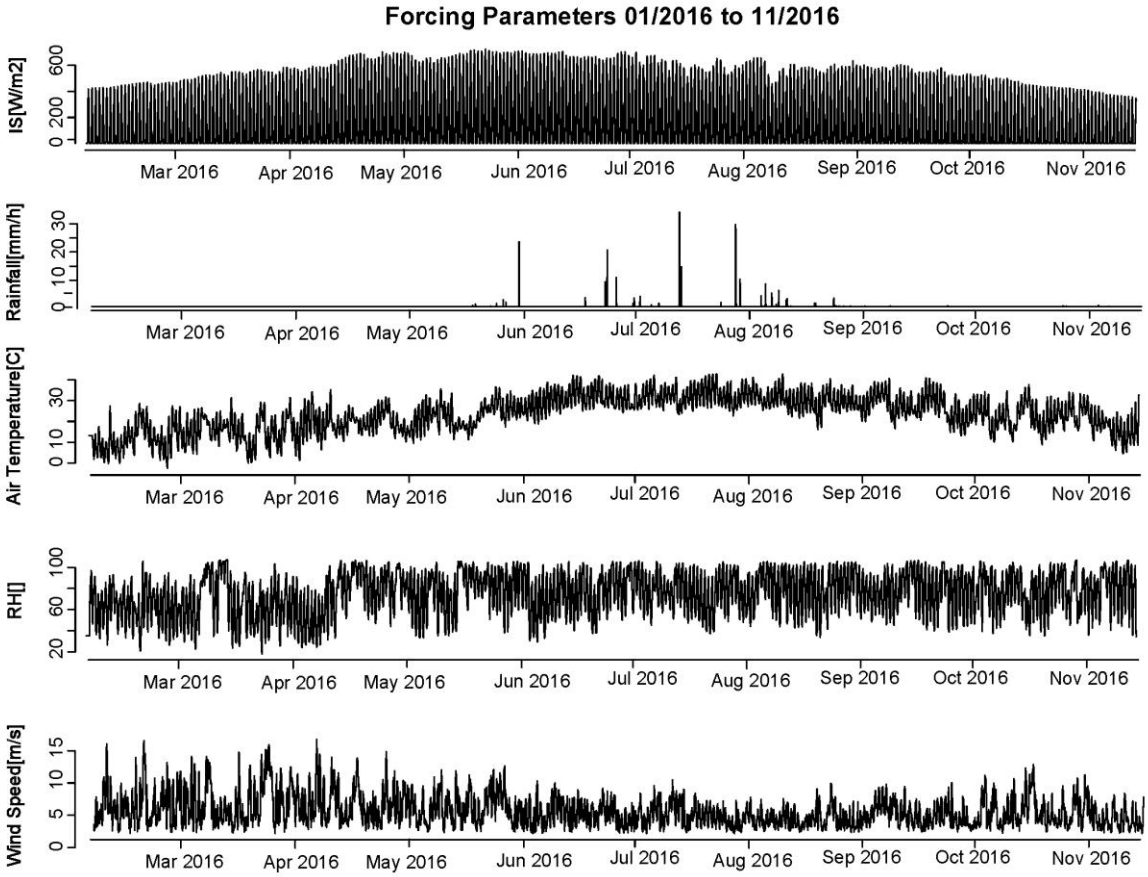

Figure 33. US-A74 observed atmospheric forcing for model calibration. From the top down the time series correspond to incoming solar radiation (IS, W/m2), precipitation (P, mm/h), air temperature (T, °C), relative humidity (RH, %) and wind speed (WS, m/s).

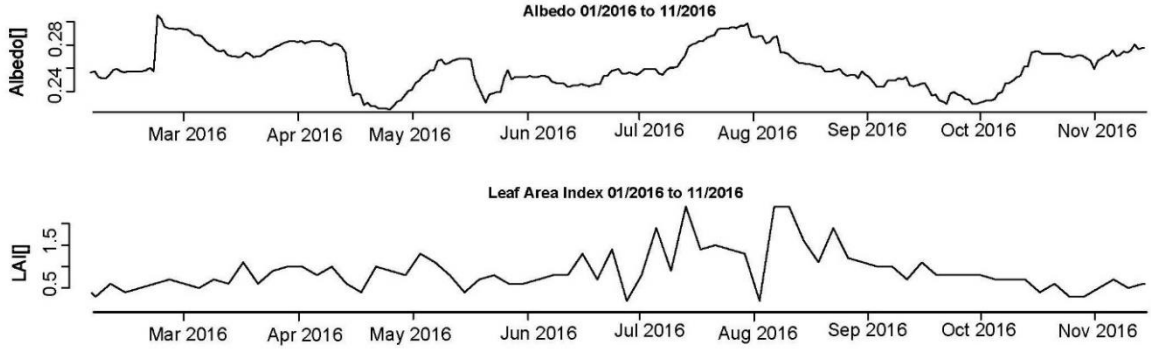

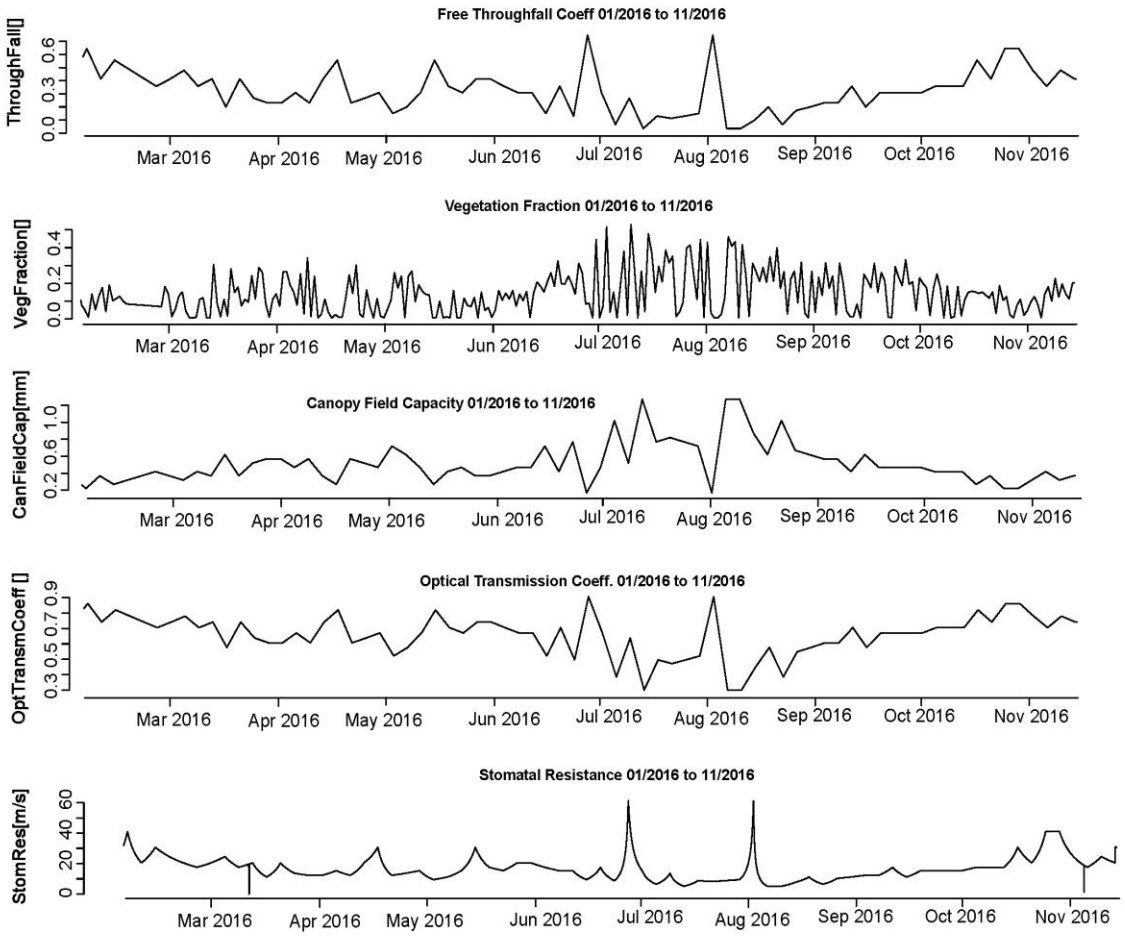

Figure 34. Remotely-sensed derived vegetation parameters for tRIBS model transferability at US-A74. From the top down, the time series correspond to the albedo (Al), Leaf Area Index (LAI), throughfall coefficient (s), vegetation fraction (Vf), canopy field capacity (p), optical transmission coefficient (Kt) and plant stomatal resistance (Rs).

Results of the model parameter transferability are illustrated in Figures 35 and 36 and Table 13. All show a strong ability to predict the variables of interest, particularly NR, H, SST and RST. However, LE and G both present lower than 0.5 and 0 NS respectively where the model tends to underestimate high values. The time series of Figure 36 illustrate that the components of the energy balance are well estimated and,

even if that there are some under and over estimations of the variables, the range of values remains accurate. RST is predicted with higher accuracy when compared to SST.

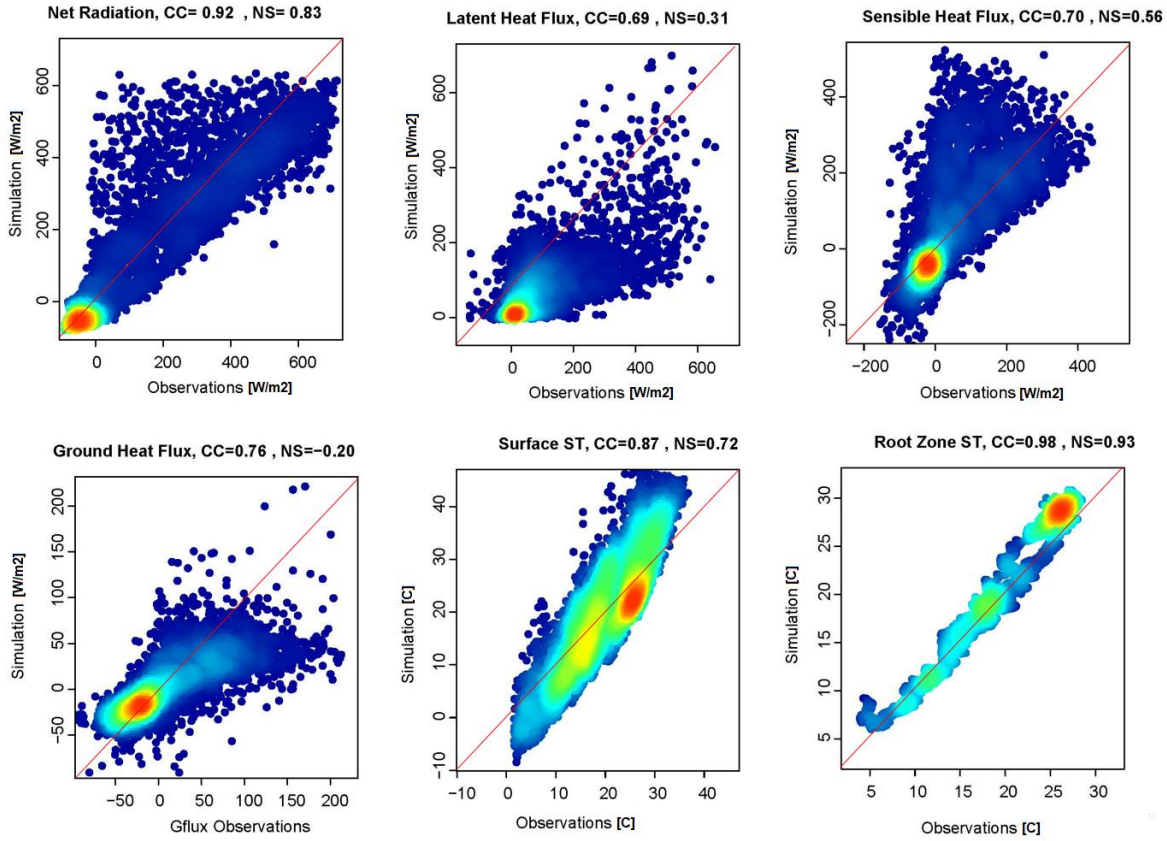

Figure 35. US-A74 density scatterplots of the transferability results at US-A74. In all panels the x-axis represents the observed and the y-axis the simulated values.

Table 13. US-A74 parameter transferability evaluation statistics. Net radiation (NR) latent heat flux (LE), sensible heat flux (H), ground heat flux (G), soil surface temperature (SST), and soil root zone temperature (SRT).

Variable→	**NR(W/m^2)**	**LE(W/m^2)**	**H(W/m^2)**	**G(W/m^2)**	**SST(C)**	**RST(C)**	**SSM**
CC	0.92	0.69	0.7	0.76	0.79	0.98	-0.47
BIAS	0.13	0.13	-0.32	13.27	-0.05	-0.07	248.85
RMSE	78.47	92.60	106.90	33.20	6.70	1.99	30.24
NS	0.83	0.31	0.56	-0.11	0.61	0.93	-0.03

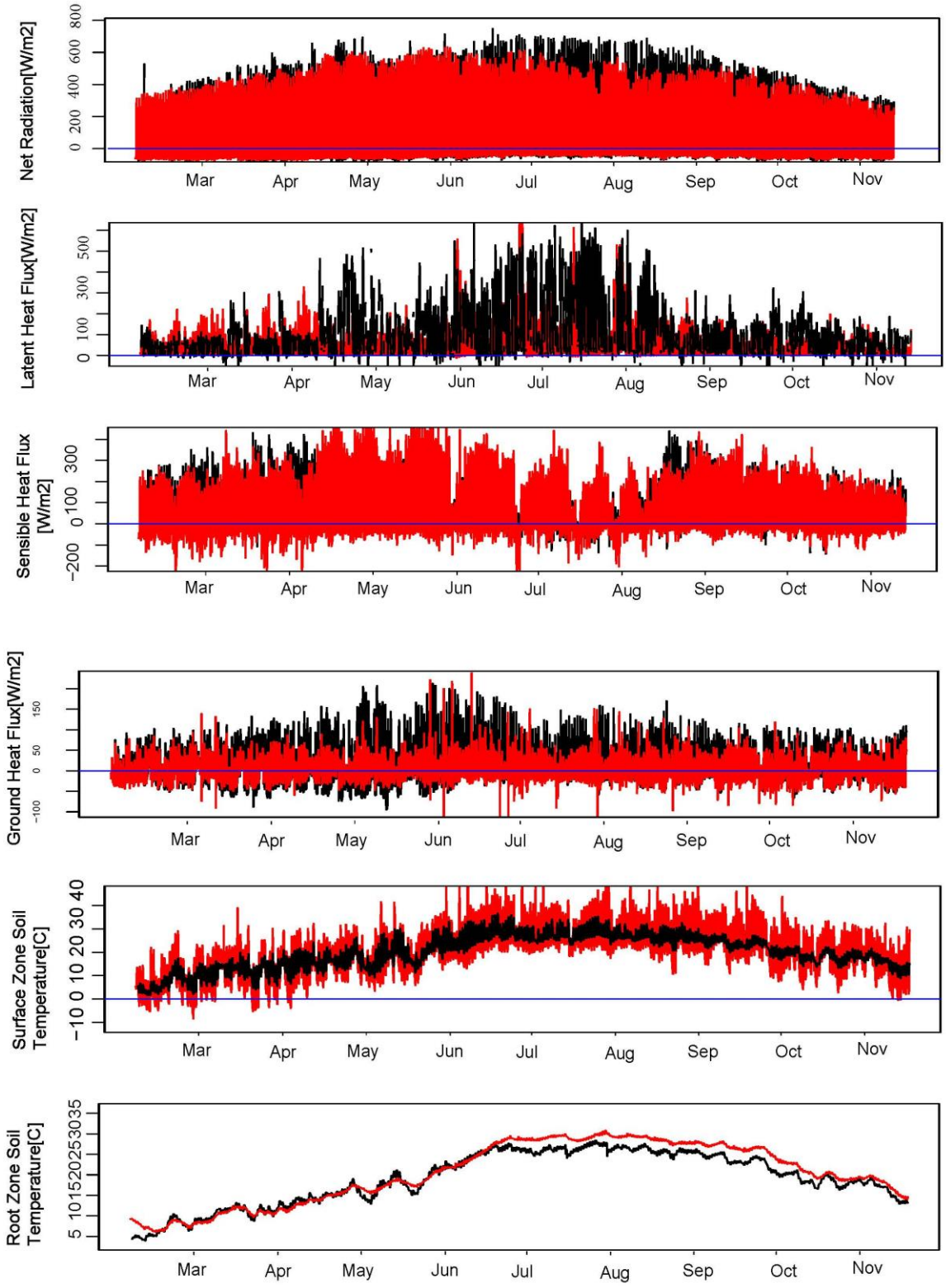

Figure 36. US-A74 transferability time series results. Red and black lines represent simulated and observed values respectively. From top down the variables are net radiation (NR) latent heat flux (LE),

sensible heat flux (H), ground heat flux (G), soil surface temperature (SST), and soil root zone temperature (SRT).

3.4.1 US-A32

The forcing parameters for the Marena transferability experiment at the US-A32 site, are presented in figure 37 and 38. The maximum incoming short wave values are found during late April to September and the minimum in December. The summer time was characterized by high temperatures, low wind speed and most of the larger precipitation events of the year. Albedo seemed inversely-related to leaf area index. Vegetation fraction (Vf), contrarious to other sites, shows the lowest values during the summer time. =Vf has a high variation between 0.1 and 0.4 during most of the year.

Stomatal resistance (Rs) presents its lowest value of 10 s/m during the cold season and gets higher during the Summer time for this location.

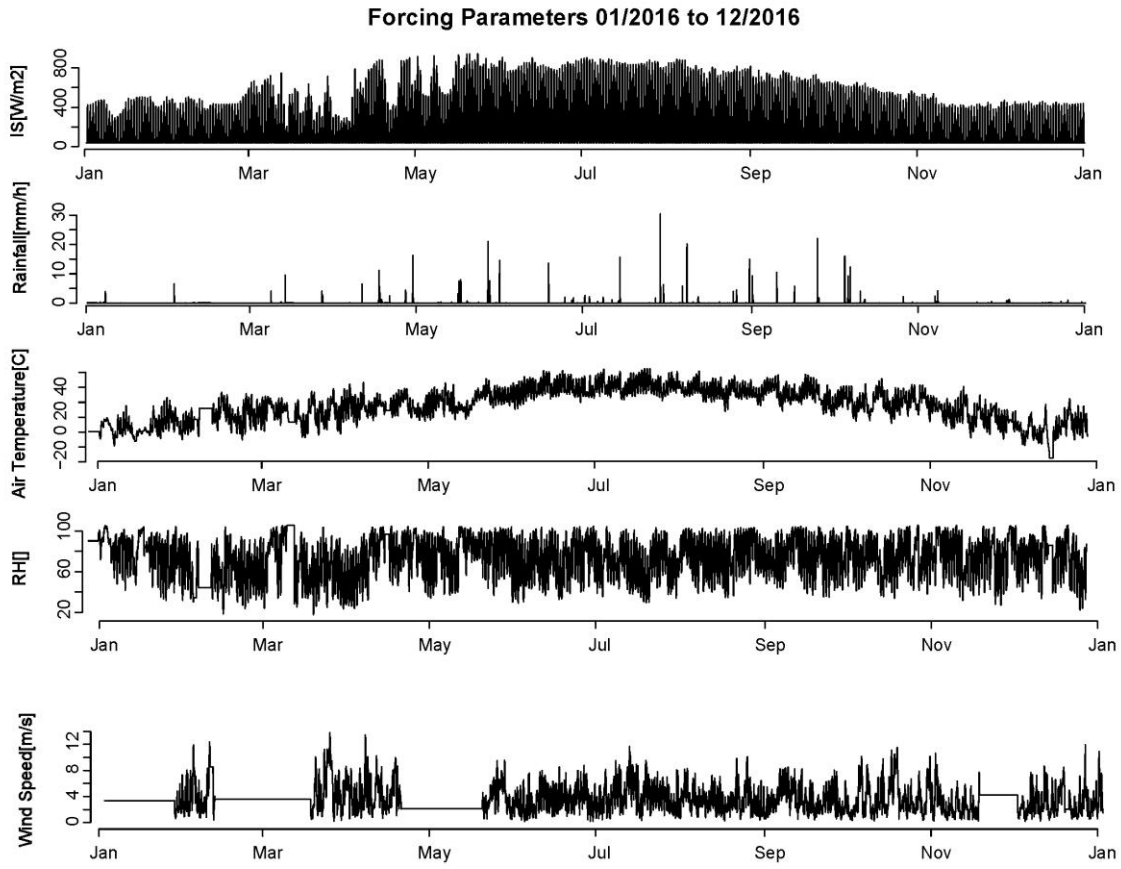

Figure 37. US-A32 observed atmospheric forcing for model calibration. From the top down the time series correspond to incoming solar radiation (IS, W/m2), precipitation (P, mm/h), air temperature (T, °C), relative humidity (RH, %) and wind speed (WS, m/s).

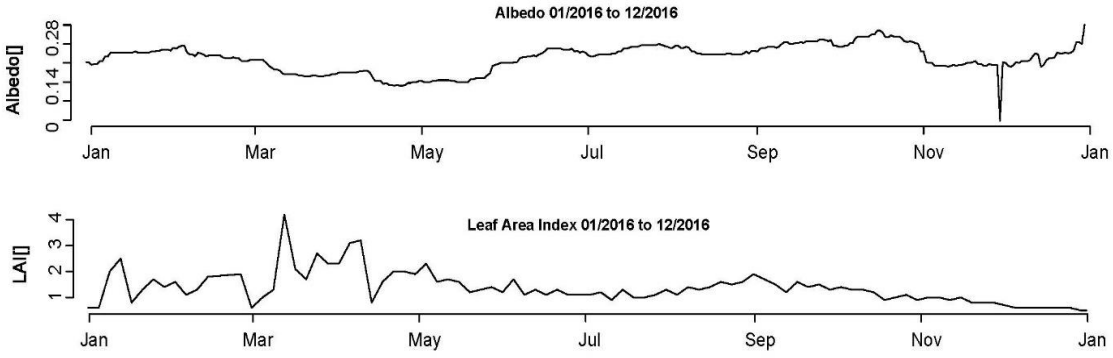

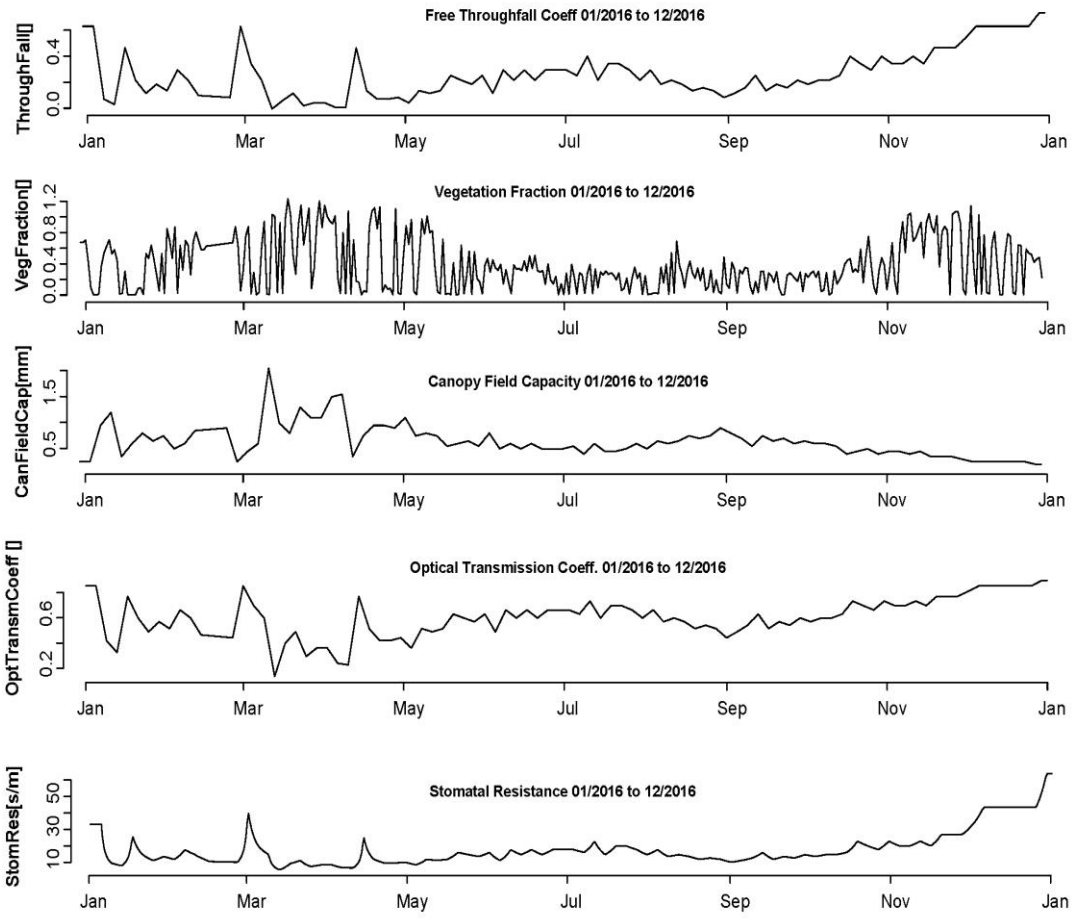

Figure 38. Remotely-sensed derived vegetation parameters for tRIBS model transferability at US-A32. From the top down, the time series correspond to the albedo (Al), Leaf Area Index (LAI), throughfall coefficient (s), vegetation fraction (Vf), canopy field capacity (p), optical transmission coefficient (Kt) and plant stomatal resistance (Rs).

Figures 39 and 40 and Table 14 illustrate that the model has a strong ability to predict all predictands except possibly by SSM and G. In the case of SSM, the NS=0.18 value is still better than the historic mean.

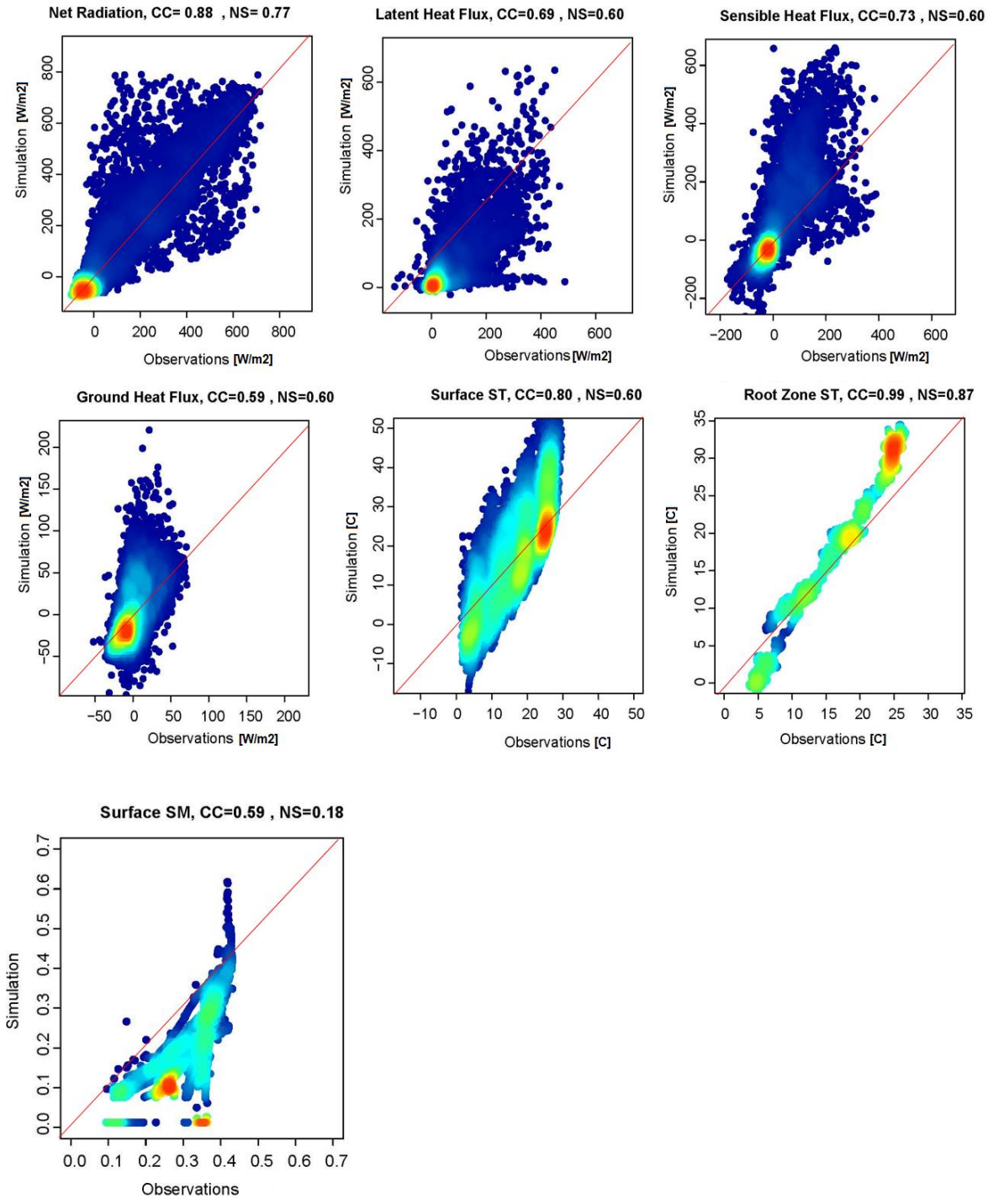

Figure 39. Density scatterplots of the transferability results at US-A32. In all panels the x-axis represents the observed and the y-axis the simulated values.

Table 14. US-A32 Transferability statistics results. Net radiation (NR) latent heat flux (LE), sensible heat flux (H), soil root zone temperature (RST), and soil surface soil moisture (SSM).

Variable→	**NR(W/m^2)**	**LE(W/m^2)**	**H(W/m^2)**	**G(W/m^2)**	**SST(C)**	**RST(C)**	**SSM**
CC	0.88	0.69	0.73	0.59	0.8	0.99	0.59
BIAS	-0.12	-0.15	-0.68	-4.1	-0.1	-0.1	0.8
RMSE	105.61	75.99	122.018	28.80	8.852	3.81	0.1612
NS	0.77	0.6	0.6	0.36	0.6	0.87	0.18

The time series of Figure 40 illustrate that the components of the energy balance are well estimated and, even if there are some under and over estimations of the variables, the range of values remains accurate. The root zone soil temperature is described with good accuracy. Finally, the time series of surface soil moisture (SSM) illustrates the model performance tends to underestimate soil moisture values.

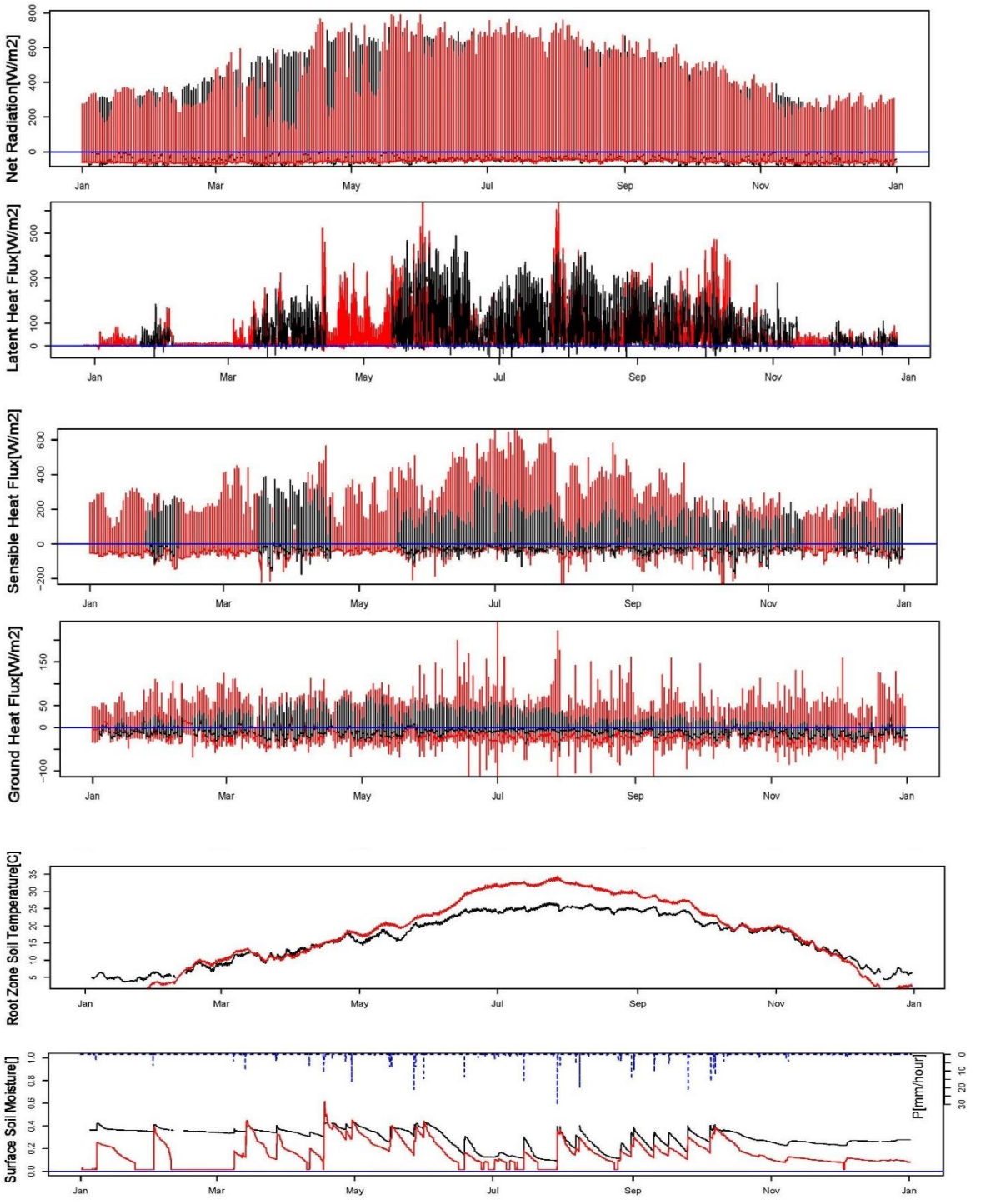

Figure 40. US-A32 transferability time series results. Red and black lines represent simulated and observed values respectively. From top down the variables are net radiation (NR) latent heat flux (LE), sensible heat flux (H), soil root zone temperature (RST), and soil surface soil moisture (SSM).

4. Discussion

The main goals of this study were to evaluate the capability of a physically-based hydrologic model to simulate surface energy fluxes, surface and root-zone soil temperature, and moisture, identify the variables that mostly contributed to their variability and to evaluate the parameter transferability at sites with similar vegetation.

The model calibration and validation procedures resulted in adequate modeling scores, correlation coefficients >0.75 and NS>0.5, despite some exceptions particularly at simulating soil moisture. The discrepancies between model and observations can be attributed to (1) uncertainties in model parameterization, (2) model structural problems, (3) errors in the dynamic vegetation information, (4) uncertainties in the weather forcing and (5) errors in the observed data. The calibration results helped to illustrate the strengths and limitations of the model in terms of data availability and quality. In the particular case of US-ARm, the quality of soil moisture observations and disagreements with neighboring data made us exclude this variable from the simulations.

The results suggest, the fourth element (i.e. uncertainties in the weather forcing) significantly influenced the quality of the simulations as quality and continuity of variables like incoming solar radiation or precipitation was not necessarily optimal. Uncertainties in model forcing and radiation flux have produced negative impacts in other studies estimating ET and surface energy fluxes (i.e., Jiang et. al, 2001). For instance, at the US-ARm site, IS had high quality and continuity but it did not occur the same at the Marena site, where the IS values were at least 150W/m^2 smaller than all the other sites

and the annual cycle, characterized in the region for having higher radiation during the summer months and lower during the winter was not captured as illustrated in Figures 6 and 12. Furthermore, the forcing data I used for the US-ARm simulations were the gap-filled(Aubinet, 2012) data provided by FLUXNET, which different from the ones provided by the ARM facility at its SGP central facility tower and the E13 ancillary towers, these are gap-filled and we used observations at 4.25m height. Further, the FLUXNET data had temperature observations at 2.5 and 5cm soil depths, and because the model is designed to estimate soil temperatures at the surface (10 cm) and root level (100 cm) matching both levels to perform the assessment was challenging, especially for the deep-soil temperature at Marena where we had access to the root zone soil moisture data, but not the RST.

Another supporting argument to argue that the quality of the forcing data is an essential component for successful simulation results, was shown in section 3.3 through multiple regression analysis that showed that IS had the strongest influence on the predictions of SEF, but that influence is re-distributed in other forcing variables and vegetation parameters, when the IS data quality and continuity is not the best. In addition, the results made clear the importance of the relative humidity, soil water content, and soil temperature influence to estimate the surface energy fluxes. The soil moisture and relative humidity are linked with land-atmosphere interactions and influence the amount of energy necessary to evaporate water (Bertoldi et al., 2010; Garai et al.,2013; Xiang, Vivoni, & Gochis et al., 2014). Moreover, albedo and wind speed that have strong

influence on the SEF in forest environments had a minor contribution in the crops and grassland sites used in this study.

The use of dynamic vegetation parameters constituted a clear proof of the value of including vegetation cover and activity in the estimation of evapotranspiration and its partitioning components. The importance of the vegetation timing and greening duration is critical to understand all water-energy fluxes that are related to carbon budgets. The results found that the correct parameterization of vegetation in physically-based models actively drives the amount of water exchange from the ground to the atmosphere.

Vegetation changes not only affect the estimation of latent heat flux that is associated with evapotranspiration but also other variables like ground and sensible heat fluxes. However, this was not directly investigated in this thesis. Future work might assess the model performance when using higher-resolution products (Landsat 30m, Sentinel 20m) to estimate the vegetation components. The limitation of using higher-resolution remote sensing images is based on the need of a leaf area index model. The MODIS LAI is estimated with a model that uses surface reflectance and constant values specific to each biome over the MODIS grid. The cloud can represent a challenge to maintain good quality and continuous data, but in this study that limitation was overcome combining satellite and in-situ data. The stomatal resistance was estimated hourly using LAI and FPAR 4-day composites that were linearly interpolated to hourly, displaying a better gradient of vegetation change; the LAI was computed with hourly observations of incoming short wave radiation, allowing to reproduce the diurnal changes. Furthermore, the option of using the photosynthetic photon flux density (PPFD) sensor instead of IS

and FPAR can provide a more accurate estimation of the photosynthetic active radiation but because this project seeks to apply the model at places without an eddy covariance system, due the availability and cost of acquisition of the MODIS FPAR and incoming short wave radiation, these variables become the best option.

The model transferability tests showed the potential use of tRIBS at sites with similar vegetation without need for calibration. The simulation skill metrics for the two sites at which the model transferability was tested are better than the historic mean and provide confidence to future use of the model as a complementary tool at standard weather stations like those at the Mesonet networks.

The soil moisture results at Marena, the lack or data in US-ARm and the transferability scores support the need for quality sensors to measure the soil moisture and soil temperature variables. The reason why soil moisture simulations were less ideal can be due the occurrence of snow processes during the wintertime, where snow cover often skew the soil moisture estimations (Reichle et al., 2004; Koster et al., 2009) . Snow is an active driver in the prediction of soil moisture that limited the performance of tRIBS. The snow does not represent an issue only for soil moisture, but it also produces an error on the ratio of downward to upward flux of shortwave radiant energy estimations (Mannstein, 1985).

The parameter transferability of tRIBS was tested in similar environments aiming to support the hypothesis that the model can complement standard weather stations in

predicting energy fluxes, soil temperature, and soil moisture in areas where these variables are not measured.

5. Summary and Conclusions

This study compiled atmospheric, soils, vegetation, and hydrologic information from eddy-covariance systems to evaluate the capabilities of a process-based model that uses standard weather station measurements and remote sensing of vegetation to estimate the components of the energy budget and the soil temperatures and water content at different depths. The model was calibrated and validated through simulation skill and error scores and particularly for the energy components (including ET) and soil temperatures the Nash-Sutcliffe model efficiencies were above 0.5 suggesting a simulations of sufficient quality. Results for the soil moisture and ground heat flux simulation skill are mixed and driven by the inaccuracies in soil characterization and parameters but also uncertainties in heat flux, precipitation and soil moisture measurements themselves. In all cases, the results proved the adequate performance of the model for the entire simulation cycles (~1 year) at an hourly time scale resolution. The model keeps adequate predictability for most of the variables (NS>0).

Incoming short wave radiation is a crucial variable to estimate the surface energy components correctly. Furthermore, worsening of the data quality will re-organize the prediction weights of other variables like temperature, relative humidity and vegetation

fraction. The soil water content and vegetation fraction influence the values of latent heat flux, but soil surface temperature has the strongest influence on the other components of energy budget.

Vegetation phenology and its changes over time are necessary to correctly estimate the surface energy budget components, soil moisture and temperature. Furthermore, the estimation of biophysical parameters at high temporal resolution using remote sensing and in-situ data is strategic to produce accurate latent, sensible, and ground heat flux estimations.

Finally, the model has the potential to be used as a virtual tool in similar environments at the U.S. Southern Plains as it can be informed using data from the Mesonet network. The dynamic vegetation parameters can be produced from MODIS imagery downloaded from the official website (modis.ornl.gov) and then estimated using the biophysical expressions shown in Table 5. Future work might include the development of a stakeholder-oriented, virtual tool where tRIBS can be run online and at any point of interest with weather forcing data (e.g., Mesonet or re-analysis model outputs). Moreover, it could be utilized in conjunction with drone technologies (like those in 3D Mesonet) that would refine the remote sensing images to the tower footprint, which would help improving the spatial resolution of vegetation parameters (such as stomatal resistance) and thus the overall simulation accuracy of the results.

6. Lessons Learned and Future Work

The process of writing a thesis is extensive and enriching. The beginnings of it include substantial reading, research ideas, and attempts. The knowledge and information you get during the first stage and building a literature review or state of the art are crucial for the development of your topic and your professional growth. However, during the first months, the path of your research can change, and some of the valuable information that you compiled can be forgotten. For that reason, the first lesson I learn is to build a reference database; even if the process seems tedious and time-consuming, organizing a chart by topic with a gist of the papers you have read can be very helpful at the end.

The second lesson learned is about data management. The use of extensive data set of information can be time-consuming, and once it is processed, several copies should be deleted and details of the processing that can be left behind. The use of a research logbook with the different issues and solutions found per data set would be handy. The third lesson that I learned is that the different attempts that you do (i.e., try an alternative method or validate with a different data set) are results that can enhance your discussion and could be put in an appendix section. Finally, I learned that there are many sources of data, but you should use the one that provides you the more technical support and that preferably still in operation.

Future work of this study might include testing the model at other regions in Oklahoma, configuring tRIBS at different Mesonet stations, and validating it with a mobile eddy covariance tower. Then, setting up tRIBS in a server so it can directly obtain the Mesonet and MODIS data, and people using the Mesonet data could be able to download the variable of interest from 2002 to the present. Furthermore, the next step

will include basin-scale simulations and a methodology to bridge local scales (ECT) and regional scales (satellite), making tRIBS an accurate complementary tool for weather forecasters, agriculturists, and other stakeholders that might need these type of data.

References

Alvenäs, G., & Jansson, P. E. (1997). Model for evaporation, moisture and temperature of bare soil: calibration and sensitivity analysis. *Agricultural and Forest Meteorology*, 88(1-4), 47-56.

AMERIFLUX. (2018). *Ameriflux*. Retrieved from US Department of Energy: http://ameriflux.lbl.gov/tech/pecs/

Assouline, S. (2006). Modeling the relationship between soil bulk density and the hydraulic conductivity function. *Vadose Zone Journal*, 5(2), 697-705.

Aubinet. (2012). *Eddy Covariance: A practical Guide to Measurement and Data Analysis* (Vol. Springer Science+Business Media B.V. 2012). (P. T. Prof. Marc Aubinet, Ed.) London - New York: Springer, Atmospheric Sciences. doi:10.1007/978-94-007-2351-1

Aubinet, M., A, G., Ibrom, A., U¨, R., J, M., T, F., . . . T, V. (2000). Estimates of the annual net carbon and water exchange of forests: the EUROFLUX methodology. *Adv Ecol Res 30*, 113-175.

Baldocchi, D. (1997). Flux footprints within and over forest canopies. *Bound Layer Meteorol*, 85:273–292.

Basara, J. B., Illston, B. G., Fiebrich, C. A., Browder, P. D., Morgan, C. R., McCombs, A., . . . Crawford, K. C. (2010). The Oklahoma City Micronet. *meteorological applications*, DOI: 10.1002/met.189.

Basara, Jeffrey B.; Crawford, Kenneth C. (2002). Linear relationships between root-zone soil moisture and atmospheric processes in the planetary boundary layer. *Journal of Geophysical Research*, VOL. 107, NO. D15, 4274, 10.1029/2001JD000633.

Billesbach, D. P., Fischer, M. L., Torn, & Berry, J. (2004). A Portable Eddy Covariance System for the Measurement of Ecosystem-Atmosphere Exchange of CO2, Water Vapor, and Energy. *Journal of Atmospheric and Oceanic Technology*, 639-650.

Bodine, D., Heinselman, P. L., Cheong, B. L., Palmer, R. D., & Michaud, D. (2010). A Case Study on the Impact of Moisture Variability on Convection Initiation Using Radar Refractivity Retrievals. . *Journal of Applied Meteorology and Climatology*, 49, 1766-1778.

Bodine, D., Klein, P., Arms, S., & Shapiro, A. (2009). Variability of Surface Air Temperature over Gently Sloped Terrain. *J. Appl. Meteor. Climatol.*, 48, 1117-1141.

Brunsell, N.A.; Jones, A.R.; Jackson, T.; Feddema, J. Seasonal trends in air temperature and precipitation in IPCC AR4 GCM output for Kansas, USA: Evaluation and implications. *International Journal Climatol*. 2010, 30, 1178–1193.

Cai, X., & Leclerc, M. (2007). Forward-in-time and backward-in-time dispersion in the convective boundary layer: the concentration footprint. *Bound Layer Meteorol,* 123:201–218.

Campbell, G. S., & Norman, J. M. (1998). *An Introduction to Environmental Biophysics.* Springer.

Castelli, R., Rodriguez-Iturbe, I., & Entekhabi, D. (1996). An analytic framework for the modeling of the spatial interaction between the soil moisture and the atmosphere. *Journal of Hydrology*.

Celis, J. A., Vergara, H., & Vanegas, D. (2017). Evaluacion de mejora en el monitoreo de sequias a escala regional en Colombia, a partir de indicadores ecohidrologicos basados en teledeteccion. *Journal of Technology*, ISSN 1692-1399.

Cosh, M.H., T.J. Jackson, R. Bindlish, J. Famiglietti, and D. Ryu, 2005, A comparison of an impedance probe for estimation of surface soil water content over large region. *Journal of Hydrology*, 311:49-58.

Criss, R. E., & Winston, W. E. (2008). Do Nash values have value? Discussion and alternate proposals. *Hydrological Processes: An International Journal*, 22(14), 2723-2725.

Dietrich, W. E., and J. T. Perron (2006), The search for a topographic signature of life, *Nature*, 439(7075), 411–418.

Donohue, R. J., Roderick, M. L., & McVicar, T. R. (2010). Can dynamic vegetation information improve the accuracy of Budyko's hydrological model?. *Journal of Hydrology*, 390(1-2), 23-34.

Dore, S., Kolb, T. E., Montes-Helu, M., Eckert, S. E., Sullivan, B. W., Hungate, B. A., & Finkral, A. (2010). Carbon and water fluxes from ponderosa pine forests disturbed by wildfire and thinning. *Ecological Applications*, 20(3), 663-683.

Dorman, J., & Sellers, P. (1989). A Global Climatology of albedo, Roughnrss Lengths and Stomatal Resistance for Atmospheric General Circulation Models as Represented by the Simple Biosphere Model(SiB). *American Meteorological Society*.

Foken, T. (2008). *Micrometeorology*. Berlin, Heidelberg: Springer-Verlag.

Garrote, L., & Bras, R. L. (1995). A distributed Model for real flood forcasting using digital elevations models. *Journal of Hydrology*, 167,279-306.

Gash, J. (1986). A note on estimating the effect of a limited fetch on micrometeorological. *Bound Layer Meteorology*, 35:409–413.

Gentine, P., Polcher, J., & Entekhabi, D. (2011). Harmonic propagation of variability in surface energy balance within a coupled soil-vegetation-atmosphere system. *Water Resources Research*.

Horst, T., & Weil, J. (1992). Footprint estimation for scalar flux measurements in the atmospheric surface layer. *Bound Layer Meteorol*, 59:279–296.

Huber, D., Mechem, D., & Brunsell, N. (2014). The effects of Great Plains irrigation on the surface energy balance, regional circulation, and precipitation. *Climate, 2(2), 103-128*.

Ivanov, V. Y., Bras, R. L., & Vivoni, E. R. (2008). Vegetation-Hydrology dynamics in complex terrain of semiarid areas: 1. A mechanisitic approach to modeling dynamics feedbacks . *Water Resources Research*.

Ivanov, V. Y., Vivoni, E. R., Bras, R. L., & Entekhabi, D. (2004). Catchment hydrologic response with a fully distributed triangulated irregular network model. *Water Resources Research* .

Ivanov, V. Y., Fatichi, S., Jenerette, D., Espeleta, J., Troch, P., & Huxman, T. (2010). Hysteresis of soil moisture spatial heterogeneity and the "homogenizing" effect of vegetation. *Water Resources Research*.

J.P. Goodrich, W. O., Gioli, B., Moreaux, V., Murphy, P., Burba, G., & Zona, D. (2016). Impact of different eddy covariance sensors, site set-up, and maintenance on the annual balance of CO2 and CH4 in the harsh Arctic envrironment. *Agricultural and Forest Meteorology*, 239-251.

Jadwiga R. Ziolkowska, C. A. (2017). Benefits and Beneficiaries of the Oklahoma Mesonet: A Multisectoral Ripple Effect Analysis . *American Meteorological Society*.

Jiang, L., & Islam, S. (2001). Estimation of surface evaporation map over southern Great Plains using remote sensing data. *Water resources research*, 37(2), 329-340.

Kim, Y., and E. A. B. Eltahir (2004), Role of topography in facilitating coexistence of trees and grasses within savannas, *Water Resources* Res., 40, W07505, doi:10.1029/2003WR002578.

Klaassen, W., & Sogachev, A. (2006). Flux footprint simulation downwind of a forest edge. *Bound Layer Meteorol*, 121:459–473.

Kljun, N. R. (2002). A 3D Backward Lagrangian Footprint Model for a Wide Range of Boundary Layer Stratifications. *Bound.-Lay. Meteorol*, 103, 205–226.

Kljun, N., Calanca, P., Rotach, M. W., & Schmid, H. P. (2015). A simple two-dimensional parameterisation for Flux Footprint Prediction (FFP). *Published by Copernicus Publications on behalf of the European Geosciences Union.*

Kormann, & Meixner, F. (2001). An analytic footprint model for neutral stratification. . *Bound Layer Meteorol* , 99:207–224.

Koster, R. D., Guo, Z., Yang, R., Dirmeyer, P. A., Mitchell, K., & Puma, M. J. (2009). On the nature of soil moisture in land surface models. *Journal of Climate*, 22(16), 4322-4335.

Leclerc, M., & Thurtell, G. (1990). Footprint prediction of scalar fluxes using a Markovian analysis. *Bound Layer Meteoroly*, 52:247–258.

Leclerc, M., Shen, S., & Lamb, B. (1997). Observations and large-eddy simulation modeling of footprints in the lower convective boundary layer. *J Geophys Res*, 102(D8):9323–9334.

Lingli, H., Ivanov, V. Y., Bohrer, G., Maurer, K. D., & Vogel, C. S. (2013). Effects of fine-scale soil moisture and canopy heterogeneity on energy and water fluxes in a northern temperate mixed forest. *Agricultural and Forest Meteorology*.

Lucht, W., & Roujean, J. L. (2000). Considerations in the parametric modeling of BRDF and albedo from multiangular satellite sensor observations. *Remote Sensing Reviews*, 18(2-4), 343-379.

Maggard, A. O., Willa, R. E., Wilson, D., Meeka, C. R., & Vogel, J. (2016). Fertilization reduced stomatal conductance but not photosynthesis of Pinus taeda which

compensated for lower water availability in regards to growth. *Forest Ecology and Management*.

Mannstein, H. (1985). The Interpretation of Albedo Measurements on a Snowcovered Slope. *archives for meteorology, geophysics, and bioclimatology*.

McPherson, R. A. (2007). A review of vegetation—atmosphere interactions and their influences on mesoscale phenomena. *Progress in Physical Geography*, 31(3), 261-285.

McPherson, R. A., FIEBRICH, C. A., CRAWFORD, K. C., ELLIOTT, R. L., KILBY, J. R., GRIMSLEY, D. L., MELVIN, A. D. (2007). Statewide Monitoring of the Mesoscale Environment: A Technical Update on the on the Oklahoma Mesonet . *journal of atmospheric and oceanic technology*, DOI:10.1175/JTECH1976.1.

MendezBarroso, L. A., Vivoni, E. R., Morua, A. R., Mascaro, G., Yepez, E. A., Rodriguez, J. C., . . . Hernandez, J. A. (2014). A modeling approach reveals differences in evapotranspiration and its partitioning in two semiarid ecosystems in Northwest Mexico. *American Geophysical Union, Water Resources Research*, 50, 3229-3252.

Monteith, J. (1965). Evaporation and the Environment. *19th Symposia of the Society for Experimental Biology*, 19, 205-234.

Montgomery, R. (1948). Vertical eddy flux of heat in the atmosphere. . *Journal of Meteorology*, 5:265–274.

Moreno, H. A., Vivoni, E., & Gochis, D. J. (2012). Utility of Quantitative Precipitation Estimates for high resolution hydrologic. *Journal of Hydrology*.

Moreno, H. A., Vivoni, E. R., & Gochis, D. J. (2013). Limits to flood forecasting in the Colorado Front Range for two summer convection periods using radar nowcasting and a distributed hydrologic model. *Journal of Hydrometeorology*, 14(4), 1075-1097.

Moreno, Hernan A.; Gupta, Hoshin V.; Sampson, David A. (2016). Modeling the distributed effects of forest thinning on the long-term water balance and streamflow extremes for a semi-arid basin in the southwestern US. *Hydrology and Earth Systems Sciences*.

Obukhov, A. (1951). Charakteristiki mikrostruktury vetra v prizemnom sloje atmosfery (Characteristics of the micro-structure of the wind in the surface layer of the atmosphere). *Izv ANSSSR ser Geofiz*, 3:49–68.

Ocheltree, T. W., & Loescher, H. W. (2007). Design of the AmeriFluxAmeriFluxAmeriFlux Portable Eddy Covariance System and Uncertainty Analysis of Carbon Measurements. *Journal of Atmospheric and Oceanic Technology*, 1389-1406.

Olajuyigbe, S., Tobin, B., Saunders, M., & Nieuwenhuis, M. (2012). Forest thinning and soil respiration in a Sitka spruce forest in Ireland. Agricultural and Forest Meteorology, 157, 86-95.

Oklahoma Climatological Survey. (2004). *Oklahoma Annual Climate Summary 2002.* Norman, Oklahoma: board of Regents of The University of Oklahoma.

Oklahoma Department of Wildlife Conservation . (2017). *Vegetation Classification Project: Interpretative Booklet.* Oklahoma Department of Wildlife Conservation.

Palladinoa, M., Staianob, A., D'Ursoa, G., Minacapillic, M., & Ralloc, G. (2013). Mass and Surface Energy Balance Approaches for Monitoring Water Stress in Vineyards. *Procedia Environmental Sciences*, 231-238.

Pasquill. (1972). Some aspects of boundary layer description. *Real Meteorology Society*, 469-494.

Paw, U. K. T., Baldocchi, D. D., Meyers, T. P., & Wilson, K. B. (2000). Correction of eddy-covariance measurements incorporating both advective effects and density fluxes. *Boundary-Layer Meteorology*, 97,487–511.

Penman, H. (1948). Natural evaporation from open water, bare soil and grass. *Proceedings of the Royal Society a Physical, Mathematical and Engineering Sciences*, DOI: 10.1098/rspa.1948.0037 .

Peppler, R., Kehoe, K. E., Monroe, J., Theisen, A., & Moore, S. (2016). The ARM Data Quality Program. *Meteorological Monographs*, 12.1-12.14. doi:10.1175/AMSMONOGRAPHS-D-15-0039.1

Pettorelli, N., Vik, J. O., Mysterud, A., Gaillard, J. M., Tucker, C. J., & Stenseth, N. C. (2005). Using the satellite-derived NDVI to assess ecological responses to environmental change. *Trends in ecology & evolution*, 20(9), 503-510.

Pielke, R. A., Avissar, S. R., Raupach, M., Dolman, A. J., Zeng, X., & Denning, A. S. (1998). Interactions between the atmosphere and terrestrial ecosystems: influence on weather and climate. *Global Change Biology*.

Pitman, J. I. (1989). Rainfall interception by bracken in open habitats — Relations between leaf area, canopy storage and drainage rate. *Journal of Hydrology*.

Rannik, U., Aubinet, M., Kurbanmuradov, O., Sabelfeld, K., Markkanen, T., & Vesala, T. (2000). Footprint analysis for the measurements over a heterogeneous forest. *Bound Layer Meteorol*, 97:137–166.

Rannik, U., Markkanen, T., Raittila, J., Hari, P., & Vesala, T. (2003). Turbulence statistics inside and over forest: influence on footprint prediction. *Bound Layer Meteorol*, 109:163–189.

Rawls, W. J., Brakensiek, D. L., & Saxton, K. E. (1982). Estimation of Soil water properties. *American Society of Agricultural Engineers*.

Reichle, R. H., & Koster, R. D. (2004). Bias reduction in short records of satellite soil moisture. *Geophysical Research Letters*, 31(19).

Rogers, R., & Yau, M. (1989). A Short Course in Cloud Physics. *Pergamon Press, Oxford*.

Sánchez, J., Bisquert, M., Rubio, E., & Caselles, V. (2015). Impact of land cover change induced by a fire event on the surface energy fluxes derived from remote sensing. *Remote Sensing*, 7(11), 14899-14915.

Schmidt, A., Hanson, C., Chan, W. S., & Law, B. E. (2012). Empirical assessment of uncertainties of meteorological parameters and turbulent fluxes in the AmeriFlux network . *Journal of Geophysical Research*, doi:10.1029/2012JG002100.

Schmidt, L. S., Aðalgeirsdóttir, G., Guðmundsson, S., Langen, P. L., Pálsson, F., Mottram, R., . . . Björnsso, H. (2017). The importance of accurate glacier albedo for estimates of surface mass balance on Vatnajökull: Evaluating the surface

energy budget in a Regional Climate Model with automatic weather station Observations. *The Cryosphere*.

Schuepp, P., Leclerc, M., MacPherson, J., & Desjardins, R. (1990). Footprint prediction of scalar fluxes from analytical solutions of the diffusion equation. *Bound Layer Meteorology*, 50:355–373.

Shuttleworth, W. (1992). *Evaporation. In: D.R. Maidment (Editor), Handbook of Hydrology*. New York: McGraw-Hill.

Sogachev, A., & Lloyd, J. (2004). Using a one-and-a-half order closure model of the atmospheric boundary layer for surface flux footprint estimation. *Bound Layer Meteoroly* , 112:467–502.

Sogachev, A.; Rannik, U; Vesala, T. (2004). On flux footprints over the complex terrain covered by a heterogeneous forest. *Agric For Meteorology*, 127:143–158.

Souza, E. P., Rennó, N. O., & Silva Dias, M. A. (2000). Convective circulations induced by surface heterogeneities. *Journal of the atmospheric sciences*, 57(17), 2915-2922.

Steinfeld, G., Raasch, S., & Markkanen, T. (2008). Footprints in homogeneously and heterogeneously driven boundary layers derived from a Lagrangian Stochastic particle model embedded into large-eddy simulation. *Bound Layer Meteorology*, 129:225–248.

Strong, C., Fuentes, J., & Baldocchi, D. (2004). Reactive hydrocarbon flux footprints during canopy senescence. *Agric For Meteorol*, 127:159–173.

Swinbank, W. (1951). The measurement of vertical transfer of heat and water vapor by eddies in the lower atmosphere. *Journal of Meteorology*, 8:135–145.

Taylor, C. M., Saïd, F., & Lebel, T. (1997). Interactions between the land surface and mesoscale rainfall variability during HAPEX-Sahel. *Monthly Weather Review*, 125(9), 2211-2227.

Vesala, T., J¨arvi, L., Launiainen, S., ASogachev, Rannik, U., Mammarella, I., . . . Nikinmaa, E. (2008). Surface-atmosphere interactions over complex urban terrain in Helsinki, Finland. *Tellus*, 60B:188–199.

Vesala, T., Kljun, N., Rannik, ¨., Sogachev, A., T, M., Sabelfeld, K., . . . Leclerc, M. (2010). Flux and concentration footprint modelling. In: Modelling of pollutants in complex environmental systems. *vol II. ILM Publications*, St Albans, pp 339–355.

Vivoni, E. R., Rodrı´guez, J. C., & Watts, C. J. (2010). On the spatiotemporal variability of soil moisture and evapotranspiration in a mountainous basin within the North American monsoon region . *Water Resources*, VOL. 46, W02509, doi:10.1029/2009WR008240.

Vrugt, J. A., & Braak, C. J. (2011). DREAM(D): an adaptive Markov Chain Monte Carlo simulation algorithm to solve discrete, noncontinuous, and combinatorial posterior parameter estimation problems. *Hydrology and Earth Sciences Systems*.

Waglea, P., Bhattaraib, N., Gowdaa, P. H., & Kakanic, V. G. (2017). Performance of five surface energy balance models for estimating daily evapotranspiration in high biomass sorghumily. *ISPRS Journal of Photogrammetry and Remote Sensing*.

Wilson, K. B., Baldocchi, D. D., Aubinet, M., Berbigier, P., Bernhofer, C., Dolman, H., & Grelle, A. (2002). Energy partitioning between latent and sensible heat flux

during the warm season at FLUXNET sites. *Water Resources Research*, 38(12), 30-1.

Xiang, T., Vivoni, E., Gochis, D. J., & Mascaro, G. (2017). On the diurnal cycle of surface energy fluxes in the North American monsoon region using the WRF-Hydro modeling system. *Journal of Geophysical Research: Atmospheres*, 122(17), 9024-9049.

Xiang, T., Vivoni, E. R., & Gochis, D. J. (2014). Seasonal Evolution of ecohydrological controls on land surface temperature over complex terrain. *Water Resources*.

Y., I. V., Vivoni, E. R., Bras, R. L., & Entekhabi, D. (2004). Catchment hydrologic response with a fully distributed triangulated irregular network model . *Water Resour. Res., 40 , W11102, doi:10.1029/2004WR003218.*

Yan, H., Wang, S., Billesbach, D., Oechel, W., Zhang, J., Meyers, T., . . . Scott, R. (2012). Global estimation of evapotranspiration using a leaf area index-based surface energy and water balance model . *Remote Sensing Environment*.

Zhang, L., HU, Z., Fan, J., Zhou, D., & Tang, F. (2014). A meta-analysis of the canopy light extinction coefficient in terrestrial ecosystems. *Front. Earth Sci.*, 599-609.

Zhou, L., Dickinson, R. E., Tian, Y., Zeng, X., Dai, Y., Yang, Z. L., & Myneni, R. B. (2003). Comparison of seasonal and spatial variations of albedos from Moderate-Resolution Imaging Spectroradiometer (MODIS) and Common Land Model. *Journal of Geophysical Research: Atmospheres*, 108(D15).

Appendix

Table A. Main fetch models remarks. Adapted from Foken (2008), Vesala, et al., (2010), Aubinet, (2012).

Author	*Remarks*
(Pasquill, 1972)	First model description, concept of effective fetch
(Gash, 1986)	Neutral stratification, concept of cumulative fetch
(Schuepp, Leclerc, MacPherson, & Desjardins, 1990)	Use of source areas, but neutral stratification and averaged wind velocity
(Leclerc & Thurtell, Footprint prediction of scalar fluxes using a Markovian analysis., 1990)	Lagrangian footprint model
(Horst & Weil, 1992)	One-dimensional footprint model
(Schmid, 1994), (Schmid, 1997)	Separation of footprints for scalars and fluxes
(Leclerc et al. 1997)	LES model for footprints
(Baldocchi, 1997)	Footprint model within forests
(Rannik, et al., 2000)(Rannik, et al., 2003)	Lagrangian model for forests
Kormann and Meixner (2001) *(Kormann & Meixner, 2001)*	Analytical model with exponential wind profile
(Kljun et al. 2002)	Three-dimensional Lagrangian model for various turbulence stratifications with backward trajectories
(Sogachev & Lloyd, 2004)	Boundary-layer model with 1.5 order closure
(Sogachev, A.; Rannik, U; Vesala, T, 2004)	Footprint estimates for a non-flat topography

Author	*Remarks*
(Strong, Fuentes, & Baldocchi, 2004)	Footprint model with reactive chemical compounds
(Cai & Leclerc, 2007)	Footprints from backward and forward in-time particle simulations driven with LES data
(Klaassen & Sogachev, 2006)	Footprint estimates for a forest edge
(Vesala, et al., 2008)	Footprint estimates for a complex urban surface
(Steinfeld, Raasch, & Markkanen, 2008)	Footprint model with LES-embedded particles
(Kljun et al.2015)	Two dimensional parametrization for FFP

ARm

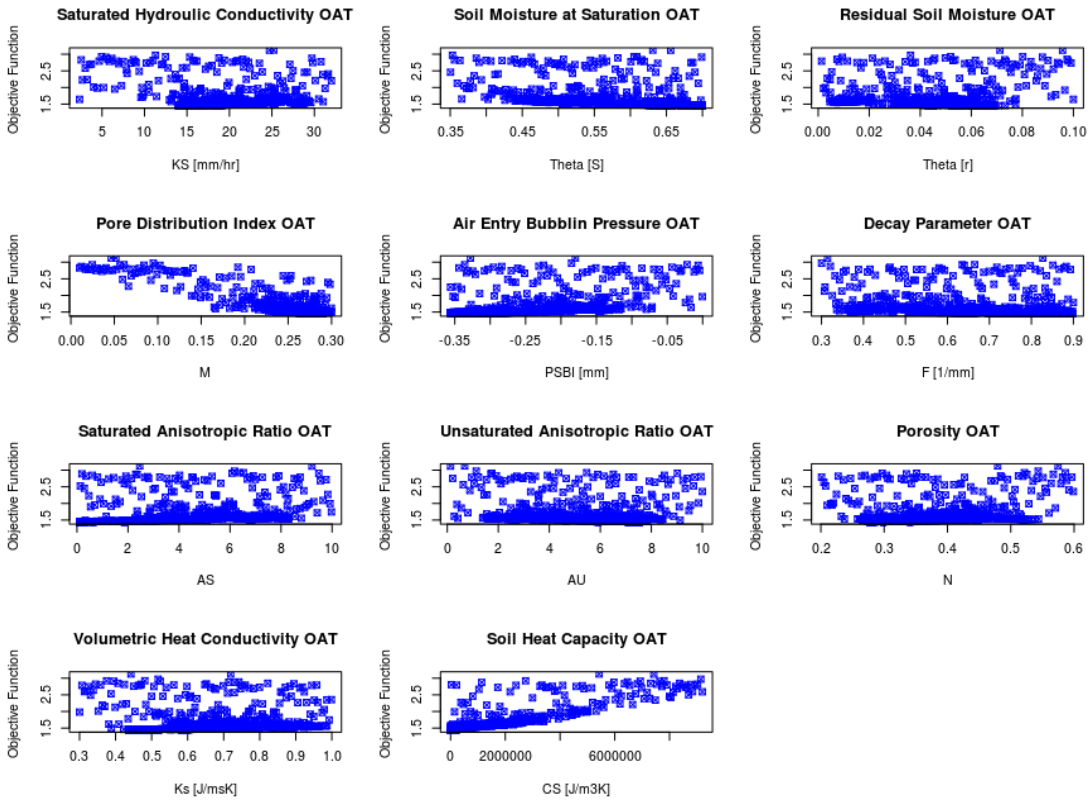

Figure 41. One At a Time Sensitivity analysis of the soil parameters based on the SCE results at US-Arm.

Table B. US-ARm best parameters results.

Parameter	**K_s**	**θ_s**	**θ_r**	**m**	**Ψ_b**	**f**	**As**	**Au**	**n**	**Ks**	**C_s**
Silty Clay Loam	21.84[a]	0.552[a]	0.017[a]	0.57[a]	-0.373[a]	5E-7[a]	01.109[a]	1.109[a]	0.431[a]	0.989[a]	1061340[a]
	[a]OAT parameters results.										

Marena

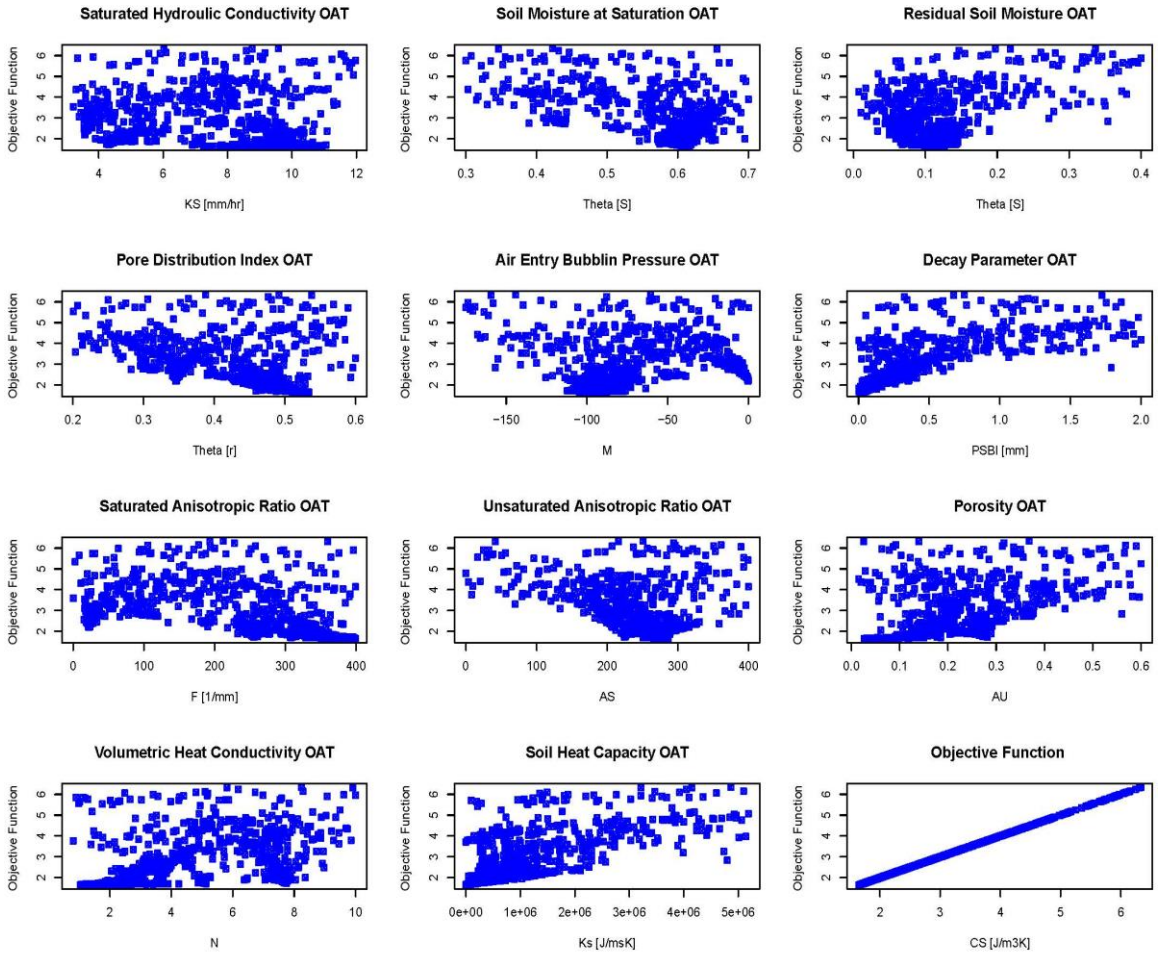

Figure 42. One At a Time Sensitivity analysis of the soil parameters based on the SCE results at Marena.

Table C. Marena best parameters results.

Parameter	**K_s**	**θ_s**	**θ_r**	**m**	**Ψ_b**	**f**	**As**	**Au**	**n**	**Ks**	**C_s**
Loam Clay	4.85[a]	0.61[a]	0.11[a]	0.52 [a]	-99.2[a]	0.07	388[a]	388 [a]	0.51[a]	1.6 [a]	1383[a]
	[a]OAT parameters results.										